UNIVERSITY OF CALIFORNIA,
IRVINE

Trace Gas Emissions from Biomass Burning: Impacts on Human Health, Local Air Quality, and Global Climate

DISSERTATION

submitted in partial satisfaction of the requirements
for the degree of

DOCTOR OF PHILOSOPHY

in Chemistry

by

Alexander William Jarnot

Dissertation Committee:
Professor Donald R. Blake, Chair
Professor Ann Marie Carlton
Professor Sergey Nizkorodov

2021

DEDICATION

To

My parents, Drs. Bruce and Miranda Jarnot,

Dr. Donald Blake,

And

My dearest Caroline, always by my side

“Never for me the lowered banner, never the last endeavour.”
-Sir Ernest Shackleton

TABLE OF CONTENTS

LIST OF FIGURES

LIST OF TABLES

ACKNOWLEDGMENTS

I would like to express the deepest appreciation to my committee chair, Professor Donald R. Blake, who has been like a father to me even before I was a graduate student, and on through my graduate student career, and who I am sure will continue to be even long into the rest of my life, as he is for so many others. Don has been more than an academic advisor, and has stood by me and helped me through so much during my career. Don truly embodies the finest spirit of science, and I am ever grateful to him.

I would like to express my sincere gratitude to Simone Meinardi, Brent Love, Gloria Liu, and Fred Murabito for their tireless efforts every day in the lab, especially during the FIREX-AQ and SARP campaigns when they analyzed canister samples every day, twenty-four hours a day for months. These individuals also taught me so much about analytical methods, best practices in the lab, and came and supported me at my practice talks for my advancement exam. I owe them all a huge debt of gratitude.

I would like to thank Barbara Chisholm for her immense efforts assisting me during my time as a graduate student. She works tirelessly to support me at every step of the way. Also, without her I would still be lost in a Baja desert somewhere.

I would like to thank Dr. Eric Apel and Dr. Becky Hornbrook for their kindness, patience, and willingness to teach me during my times with them. They allowed me to learn to use the TOGA instrument, and even let me operate it in-flight during a field project, when originally, I was only in the field as a second set of hands to move equipment. They treated me like another scientist instead of just a graduate student, and I am proud to have alongside them. I am extremely grateful for their advice and help during my career thus far.

I would like to thank Dr. Nicola Blake, Dr. Isobel Simpson, and Dr. Barbara Barletta for the immense amount of insight, advice, support, and help they have given me over the years. I have gained an immense amount of knowledge from them, and would not be where I am without them.

I would like to thank Dr. Emily Fischer and Dr. Ilana Pollack for their guidance, patience, support, and collaboration with the research using positive matrix factorization. Ilana spent a great deal of time teaching me the proper use of the technique, and was extremely patient with me during the learning process. Dr. Fischer also spent a great deal of her own time mentoring me, even though I am not one of her students. I truly appreciate their guidance and mentorship.

A portion of this material is based upon work supported by the National Center for Atmospheric Research, which is a major facility sponsored by the National Science Foundation under Cooperative Agreement No. 1755088. Any opinions, findings and conclusions or recommendations expressed in this material do not necessarily reflect the views of the National Science Foundation.

VITA

Education

PhD University of California - Irvine, Chemistry ***Expected*** November 2021
Dissertation: "The Impact of Biomass Burning Emissions on Urban Air Quality"

MS University of California - Irvine, Chemistry December 2018
Advisor: Donald R Blake

BA Hood College, Chemistry June 2017
Minors in Physics, Studio Art

Honors and Awards

NCAR Graduate Visitor Fellowship 2021

Michael E Gebel Award 2020
Awarded for excellence in environmental chemistry research.

NASA Group Achievement Award 2020
Awarded for outstanding scientific achievements of the Fire Influence on Regional to Global Environments Experiment – Air Quality (FIREX-AQ) airborne Earth science mission team.

Loh Down on Science Fellowship 2018
Distilled scientific findings into scripts to be aired on the NPR radio show *The Loh Down on Science.*

Eagle Scout 2013

Research Experience

Graduate Student Researcher, University of California - Irvine, Irvine, CA 2021
Advisor: Donald R Blake

- Researcher in the Rowland-Blake lab: a high-throughput, whole air sampling lab which uses ultra-high precision, multi-column gas chromatography and other techniques to measure trace gases to sub-ppt limits of detection.
- Flew on multiple airborne campaigns, and operated air sampling instrumentation while aboard.
- Integrated, maintained, repaired, and de-integrated instrumentation from research aircraft.
- Assisted in the design and fabrication of gas chromatography manifolds and systems.

- Kept up day-to-day maintenance of lab equipment, including gas cylinder changes, column repair and maintenance.
- Prepared whole air sampling canisters for sample collection and subsequent use on the Rowland-Blake lab's high-precision gas chromatography systems.
- Collected and analyzed whole air samples for over 100 distinct trace gas species to sub-part-per-trillion concentrations using three multi-column gas chromatography systems.
- Calculated response factors for each species, accounting for system drift and filament degradation.
- Built gas columns for use in laboratory cryo-trapping systems.

Hood College, Frederick, MD 2015 - 2016
Student Research Intern
Advisor: Christopher P Stromberg

- Set up and integrated a handheld x-ray fluorescence (XRF) spectrometer into the Hood College chemistry department instrumentation room.
- Designed, tested, and wrote laboratory assignments utilizing handheld x-ray fluorescence spectrometry for use in the undergraduate curriculum for all course levels.
- Prepared and presented safe demonstration experiments for visiting student days, open houses and national conferences.

Professional Experience

NASA Student Airborne Research Program, Irvine, CA 2020 & 2021
Mentor

- The NASA Student Airborne Research Program (SARP) is an annual summer program for twenty-eight senior undergraduates to take part in airborne research.
- Aided in airborne logistics prior to the transition to an online program due to the pandemic, including selecting sample targets and instrument uploading.
- Closely mentored a group of seven students and helped them develop individual research projects to be presented at a national conference.

Teaching Experience

University of California - Irvine, Irvine, CA September 2017 - Present
Teaching Assistant, Department of Chemistry

- Led discussion sessions, held office hours, administered quizzes and proctored exams for large lecture courses.
- Led general and organic chemistry laboratory sections. Oversaw four sections of twenty students and maintained a safe, yet efficient working environment.
- Helped transition large lecture courses to an online format.

Journal Publications

O'Dell, K., et al., (2020). Hazardous Air Pollutants in Fresh and Aged Western US Wildfire Smoke and Implications for Long-Term Exposure. *Environmental Science and Technology*, *54*(19), 11838–11847. https://doi.org/10.1021/acs.est.0c04497

Presentations and Invited Lectures

Poster Presentation, "The Impact of Smoke on Boundary Layer Trace Gas Abundance in the California Central Valley," American Meteorological Society, Winter 2021

Poster Presentation, "The Impact of Smoke on Boundary Layer Trace Gas Abundance in the California Central Valley," American Geophysical Union, Fall 2020

Poster Presentation, "A Comparison of Trace Gas Trends in Urban Areas Collected via Whole Air Sampling during the COVID-19 Pandemic," American Geophysical Union, Fall 2020

Oral Presentation, "Interactions of Urban Plumes with Biomass Burning Emissions During the 2018 WE-CAN Field Campaign," American Geophysical Union, Fall 2019

Field Campaigns

Fire Influence on Regional to Global Environments Experiment - Air Quality (FIREX-AQ)

- Sponsoring Organizations: NASA, NOAA
- Location: Boise, ID

Western Wildfire Experiment for Cloud chemistry, Aerosol absorption and Nitrogen (WE-CAN)

- Sponsoring Organizations: NSF, NCAR, CU Boulder
- Location: Boise, ID

Professional Training

Machine Shop Training
UCI Physical Sciences Machine Shop, Irvine, November 2018
Description: Learned shop safety. Learned how to properly design parts and read schematics. Learned basics of machining processes (e.g., single-point threading). Completed a build from raw materials to finished product utilizing the lathe, band saw, belt sander, and mill.

Professional Affiliations

American Geophysical Union, 2016 – Present

American Meteorological Society, 2020 – Present

Professional Service

Session Moderator
WE-CAN Science Team Meeting, 2018

Computer Skills

Languages: R, Python, Igor Pro

Skills: data analysis, chemical box modeling, machine learning, positive matrix factorization

ABSTRACT

Trace Gas Emissions from Biomass Burning: Impacts on Human Health, Local Air Quality, and Global Climate

By

Alexander William Jarnot

Doctor of Philosophy in Chemistry

University of California, Irvine, 2021

Professor Donald R. Blake, Chair

Wildfires have been increasing in frequency and severity over the past few decades. Wildfires, agricultural fires, land use burns, and other forms of biomass burning are sources of particulate matter and trace gases, including carbon monoxide, to the atmosphere. These gases are detrimental to air quality and the Earth's climate, and can react to form tropospheric ozone. Many of these trace gases, like benzene, are also hazardous to human health. Here the trace gases from biomass burning in the United States are examined, and the effects on human health, air quality, and climate are reported.

Several large-scale field campaigns have been mounted to study the emissions of fires. These campaigns are usually focused on collecting data from very fresh and aged fire smoke with little influence from background emissions. Therefore, the interactions between fire smoke and urban air have not been well studied. Positive matrix factorization is used here to analyze mixed smoke and urban air masses to tease out the relative emissions contributions from each source.

The emission ratios of trace gas compounds to carbon monoxide are also studied to see if the types of fuels, environment, or burn conditions affect the relative emissions of particular trace gases between different fires. While most trace gases are emitted at relatively consistent rates between different fires and fuels, ethyne, methyl chloride, and methyl bromide exhibited significantly different emission ratios between western wildfires and smaller southeastern agricultural fires.

Finally, chemical box modeling is used to examine the effects of biomass burning emissions on the chemistry of urban air quality. Using inputs for trace gas emissions based on observed data a box model was run for three conditions: urban emissions only, smoke mixed with urban emissions, and heavy smoke mixed with urban emissions. The results indicate that smoke emissions can augment ozone production in urban areas. These results are compared to observations from Pasadena, CA during the 2020 Bobcat Fire.

1. Introduction

On a list of the things taken for granted, “oceans & air” would be written at the top. Air isn’t something you think about. Yet it is all around us, and contains what is most necessary for life to exist. It is a deceptively simple soup made of just 78% nitrogen, 21% oxygen, a little less than 1% argon, and about 0.1% that is usually defined in textbooks as “other”. However, this seemingly insignificant “other”, a unique amalgamation of thousands of gases, has a bearing on everything from the smell of your favorite bakery to the Earth’s climate. Not only that, this amalgamation is deceptively alive, in a chemical sense. Each passing moment, molecules are being born, combining, and dying right under your nose. This chemical life is extremely complex, fraught with drama. The gases can undergo radical transfers, cyclizations, peroxide formations - reactions most organic chemists could only dream of performing. Yet, they’re common occurrences in the field of atmospheric chemistry. Moreover, gases can clump to form particles, opening up the possibilities for reactions within.

While air quality and pollution have been known since the Middle Ages, the first scientifically rigorous study of the atmosphere and the gases that make it up began with Joseph Luis Gay-Lussac, who took the first high-altitude whole air samples at six thousand meters above the ground in a hot air balloon in 1804 (Clark, 1952). While studying this sample he discovered that the proportions between the gases he could measure (e.g., oxygen, nitrogen) remained constant, while pressure and humidity decreased at higher altitudes. These discoveries, along with the record-setting balloon flight, were the events that led to the beginning of atmospheric research. The field has grown significantly since then, with over one hundred scientific journals and conferences dedicated to the field.

Within atmospheric research, there is a quickly growing sub-discipline focused on wildfires, their emissions, and the effects of those emissions on air quality and climate. Studies by Andreae, Crutzen, Delany, Greenberg and others in the mid-1980s found that biomass burning was a significant source of VOCs, carbon monoxide, ozone, and nitrogen oxides (e.g., Crutzen et al., 1979; Delany et al., 1984; Greenberg et al., 1985; Crutzen et al., 1985). However, this sub-discipline really took off following the NASA Atmospheric Boundary Layer Experiment - 2A (ABLE-2A) during July - August 1985, which took place in the Amazon rainforest during its dry season (Harriss et al., 1988). Instruments aboard the NASA aircraft and mounted on towers, balloons, and sondes sampled the boundary layer over the course of the month, which was impacted by smoke from over six thousand wildfires that burned at the peak of the dry season. While the focus of the mission was not on biomass burning emissions, the data contained interesting results that had profound implications for the global climate. Figure 1.1 shows carbon monoxide measurements observed during two flights – the first in late July and another in early August. The measurements show an enormous increase in CO concentrations over the Amazon between the two flights. This is because the Amazon wildfire season started around the beginning of August, and the CO enhancement observed was because of the recent fire activity in the region. Previously, the extent to which wildfires contributed VOCs, nitrogen oxides, ozone, and aerosols to the boundary layer was not well understood. ABLE-2A provided insight into constraining the quantity of these climate-forcing species being released into the atmosphere.

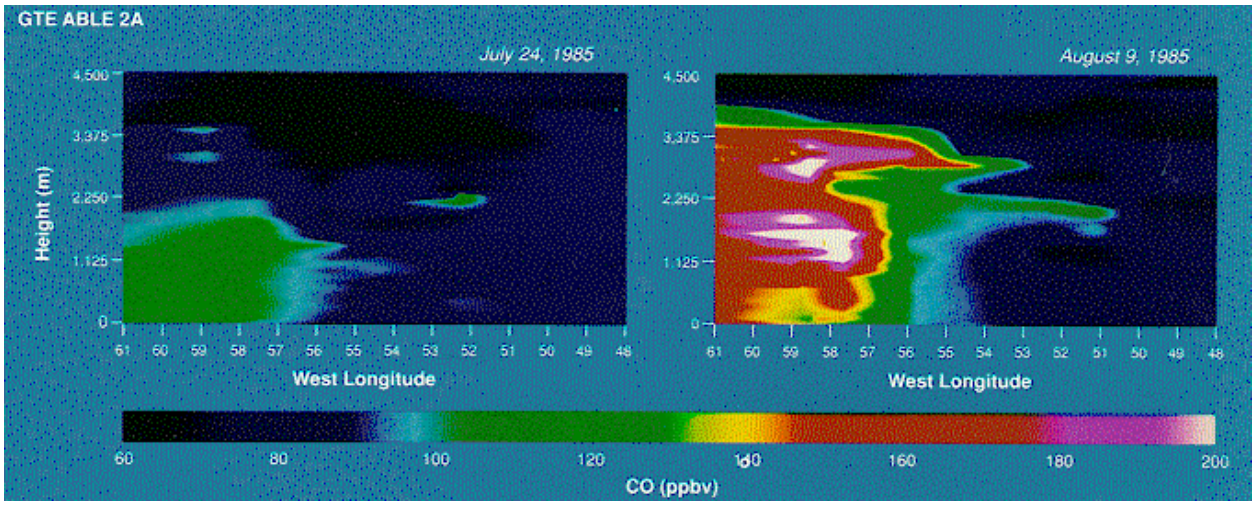

Figure 1.1 Plots of carbon monoxide concentrations versus altitude observed during the 1985 NASA ABLE-2A airborne campaign. Note the biomass burning plume observed in the righthand plot, which was collected at the peak of the Amazon wildfire season. (Figure 3 from NASA ABLE Summary, 1985)

While the field of biomass burning research has grown significantly since ABLE-2A, there are a few researchers who stand out in the amount of time and resources they have put into this discipline. Namely, Bob Yokelson (University of Montana), Peter Hobbs (University of Washington), and Jim Crawford (NASA Langley) have been leading the field with conducting experiments and leading field campaigns to study the effects of wildfires on air quality and climate. Yokelson especially has dedicated his career to studying biomass burning, most notably by leading the Missoula Fire Lab experiments. The fire lab hosts a large room that acts as the burn chamber. In the center of the room is a ventilation stack that serves as exhaust for the smoke. Controlled burns are conducted on a plinth in the center of the chamber underneath the exhaust vent. The room also has large doors which are opened between burns to clear out the smoke. The room and exhaust vent were outfitted with analytical instruments to measure different aspects of the smoke composition, from VOCs to aerosols to particulate matter such as ash. Yokelson and the fire lab team have conducted hundreds of burns with dozens of different

types of fuels (pine, leaf litter, duff, etc.) under different conditions (wet, dry, etc.) to determine how different fuels burn, and what kinds of emissions they release (Stockwell et al., 2014). The team has been able to calculate emission factors for dozens of trace gases across the fuels they have tested (Liu et al., 2017). These emission factors are important for modelers to be able to calculate global emissions inventories for biomass burning.

As stated earlier, the field of biomass burning research has been growing quickly. The number of publications written on biomass burning has skyrocketed in the last forty years. Since 2015, six large-scale airborne campaigns (WE-CAN, FIREX-AQ, BB-FLUX, BBOP, MOYA, WINTER) have been mounted to analyze biomass burning emissions. While *in situ* analysis is still on the rise and very necessary for understanding biomass burnings effect on climate, the future of the field lies in modeling and satellite validation. Field campaigns are time and resource-intensive, and are limited in their coverage. Ideally, one would be able to measure fire emissions globally, daily. This is where modeling and satellite observations enter. While they have long been tools in atmospheric science, the accuracy and reliability of biomass burning emissions inventories (thanks to experiments such as those performed at the fire lab and field campaigns) now means biomass burning emissions for some cases can be accurately estimated using satellite observations. These emissions estimates are now being used to improve projections for how fires will impact the Earth's climate now and going forward.

But how do biomass burning emissions affect our climate? Carbon monoxide, carbon dioxide, VOCs, and aerosols such as black and brown carbon, all emitted from fires, have been shown to have a climate warming effect in the atmosphere. Nitrogen oxides, also emitted from fires, will have an intrinsic net cooling effect, yet also have the ability to participate in ozone and secondary organic aerosol formation, which degrade air quality and pose health risks (IPCC,

2021). Figure 1.2 summarizes the effects that biomass burning emissions have on the overall radiative forcing for the planet compared to other radiative forcers. Note that the error associated with the effects of particulate matter from biomass burning, for instance, is relatively large (± ~70% for organic carbon-based particles). This denotes a large degree of uncertainty in the overall effects of biomass burning emissions on radiative forcing, and is why research in this area is necessary.

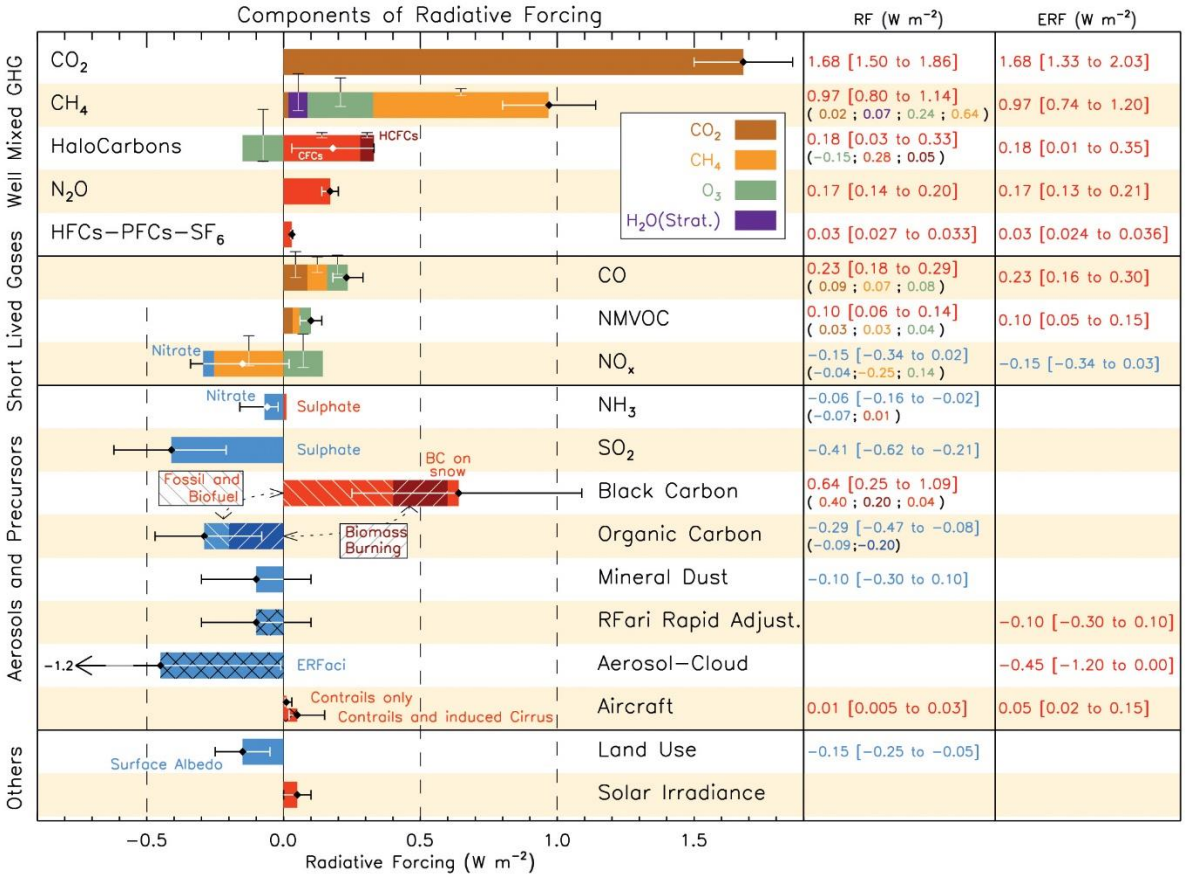

Figure 1.2 Climate forcing impacts of gases and their contributing emission sources. Note the large error bars associated with biomass burning emissions. (Figure TS.7 from IPCC AR6, 2021)

To make matters worse, wildfires are only going to become more frequent and more intense (Abatzaglou et al., 2016; Abatzaglou et al., 2019). We have already seen this in the western US

just in the past decade. For example, in 2017 California saw the largest and most destructive wildfire in the state's history - the Thomas fire (Nauslar et al., 2018). The fire burned over two hundred and eighty thousand acres including one thousand and sixty-three structures during the course of four months. Even after the fire was officially declared out, hotspots in the burn scar continued to be discovered for another three months. Again, this fire was the largest and most destructive fire in California's one hundred- and seventy-one-year statehood, and the 54th largest in North America to date. Less than five years later, the Thomas fire is now only the seventh-largest wildfire in California history. In North America, ten of the twenty largest wildfires in recorded history have occurred since 2000. But this is the new normal. As shocking as this may be, this will continue to happen. Climate change is causing places like the western United States to become hotter and drier. As areas like this get less rainfall and temperature increases, fuel such as forests and grasslands dry out. As the world's population increases, ignition sources increase (88% of wildfires are human-ignited; Hoover et al., 2021), and with an abundance of dry fuel, fires will only burn hotter and faster.

This is happening across the planet wherever the land is becoming hotter and dryer. Places like the boreal forests in Canada, the Australian bush, Greek islands, and Siberian permafrost are some notable examples of locations where wildfires have captured humanity's attention in recent years. Hotter fires mean more intense fires, and more intense fires means a greater chance of pyrocumulonimbus cloud formation. When a pyrocumulonimbus, or PyroCb, forms it means the fire that formed it has enough energy to create a strong vertical convection, and in turn its own weather system. PyroCbs are characterized by a classic thunderstorm anvil cloud, and with the amount of convection and energy in the cloud there is often lightning activity (Apel et al., 2015). More importantly this convection can reach the upper troposphere, bringing very dry air down to

the surface, which exacerbates the fuel dryness and aids in the fire spread (McRae et al., 2015). This poses a serious issue for firefighting efforts. Extreme fire events that generate their own weather are unpredictable and dangerous, and can easily spread quicker than anticipated. Research is being done to try to predict how fires spread under different conditions, and to plan the most efficient routes for firefighters to flee an encroaching fire (Sullivan et al., 2020). However, as fires grow larger and drier fuels allow the fire fronts to spread quicker, firefighters will have a much more difficult time containing them. This means fires will burn longer and emit more smoke. The problems don't stop there. Climate change effects mean the fire season - the times of the year where fires most commonly occur - will get longer and longer over time. As the planet warms spring and winter, that traditionally brought rain, are drier and fires start earlier and burn longer into the year.

Biomass burning emissions are also a threat to local air quality and health. Fires directly emit hazardous air pollutants including benzene, toluene, acetonitrile, hydrogen cyanide, and formaldehyde. These gases range from harmful to toxic to carcinogenic. These compounds also persist in the boundary layer for days to weeks, which allows them to travel hundreds of miles from the fire source while remaining at harmful concentrations. People living directly downwind of a fire, and firefighters or farm hands working in the path of a fire are exposed to greatly enhanced concentrations of these compounds. Additionally, there are gases released by fires that may not be dangerous on their own, but aid in the formation of ground-level ozone - a strong oxidant and the main component of smog. Ozone is harmful when inhaled, as it causes damage to the lungs. Ozone is also harmful to crops and other plants, as it damages their leaves. Fires also emit particulate matter which, if inhaled, can lead to breathing problems like emphysema. Particles smaller than ten microns in diameter can enter the bloodstream.

This research will focus on the gaseous emissions from wildfires and their effects on air quality and climate. Historically, fire research has focused on how emissions have contributed to the global VOC, NO_x, CO, and CO_2 budgets and how they affect climate forcing (Hobbs et al., 1997; Paris et al., 2009; Burling et al., 2010). Recently, with the uptick in major fires affecting residential areas, that focus has shifted to how these emissions affect air quality (Liu et al., 2017; Sekimoto et al., 2018; Lindaas et al., 2021). After it was discovered how much climate change is influencing fire frequency, a number of researchers have started to study wildfire emissions as they affect air quality and human health. Dan Jaffe (University of Washington) and his students especially have done a great deal of work studying how fire emissions affect air quality in urban areas. Emily Fischer (Colorado State University) and her student Kate O'Dell have also done a significant amount of work studying the effects of fire emissions on human health, and quantifying the number of hazardous air pollutants (defined by the US EPA as compounds that are known or suspected to cause serious health effects) released from fires (O'Dell et al., 2020). However, there is a dearth of information regarding biomass burning VOCs and their regional air quality effects, effects from agricultural fires, and large-scale climate forcing from fire emissions - especially from VOCs. This research analyzes VOC emissions from fires and how they interact with rural and urban air masses. Agricultural fire emissions and their effects on local air quality and underserved communities will also be assessed. Finally, fire emissions will be studied to determine their effects on continental air quality and climate forcing.

1.1 The Structure of Earth's Atmosphere

The atmosphere has five layers, each one distinct and important to the Earth's meteorology and climate. All known life, weather, and climate exists within these thin layers. Figure 1.3 summarizes the approximate locations of each layer and the boundaries between them. Also plotted is the general temperature profile throughout the atmosphere (Figure 1.3, solid line). Note that the temperature change undergoes a change in sign at each boundary. Because there is very little mixing above the stratosphere, the vast majority of all gases relevant to this research are contained below the stratopause. Therefore, the stratopause and layers residing above it will not be discussed here (Figure 1.3).

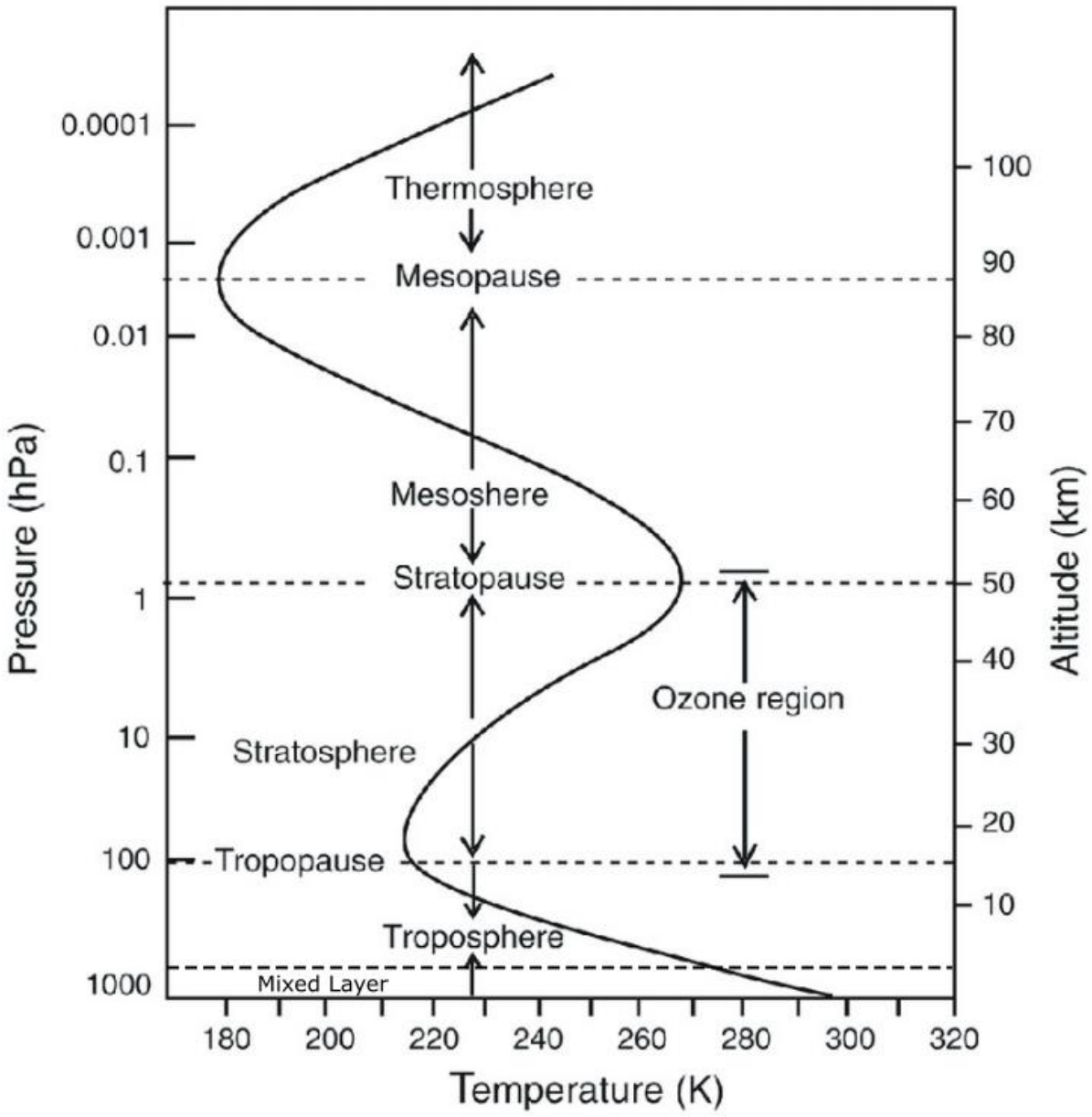

Figure 1.3 Vertical profile of ambient temperature in the atmosphere (Adapted from Mohanakumar, 2008).

Starting at the surface of the Earth and extending up to approximately 15 km is the troposphere. Contained within the troposphere are two general regions: the mixed layer (ML), and the free troposphere. The ML lies between the Earth's surface and the free troposphere.

Because the ML is in direct contact with the Earth's surface, it is greatly affected by surface heating. This heating causes turbulent mixing within the ML.

Consider an air parcel, or small "balloon" of air. If the air parcel were to move adiabatically through the atmosphere, it's internal temperature would change according to the adiabatic expansion equation based on the Ideal Gas Law (Equation 1.2).

$$T = T_0 \left(\frac{V_0}{V}\right)^{nR/C_v} \qquad \text{Eq. 1.2}$$

If the temperature of the air parcel (T) is greater than that of the surrounding air (T_0), then the air parcel will be positively buoyant and will rise through the atmosphere. If $T < T_0$, then the air parcel will be negatively buoyant; if $T = T_0$, then the parcel will be neutrally buoyant. Under stable conditions, the parcel's internal temperature will be equal to that of its surroundings, so it will always stay neutrally buoyant. It isn't until there is some outside disturbance that displaces this hypothetical parcel that it will change its buoyancy (Stull, 2017). In Earth's atmosphere this is caused by the heating of the Earth's surface, as stated previously. As the surface heats, it warms the air in contact with it creating surface winds. These winds are the disturbances that can create instability within the ML. Conversely, during the night the surface cools off, causing the surface to be cooler than the surrounding air. This tends to lend more stability to the ML, which is why the ML generally becomes less turbulent overnight (Stull, 2017).

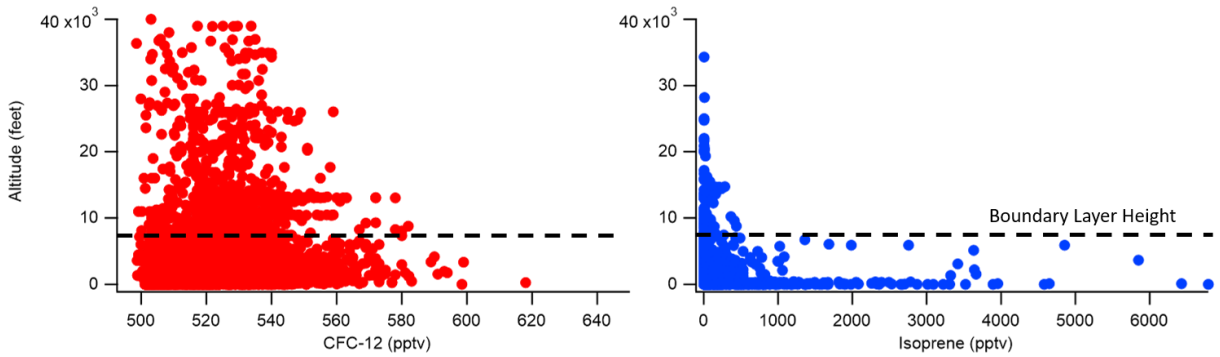

Figure 1.4 Vertical profiles for two trace gases, measured by the UCI Rowland-Blake group during SARP 2009-2019. Samples were collected aboard research aircraft and on the ground throughout southern CA. The average boundary layer height is marked with a dashed line.

Therefore, the ML is typically well-mixed and can generally be considered homogeneous, especially in warmer climates where there is more vertical turbulence. Under fair weather circumstances, pollutants emitted at the surface are typically dispersed vertically throughout the ML within a few hours. Figure 1.4 shows data collected during NASA Student Airborne Research Program (SARP) flights around the LA Basin and Central Valley from 2009-2019. Isoprene, being a very short-lived gas, does not live long enough to enter the free troposphere in any significant quantities under normal circumstances, and therefore a steep gradient in concentration forms between the mixed layer and free troposphere (Figure 1.4, right panel). CFC-12, however, is very long lived, and therefore a uniform vertical concentration profile forms throughout the mixed layer and free troposphere (Figure 1.4, left panel).

Between the ML and free troposphere sits a capping inversion layer. In a purely "normal" atmosphere, the ambient temperature decreases with altitude. Over time the cooler air above, being denser than the warmer air below, will sink to replace the warmer surface air, causing turbulence within the troposphere. However, because of the radiation from the Sun, Earth's atmosphere experiences a temperature inversion within the troposphere. As air masses within the

troposphere carried by prevailing winds sink (known as subsidence) they compress and therefore heat (by the ideal gas law) the air below them. This forms an area of temperature inversion from the typical temperature profile of the troposphere.

This inversion lends an immense amount of stability to the layer separating the boundary layer from the free troposphere. It acts as a "lid" on the boundary layer, preventing mixing between it and the free troposphere. Because of this, subsidence inversion layers are also known as capping inversions (Gossard & Moninger 1975). Capping inversions prevent mixing between the boundary layer and free troposphere, because an air parcel would have difficulty traveling through the inversion. As it rises into the much cooler air of the free troposphere resting above the inversion, it would become denser and sink back down, and any air sinking would warm up and rise again. This is what gives the capping inversion it's stability. All of the emissions from the Earth's surface are trapped within the boundary layer below; therefore, extremely short-lived gases rarely make it into the free troposphere before they are removed chemically from the atmosphere via oxidation.

Resting above the inversion layer and extending up to the tropopause is the free troposphere (FT). This layer is cooler, dryer, and much less turbulent than the ML. Because of the stability of the capping inversion layer trace gases emitted in the ML remain in the ML, except for longer-lived compounds such as chlorofluorocarbons (CFCs) which eventually mix into the FT. However, extreme events such as volcanic eruptions and large fires can generate enough vertical lift to break through the inversion layer, injecting trace gases directly into the FT (Liang et al., 2013).

Sitting atop the FT is the tropopause, another type of inversion layer - where the vertical temperature profile changes sharply. However, the tropopause is extremely stable, preventing

nearly all mixing between the FT and stratosphere above. On rare occasions mixing does occur between the upper FT and lower stratosphere. Extremely long-lived compounds such as CFCs will eventually mix upwards into the stratosphere because of the slow convective forces within the atmosphere.

The stratosphere is an especially important layer within the atmosphere. It is very dry, and contains very few trace gases. The primary trace constituents are carbon dioxide and ozone, both at part-per-million concentrations (Liang et al., 2013). The mixing ratio of ozone in the stratosphere is significantly greater than in the troposphere as ozone is formed readily from available oxygen being photolyzed by ultraviolet sunlight.

On the macro scale, air travels around the planet within global air masses called cells. These are formed by (1) the movement of air as it warms at the equator and cools at the poles, and (2) friction between the Earth's surface and the atmosphere as the planet rotates. First, air is heated more in the tropics as this region receives more sunlight than the extreme latitudes. Warm surface air will then rise over time high into the atmosphere. Without any planetary rotation, this air would then be transported to the poles, where it would cool and sink back to the surface (Brewer 1949). Then, the air mass would eventually be transported back towards the equator to start the cycle anew. However, the Earth rotates, which complicates the situation. There is friction between the land masses on Earth's surface and the boundary layer. This friction tends to cause flow along the direction of rotation. This flow coupled with the circulation caused by the air's normal heating and cooling. The results of these air mass movements are the Hadley, Ferrel, and polar cells (Brewer 1949; NOAA 2021), which carry air across the globe within bands, or cells. In the northern hemisphere at mid-latitudes, the prevailing winds travel from west to east carrying trace gases and particulate matter across the Pacific and eastward across the United

States (the area of focus of this research). In the southern latitudes of the northern hemisphere (< 30° N) winds generally travel from east to west, and is how smoke and Saharan dust travel from the African continent across the Atlantic and into the Gulf of Mexico and southern United States. Note in Figure 1.5 that the prevailing wind trends travel the same direction across the equator in the southern hemisphere.

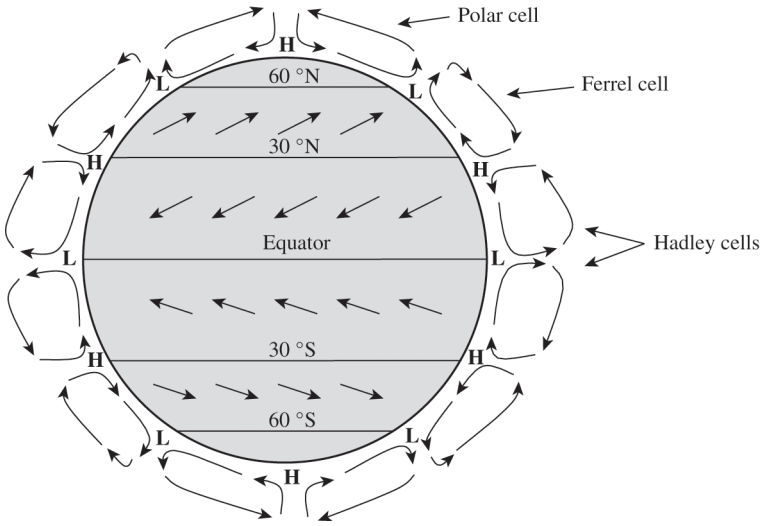

Figure 1.5 Diagram showing the prevailing winds and circulation cells around the planet. Note that the prevailing winds above 30 N are westerly (Figure 3.4 from Seigneur, 2019).

1.2 Effects of Trace Gases on Climate

The modern atmosphere is composed chiefly of diatomic nitrogen. As a molecule held together by a triple bond, it is for all intents and purposes an inert gas. It is exactly because it is so inert that it became the primary constituent of today's atmosphere.

The second most common gas in the Earth's atmosphere is diatomic oxygen. Comprising approximately 21% of the atmosphere at sea level, it is the major oxidative source for the atmosphere.

Argon makes up about just under 1% of the atmosphere. A remnant of millennia of radioactive decay, argon is a noble gas, and therefore inert.

The next major component of the atmosphere is carbon dioxide. It has a variety of sources, including combustion and aerobic decomposition. As far as reaction chemistry goes, carbon dioxide is relatively inert. However, it's critical characteristic is that unlike nitrogen, oxygen, and argon, carbon dioxide has infrared-active bending modes. This means that it absorbs infrared (IR) radiation, and stores the energy as vibrations within the molecule. These vibrations dissipate the energy over time to their surroundings as heat. The energy can also be re-emitted as infrared radiation. This action is important for the energy balance of the Earth's atmosphere. Because of this property, and its abundance in the atmosphere, carbon dioxide is the molecule by which the warming properties of all other atmospheric gases are measured.

Methane is another gas commonly found in the atmosphere. It has a variety of sources, including anaerobic decomposition, thermogenic processes, and natural gas. Like carbon dioxide and water vapor, it is IR-active. Yet, methane is approximately eighty times more efficient at warming than carbon dioxide over a twenty-year period (IPCC, 2021). Coupled with the fact that methane has an atmospheric lifetime of about a decade, understanding the sources and sinks of methane is critical to predicting its effect on climate.

Methane's importance and lifetime in the atmosphere gives it a special place among the trace gases. Therefore, volatile organic compounds that aren't methane are commonly referred to as non-methane hydrocarbons (NMHCs). These NMHCs are all inherently IR-active. Because of

the large variations in the structures and abundances of the many, many known NMHCs, each will have their own warming potential. Collectively they have an impact on the climate, like methane and carbon dioxide. However, they are short-lived and thus have a trivial impact on the climate forcing.

There are also many other trace gases present in the atmosphere besides the ones mentioned previously. These each have their own physical properties that give them the ability to absorb and re-emit radiation, react with other molecules, and clump together to form particles. Many NMHCs and trace gases can also be inherently toxic or otherwise harmful to humans and animals that may breathe them. For this reason, it is important to understand how these molecules are formed, how they may react, how abundant they are in the atmosphere, and how they ultimately affect the climate and those who live in it.

1.3 Climate Change

The entire energy budget of the Earth has a single source - the Sun. The Sun radiates energy in the form of photons, which impart their energy onto the surface of the Earth. The Earth, being a blackbody, also radiates energy back into space. If Earth did not have an atmosphere, this would be the normal case. In fact, if the Earth's atmosphere only consisted of nitrogen and oxygen, then the average temperature of the surface of the Earth would be about 255 K.

However, this is clearly not the case. Because the atmosphere acts as an insulator, the routes of energy transfer between the Earth and space change slightly. First, as IR photons are emitted from the Earth's surface, instead of escaping into space, many are intercepted by IR-active gases

(e.g., CO_2, H_2O, CH_4). The energy is then dissipated to the surroundings or re-emitted in all directions. This way, some of the energy is kept on Earth, while the rest escapes as losses to space. The process of IR-active gases in the atmosphere trapping energy is known as the *greenhouse effect*. The consequence of the greenhouse effect is a net warming of the Earth's surface.

There is another consequence of the Earth's atmosphere that affects the energy balance known as the *whitehouse effect*. The whitehouse effect is caused by aerosols which can scatter incoming radiation off into space. The scattering is because of the high reflectivity, or *albedo*, of certain types of aerosols. The whitehouse effect ultimately causes a net cooling of the Earth's surface. An important note is that aerosol formation can be traced back to trace gases. As trace gases react and become oxidized, they can ultimately condense together to form particles. These particles can also act as seeds around which clouds can form. Therefore, trace gases have a large effect on the Earth's overall energy balance. This effect is known as *climate forcing,* and is defined simply as the difference in radiative flux for a given change in the concentration of a given species (IPCC, 1990).

Carbon dioxide is a greenhouse gas and therefore a molecule of CO_2 will have an impact on climate as long as it is in the atmosphere. The exact effect it will have is defined by its global warming potential or GWP. The exact GWP is defined in equation 1.3.

$$GWP = \int_0^T a(x) * [x(t)]dt \qquad \text{Eq. 1.3}$$

Where a is the forcing because of an instantaneous release of the given species (defined as 1 kg), and x(t) is the concentration of the species remaining after a given time T (IPCC, 1990). However, it is often simpler and just as efficient to report the relative GWP for a given gas, which is the ratio of the GWP of the given gas to that of CO_2. Therefore, CO_2 has a relative GWP of one, and all other gases will have a relative GWP of greater or less than one. Any reference to GWP here will refer to relative GWP.

1.4 Air Pollution

Ozone is an important gas that will feature heavily in this research. Ozone is an essential component of the stratosphere as it absorbs UV-A and UV-B radiation emitted from the Sun before it reaches the Earth's surface. This radiation will kill cells it interacts with and therefore is extremely harmful to life on Earth. While ozone is necessary in the stratosphere, it is hazardous and poses a health hazard when it is present in the lower troposphere where it is exposed to the surface. A strong oxidant, ozone will damage animal and plant cells, and other materials. In large enough concentrations, ozone will damage lung tissue when inhaled, causing asthma and other respiratory conditions. It also causes damage to plants, limiting their photosynthetic capacities and opening them up to infections. It will also damage rubber, for example, causing cracking in car tires. Because of the hazard to health, it is imperative to understand and predict the formation of tropospheric ozone.

Ozone is formed via a complex series of reactions, but are bottlenecked by the concentrations of nitrogen oxides and VOCs. Therefore, the limiting reagents for ozone formation are VOCs

and NO_x, and the ambient concentrations of each these species will determine the amount of ozone that is able to be formed. That is why it is important to understand sources of both VOCs and NO_x, and why wildfires have captured the attention of the atmospheric science community as they emit both gases in significant quantities.

NO_x and VOCs abundances are the limiting factor in ozone formation, therefore plotting each gas against each other yields a surface that describes the ozone formation potential at every possible combination of NO_x and VOC concentrations (Dodge, 1984). The result is plotted in Figure 1.6, where the maximum ozone formation potential lies along the 8:1 VOC to NO_x ratio, and increases with increasing concentrations of each species along that ratio. Also shown are lines of constant ozone formation potential - isopleths - that are like topographic lines indicating height on a terrain map. Along each side of the maximum ozone formation "hill" are the VOC- and NO_x-limited regimes, respectively (Dodge, 1984).

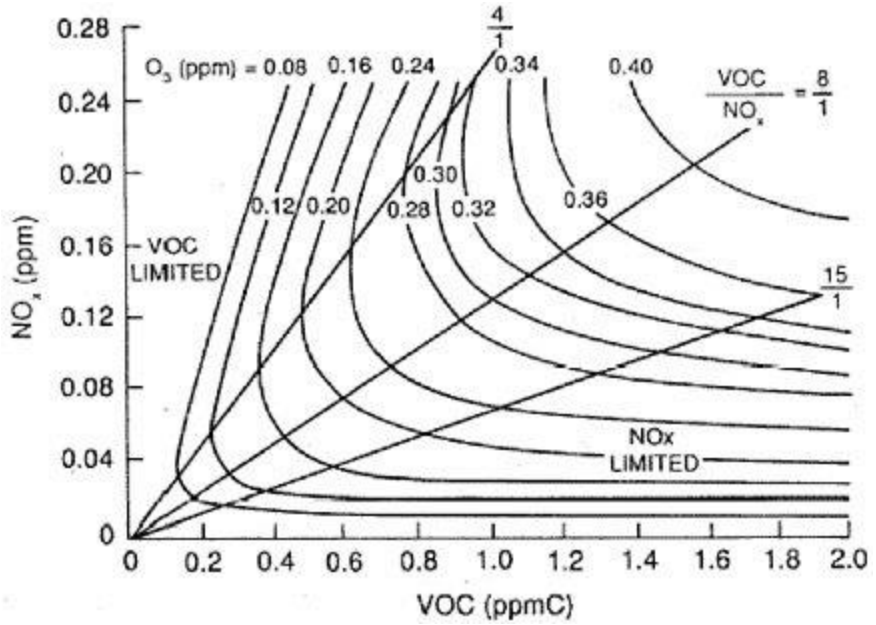

Figure 1.6 Ozone isopleth plot showing the ozone formation potential given NOx and VOC concentrations. Note the greatest ozone formation potential lies along the 8:1 VOC:NO_x line. Also note the VOC- and NO_x-limited regimes in the left-hand and lower portions of the plot, respectively (Dodge, 1984; Figure adapted from Sillman, 2002).

In these regions there is so little of one species that no matter how much of the other is present, there will be no increase in ozone formation. Understanding which regime an air basin lies in is important to understanding how ozone will be formed in that region, as the formation potential will be extremely sensitive to any input from the limited species.

The dominant oxidant in the troposphere is the hydroxyl radical (OH). Hydroxyl radicals in the remote atmosphere are formed via photochemical reactions with ozone (Eq. 1.1) and then atmospheric water (Eq. 1.2) (Levy 1971).

$$O_3 + h\nu \rightarrow O(^1D) + O_2 \qquad \text{Eq. 1.1}$$

$$O(^1D) + H_2O \rightarrow 2OH \qquad \text{Eq. 1.2}$$

Other sources include the photolysis of hydrogen peroxide (a trace gas commonly found in fire plumes), and the photolysis of HONO (also found in fire plumes). Hydroxyl radicals can also form in the presence of enhanced NO concentrations from the reaction of NO with HO_2, both of which are emitted from fires. Hydroxyl radical reactions are the primary oxidation (i.e., removal) pathway for the majority of VOCs. This chemistry is important in fire plumes as reaction with OH is the fate of most species of VOCs released from fires. Also, an important note is that OH is almost exclusively formed via photolysis, and with the lifetime of OH being on the order of about half a second (and therefore will not be transported) it can be assumed that without sunlight OH chemistry will not occur. So, in thick wildfire plumes where sunlight is blocked in the center of the plume and in the cases of huge plumes, the underside, there are distinct regions that follow daytime chemistry, and also regions that will not experience OH chemistry until they dilute enough to let in sunlight.

Ozone is the second major oxidant in the atmosphere. The key difference between OH and ozone is that ozone has a much longer lifetime than OH and therefore can be transported across long distances under the right conditions. Also, ozone is not exclusively formed via photolysis like OH. This means that in dense smoke plumes ozone can form in and be transported to the center and underside where OH cannot reach.

The lifetime of a gas molecule in the troposphere is dependent on the most likely fate of the compound. For the vast majority of compounds this will be oxidation via reaction with OH or ozone. The rate at which a given compound reacts with an oxidant is key to determining the lifetime of the compound. Knowing the reaction rate for the oxidation of the compound (for the proper oxidant), the only other information needed to calculate the lifetime is the mechanism of the reaction (rate-limited, bimolecular, termolecular, etc.), and the concentrations of the

appropriate species (depending on the type of reaction, usually that of the compound of interest and the oxidant). An important distinction between the lifetime of atmospheric compounds and lifetimes of other chemical mechanisms is that the atmospheric lifetime is traditionally denoted as the e-folding time, not the half-life or other definition. That is, the lifetime is defined as the time it takes to reduce the concentration of the compound by a factor of 1/e.

The lifetime of a compound lends information to the compound's reactivity in the troposphere, and based on the meteorology of the atmosphere can also give information on its structure. For example, isoprene has an extremely short lifetime of up to a few hours. This is not enough time for the compound to escape the mixed layer and breach into the free troposphere unless under extreme circumstances (such as a wildfire). Therefore, by plotting the concentration of isoprene versus altitude, one can determine the height of the boundary layer.

1.5 Biomass Combustion

Fire is an intrinsic part of nature. It has burned long before the birth of humanity. Neanderthals (in their time) and humans have used fire as a source of light and heat, for cooking, and for making tools for at least a million years (Wertime 1973). Fire is so intrinsic in nature that many organisms actually depend on it to procreate. For example, Ponderosa pine trees cannot disperse their seeds without the aid of a fire. The heat of the fire is what allows the seed pods to open, releasing the seeds and allowing the next generation of pines to grow. Fires also clear the forest understory and canopy, returning nutrients to the soil and allowing sunlight to reach the forest floor. This creates the conditions for new saplings and plants to grow and thrive.

Fire is comprised of three things: an ignition source, oxygen, and fuel. In the case of wildfires, the ignition source is typically either a lightning strike or human ignition. In addition, there are also smaller, controlled burns or prescribed fires that occur year-round across the globe. These are typically performed in an agricultural setting, but can also be done to clear brush or timber for land use. Early civilizations learned to control fire and realized it's potential for more than just cooking, light, and warmth (Wertime 1973). As fire consumes its fuel, and spreads easily, farmers have long used it to clear leftover crop residue from their fields, especially in areas where solid waste disposal is difficult. This practice also has the added benefit of killing pests living in the fields, and was long believed to be beneficial in returning nutrients back to the soil.

Prescribed burns are also utilized in forestry as a means of removing understory and slash from a forest. As trees are felled for logging or timber clearing, the branches are trimmed and left on the forest floor. These branches, along with leaves and other detritus is slash. If left in place the slash would dry out and decay, which poses a fire hazard. Too much dry material can easily lead to an uncontrolled wildfire, which would cause massive damage to the forest and, in many cases, local human populations. Additionally, too much low-lying brush and scrub can stunt the growth of trees like long-leaf pines and hinders forest health (Peterson et al., 2005).

Therefore, to control the amount of available fuel a fire would need in order to spread and promote growth, the slash must be removed. Because forestry often takes place in remote locations and/or deep wilderness, it is extremely difficult to remove large amounts of solid waste such as slash. Therefore, it is common practice to burn the slash and other brush in a controlled fire, being careful not to start a large, uncontrolled wildfire in the process. This removes the slash, brush, and undergrowth down to the duff, promoting growth. These practices are also used

less frequently to clear ranch lands of hazards (such as fallen trees) that could harm cattle and inhibit their feeding.

There are three main sources of gases from a fire. The first is because of the direct pyrolysis of fuel during combustion. In complete combustion, hydrocarbons react with ambient oxygen to form carbon dioxide and water vapor.

$$C_xH_y + O_2 \rightarrow CO_2 + H_2O \qquad \text{Rxn. 1.3}$$

However, complete combustion rarely occurs, especially in nature. Most fires burn inefficiently because of trapped water within the fuel and the difference in densities of the fuels. Incomplete combustion produces carbon dioxide and water, but also produces carbon monoxide and pyrolyzed hydrocarbons.

$$C_xH_y + O_2 \rightarrow CO + CO_2 + H_2O + C_xH_y + C_xH_yO_z \qquad \text{Rxn. 1.4}$$

Biomass — the total mass of organisms in a given area — is almost exclusively plant matter with respect to crops and forested areas (Jorgensen & Fath 2008). Therefore, biomass in these areas is comprised of mainly cellulose (a polysaccharide that gives the plant cell wall it's structure), lignin (a polymer sheath around the cellulose wall that lends rigidity to the plant), and hemicellulose (a simple polysaccharide that binds the lignin strands together). Figure 1.7 shows the general structure for each component. Note that the base units for cellulose and hemicellulose are the same, but cellulose forms long, polysaccharide strands while hemicellulose strands contain a large amount of branching and side chains. Another important aspect to note is that

lignin's base units contain aromatic rings, which is the source of aromatic compounds during combustion.

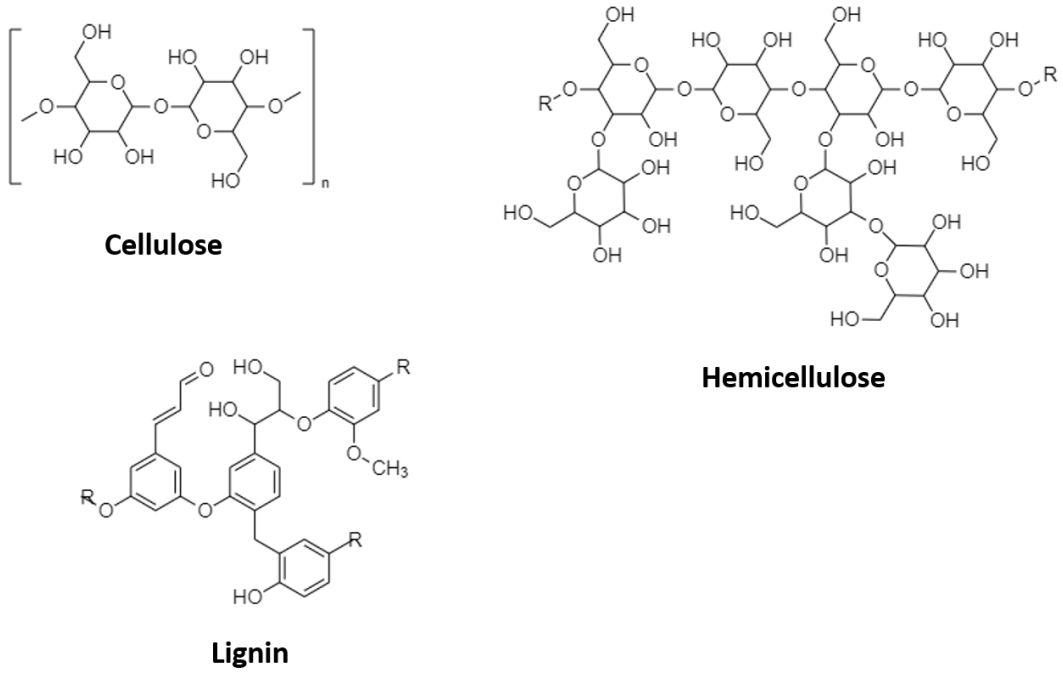

Figure 1.7 Generalized structures of cellulose, hemicellulose, and lignin. The base unit of hemicellulose is identical to cellulose; however, cellulose forms long, uniform polymer chains while hemicellulose forms irregular, branched structures. The structure of lignin varies significantly, shown is just one of the major structures observed.

There are additional components such as sap, water, and nutrients such as fixed nitrogen that exist within plant biomass. Agricultural biomass often contains fertilizers, pesticides, and minerals that vary greatly depending on the crop type and location in which it is grown.

The second source of gases is a consequence of the heat of the burning. There is a difference of a few hundred degrees Celsius (~100 C when water boils to ~200 °C when the wood starts to catch fire to ~500 °C when wood pyrolyzes) where trapped volatiles will start to boil and vaporize prior to the wood itself starts to burn. Above ~35 °C, very low molecular weight

terpenes such as isoprene start to boil out of the plant. At 100 °C, water held within the plant matter starts to boil and evaporate through transpiration out of the leaves. Between 100 °C and ~200 °C, myriad terpenes and other volatile compounds boil out of the plant structures. At approximately 200 °C, the cellulose, hemicellulose, and lignin will begin to undergo flaming combustion, or burning (Wadhwani et al., 2017). During this phase the organic polymers that make up the cellulose, hemicellulose, and lignin begin to decompose. Depending on how the polymers fragment, some compounds will volatilize as is, while other fragments will react accordingly with ambient oxygen to form oxygenated organic compounds (Lin et al., 2009; Santoso et al., 2019). Therefore, the unit structure of the polymer directly influences the structures of the emitted VOCs. Carbon atoms will also react to form carbon monoxide and carbon dioxide, with a branching ratio dependent on the ambient temperature. Low-temperature, smoldering combustion occurs after flaming combustion and pyrolysis is no longer sustainable, generally because of a lack of heat necessary to sustain the combustion reaction and ignite the venting gases. At this stage, the fuel is in the form of biochar and charcoal - biochar being plant biomass burned in a low-oxygen environment with a high hydrogen content and charcoal being the same but with a low hydrogen content and is usually from larger timber logs (Santoso et al., 2019). These structures are mainly carbon structures with their respective inclusions, and contain very little additional material as that has been combusted or volatilized. At this stage, the biochar and charcoal are still hot (>200 °C), yet the gases being released from the combustion are not hot enough to ignite (Santoso et al., 2019). The hot portions of the fuel will glow a dull red at low temperatures up to a bright orange at high temperatures following a blackbody emission curve. The compounds emitted at this stage are generally larger and more complex, as there isn't

enough heat to fragment them into very small molecules. Additionally, more carbon monoxide is emitted than carbon dioxide.

At above approximately 500 °C nearly all of the ambient oxygen has been combusted away. At this point the cellulose, hemicellulose, lignin and other organic material in the plant biomass will begin to pyrolyze, that is, burn in the absence of atmospheric oxygen (Santoso et al., 2019). The pyrolysis process involves the fragmentation of the fuel source (Lin et al., 2009). Therefore, the major products of biomass combustion are the base polymer units of cellulose, hemicellulose, and lignin (Wadhwani et al., 2017; Kawamoto 2017). There are also smaller products that form as the fuel breaks down further. These pyrolysis products are volatilized in the heat and released into the smoke plume. Pyrolysis is one of the combustion methods that forms new compounds that weren't already present in the fuel to begin with. This is how compounds such as benzene and toluene, that are normally considered anthropogenic, can be emitted in a natural phenomenon. Figure 1.8 shows the pathways that form some of the organic biomass burning tracer gases starting from the cellulosic and lignin base units. Note again that lignin is the primary source of aromatic compounds from biomass burning.

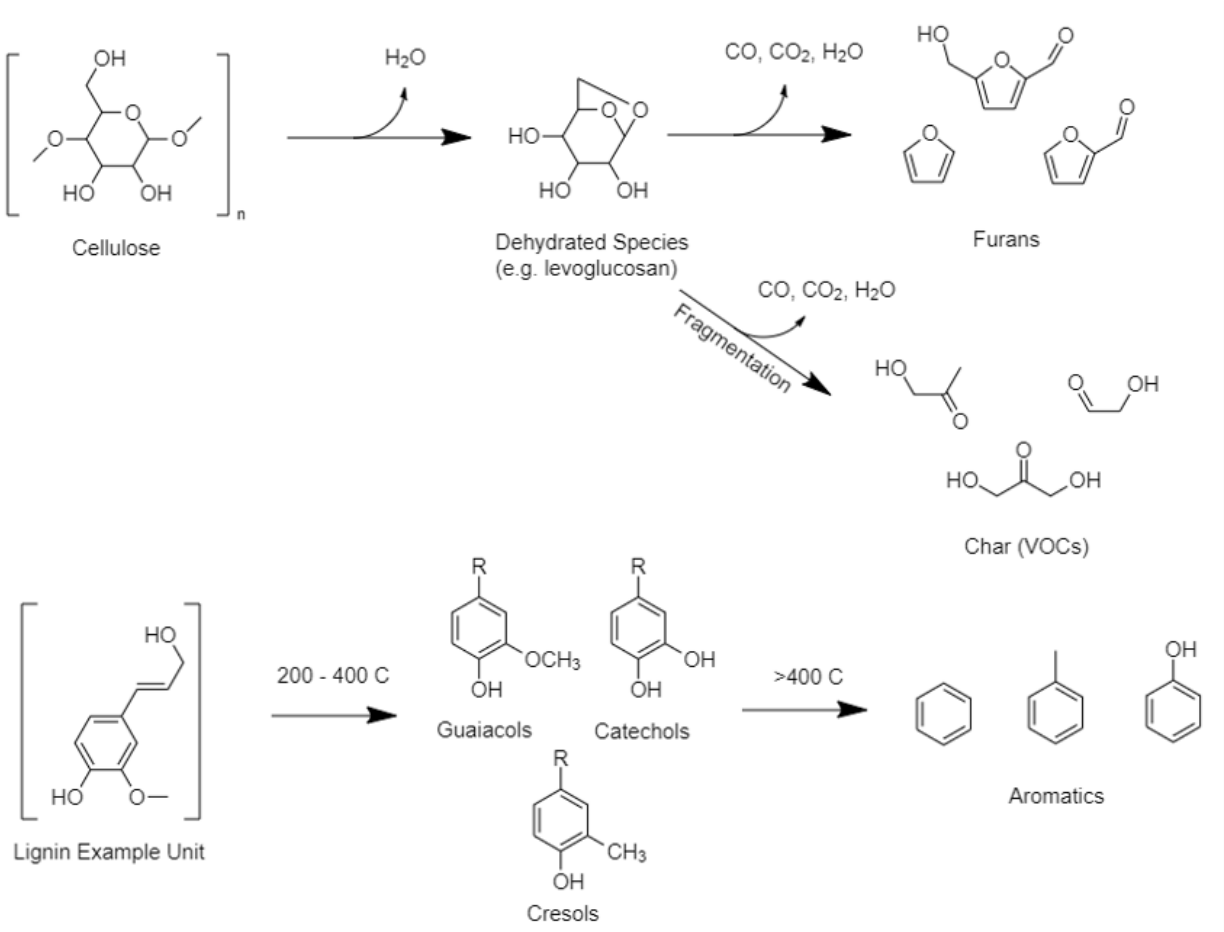

Figure 1.8 Pyrolysis of cellulose and lignin reactions. Hemicellulose follows a similar reaction mechanism to cellulose because of its similar structure. Note that lignin is the source of the aromatic gases released from fires (Based on information provided in Gunwardena et al., 2013; Huber et al., 2007; Lin et al., 2009).

The reality of biomass burning is that all of the aforementioned processes often occur simultaneously (Sekimoto et al., 2018). Some processes will dominate at certain stages in the burning process. For example, smoldering combustion will be the dominant process behind the fire front and long after the flames die out.

The third source is radical recombination. As the fuel combusts and pyrolyzes, the polysaccharides and other compounds that make up the fuel begin to break down. At high temperatures the molecules forming the fuel do not fragment cleanly, and often break down into

radical species. These species are unstable in the air, and it is more stable for them to form closed-shell complexes. Therefore, immediately after combustion and volatilization these radical compounds will react with themselves and each other, thereby forming new compounds. For example, fragments longer than six carbons can cyclize to form aromatic rings and cyclo-compounds.

The stage of the burning process in which the fire is in is often designated according to the modified combustion efficiency, or MCE. The MCE is calculated based on the branching ratio of carbon dioxide to carbon monoxide enhancements from the fire, as denoted in equation 1.4 (Yokelson et al., 1996).

$$MCE = \frac{[\Delta CO_2]}{[\Delta CO_2] + [\Delta CO]} \qquad \text{Eq. 1.4}$$

The MCE is a useful calculation to determine how efficiently a fire is burning. A fire will emit different ratios of CO to CO_2, and a different composition of VOCs depending on the efficiency at which it burns. This is because a more efficiently burning fire means a hotter fire, which means more fragmentation of the fuel. The MCE is calculated by taking the enhancement in CO and CO_2 compared to the background (the delta in Eq. 1.4 represents $[Compound_{Plume}] - [Compound_{Background}]$) to prevent contamination from outside sources such as traffic or urban areas. Because fire produces a significant amount of CO through inefficient burning, the more CO compared to CO_2 then the more inefficient the burn. Only CO_2 will be released in complete combustion. Therefore, the MCE of complete combustion would be 1 (Equation 1.4). Anything less efficient than complete combustion will yield a value less than unity. Typical values for the MCE of wildfires are ~0.8 – 0.9 for very dry, hot fires in the

western US, and ~0.6 – 0.8 for wetter, smoldering fires such as fires near the end of their burning, or in the Pacific Northwest. The MCE is calculated continuously as the fire burns, especially during field campaigns as the fire can change quickly. The ratio of emitted CO to CO_2 will remain constant in the boundary layer because of the lifetimes of the gases. That is why the MCE can be back-calculated from samples taken in the plume downwind of the fire. This provides information on the conditions in which the fire was burning when the smoke being sampled was emitted.

1.6 Trace Gas Formation During Biomass Burning

Biomass burning is a significant source of VOCs. The suite of VOCs emitted from burning includes many short- and long-lived compounds. Normally, VOCs with a lifetime shorter than about a day would not survive long enough to reach the free troposphere. However, during large enough burning events the vertical convection can be strong enough to breach through the inversion layer and inject VOCs directly into the free troposphere.

There are two main sources of VOCs during biomass burning. The first, distillation from vegetation, is a direct emission of unaltered compounds. As the fire progresses, it heats up nearby vegetation. This distills off volatile biogenic species such as alpha-pinene and isoprene, as well as trapped water. As the volatile species distill out and the vegetation dries, the leftover fuel will eventually start to combust. This transitions to the second source of VOCs: radical recombination. As the cellulose and lignin, the primary components of wood, combust the long-chain hydrocarbons will decompose into shorter radical organic species (Kawamoto et al., 2017).

These radicals then rapidly recombine to quench the radical and form completely new compounds that were not present in the fuel in the first place. Some examples of these VOCs include benzene and toluene, which are primarily considered anthropogenic compounds. Therefore, fires can be a source of typically anthropogenic compounds in remote areas. That is, remote areas that normally would not be affected by more "urban" compounds can see an influx of these during high fire periods. In addition, persistent enhancements in hazardous air pollutants (HAPs, as defined by the US EPA) such as benzene and toluene pose a significant health risk to those who live and work close to fires, like firefighters, locals, and farm workers.

1.7 Types of Biomass Burning

As the majority of the VOCs emitted from biomass burning are formed from the decomposition of the biomass itself, it makes sense that the composition of the fuel has a direct impact on the composition of the emissions. The two most important components of the biomass fuel that directly influence the emissions from the biomass burning are the carbon and nitrogen content, as these elements are the basis for the trace gases emitted from fires.

The parts of the biomass that form the fuel analyzed here are the leaves, sapwood, and heartwood. Leaves make up only about 5% of the overall mass of the tree, but because of their high surface area are one of the first parts of the tree or plant to burn and burn easily (Coggon et al., 2016). Also, they are the primary component of the forest floor litter and duff, as trees are always dropping leaves and needles which then rest on the forest floor and decompose into duff. Sapwood is the outermost layer of the tree trunk, and contains the xylem cells that transport

nutrients and water throughout the tree, and therefore has a significant water content. The sapwood is mostly composed of dead cells, like fingernails or hair on a human, and forms a protective layer between the bark and the heartwood (Krokene 2015). Sapwood is porous in structure form the xylem channels, and as its name suggests contains the resin sap that flows throughout the tree. The heartwood is the center most layer of the trunk and contains the living cells that cause tree growth (Bajpai 2018). It is much denser than the sapwood, and typically darker in color as it contains tannins and other chemicals that stain it darker.

The carbon content of different plant species has been a topic of study for years. As such, researchers from around the world have reported values of the carbon content of plants and trees in the literature. Analysis of literature reviews and publications shows that carbon content remains relatively consistent among each species and their parts. Researchers have long used the value of 45.45% carbon by weight proposed by Whittaker in 1975 as a universal value for carbon content (Whittaker 1975). While recent studies show that there is variation in carbon content among species and parts of the plant, this figure still holds true for several species (Burling et al., 2010; Ma et al., 2018). An important note is that crop species are significantly different from the woodier hardwoods like pines and oaks. This means that crops will have a different emissions profile than that of hardwood species.

As nitrogen is a critical element to plant growth and development, its content in plants is important to understand. Because of this, thousands of papers have been written reporting values of nitrogen content in hundreds of species of plants, and in all of the different parts of a plant. These values have been collected and reported by Falster et al. in the Biomass And Allometry Database (BAAD). Values for nitrogen content by percent weight are shown in Figure 1.9.

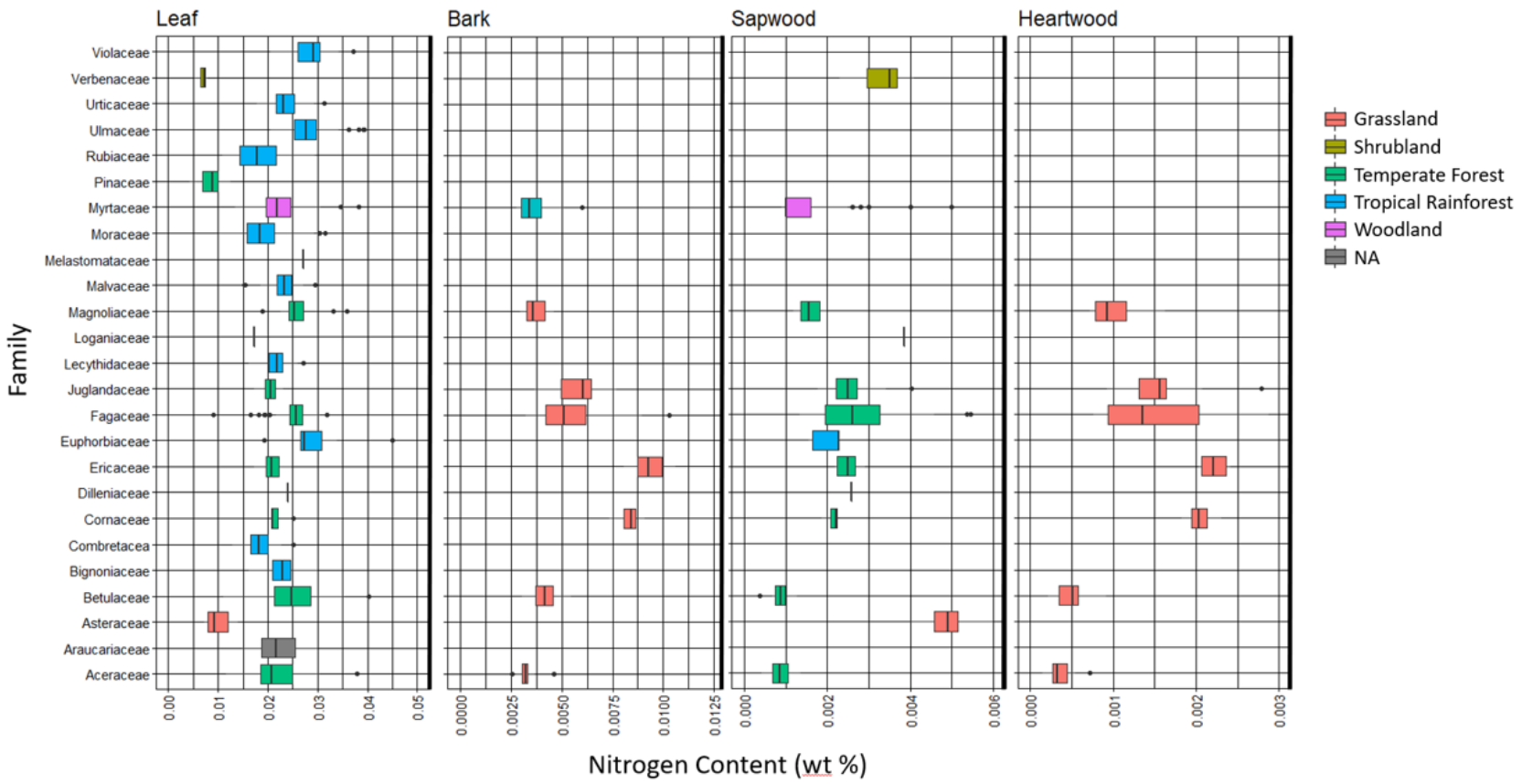

Figure 1.9 Comparison of nitrogen content found in different plant families and the different parts of the plant. Note that the leaves and bark contain the greatest nitrogen content across the families, and heartwood contains the least (Created using data provided by Falster et el., 2015).

The key piece of information to take away from Figure 1.9 is that the nitrogen content varies widely from species to species and even between different parts of the same plant. This means that fire emissions from this plant will also vary with regards to nitrogen-containing species like acetonitrile and hydrogen cyanide, which are both hazardous air pollutants.

1.8 Objective of Present Study

Biomass burning has been a topic of interest in the field of atmospheric science for decades. With the rise in wildfire events globally because of climate change, the interest in understanding the impacts of fire smoke on climate has turned to a necessity. However, despite this enormous push to study and investigate biomass burning emissions, comparatively little research has been done to study the interactions between biomass burning plumes and urban pollution (McClure et al., 2018). Yet, because of the complexity of the chemistry within each of these source plumes, there is much in the way of interesting and important chemistry to study in this overlap.

As mentioned previously, fire smoke is full of hazardous airborne pollutants and particulates. During the 2017 fire season - which was at the time the worst season on record in the US - over 3.5 million tons of VOCs were emitted from wildfires, and 2 million from prescribed burns for a total of 5.5 million tons of VOCs directly emitted from fires in 2017 alone (EPA 2021). Most of these VOCs would have been emitted at the peak of fire season, when multiple fires were burning simultaneously. The burst of VOCs and particles and ash borne from the fires fill the mixed layer, and in places like California's Central Valley where there isn't a strong, consistent wind this miasma would hang in the air for days and into weeks. People living in these places are

stuck, and forced to breathe the air that is hazardous. The only refuge is inside where one has good ventilation and some sort of filtration system. Yet, when one lives directly in the path of the smoke plume, these hazardous compounds can still be found at enhanced concentrations even inside a house or building. During the 2007 wildfire season in southern California physicians experienced a surge in emergency room visits from patients experiencing asthma and dyspnea symptoms which were attributed to breathing wildfire smoke (Dohrenwend et al., 2013). It is estimated that fifteen to twenty thousand people will die from smoke-related illnesses and complications each year in the US. In addition to these short term, acute effects of exposure to fire smoke, long-term exposure has been shown to increase the risk of cancer in humans (O'Dell et al., 2020). It has been shown that exposure to wildfire smoke leads to an increased risk for every ten people to develop cancer for every one million, which is above the national average of 0.71 per million people (O'Dell et al., 2020).

As stated in the introduction, wildfires have been increasing in frequency and severity over the past few decades because of climate change. More frequent, intense fire events mean more particles and VOCs being emitted into the atmosphere in a burst during the peak of wildfire season. These emissions will remain in the atmosphere until they are rained out or deposit onto the Earth's surface. By the time this happens, though, smoke can travel across continents and oceans, affecting people who live nowhere close to the fire and long after the last embers of the original fire have died out. While ten people in one million may not seem extreme compared to the risk from other sources like traffic (O'Dell et al., 2020), smoke can easily travel the entire distance across the US or across the Atlantic Ocean from Africa to the southern US affecting hundreds of millions of people. Suddenly, where fires may have only affected a few small towns or a large city when they were relatively infrequent and could be fought, now thousands of

people are at a much greater risk of developing cancer directly from being exposed to wildfire smoke, and hundreds of thousands will die from conditions and/or complications from breathing smoke.

Additionally, the emissions from fires affect not only human health, but plant health, and ultimately climate. Ozone is formed via reactions involving NO_x and VOCs, both of which are emitted from fires. Ozone is detrimental to human health and contributes to the asthma and dyspnea development in humans who are exposed to fire smoke. This ozone also damages plants, including crops, stunting their growth and opening them up to infection. Ozone can also be formed directly from wildfire emissions even many miles downwind of the fire. NOx sequestration in the form of PAN "holds" NO_x as a different compound that can travel far downwind of the fire without reacting to form ozone. However, eventually PAN will thermally decompose by breaking down into NO_x (Singh & Hanst, 1981). This NOx is then free to react with transported or local VOCs to form ozone that normally would not have been formed in the region, enhancing the background concentration for that area.

The NO_x, CO, CO_2, and particles emitted from fires also have a significant impact on climate. However, as stated previously the effects of these emissions on climate are not well understood. The impacts of climate change on future fire seasons are well understood, yet the ways in which these increases in fire will in turn affect climate change is not. What is known is that there will be an effect, but whether it is a net warming or net cooling effect is not well known. This question is currently the focus of much of the fire science community.

Another gap in the research is in the area of agricultural fires and prescribed burns. While the wildfires of the western US may capture the attention of the media and populace living nearby (as they should), nearly half of biomass burning emissions also come from much, much smaller

fires in the forms of controlled agricultural and brush burns (EPA 2021). These land use burns are often only a few square acres in size and therefore do not get nearly large enough to form the convective clouds seen in western wildfires, and rarely get large enough for their plumes to reach the capping inversion. These plumes dilute into the background air quickly. In the case of agricultural fires specifically, as they are performed by farmers to clear their fields after the harvest, areas where these burns occur also see a burst in fire smoke affecting local air quality. In the US this practice has been restricted since the 1990s, and while the practice still occurs it is not nearly as prevalent as in places such as sub-Saharan Africa and India. In sub-Saharan Africa for example the crop burning season is between August - October, when across the continent thousands of small individual fires are lit for land management purposes. The emissions of these fires are clearly visible from satellites (Figure 1.10).

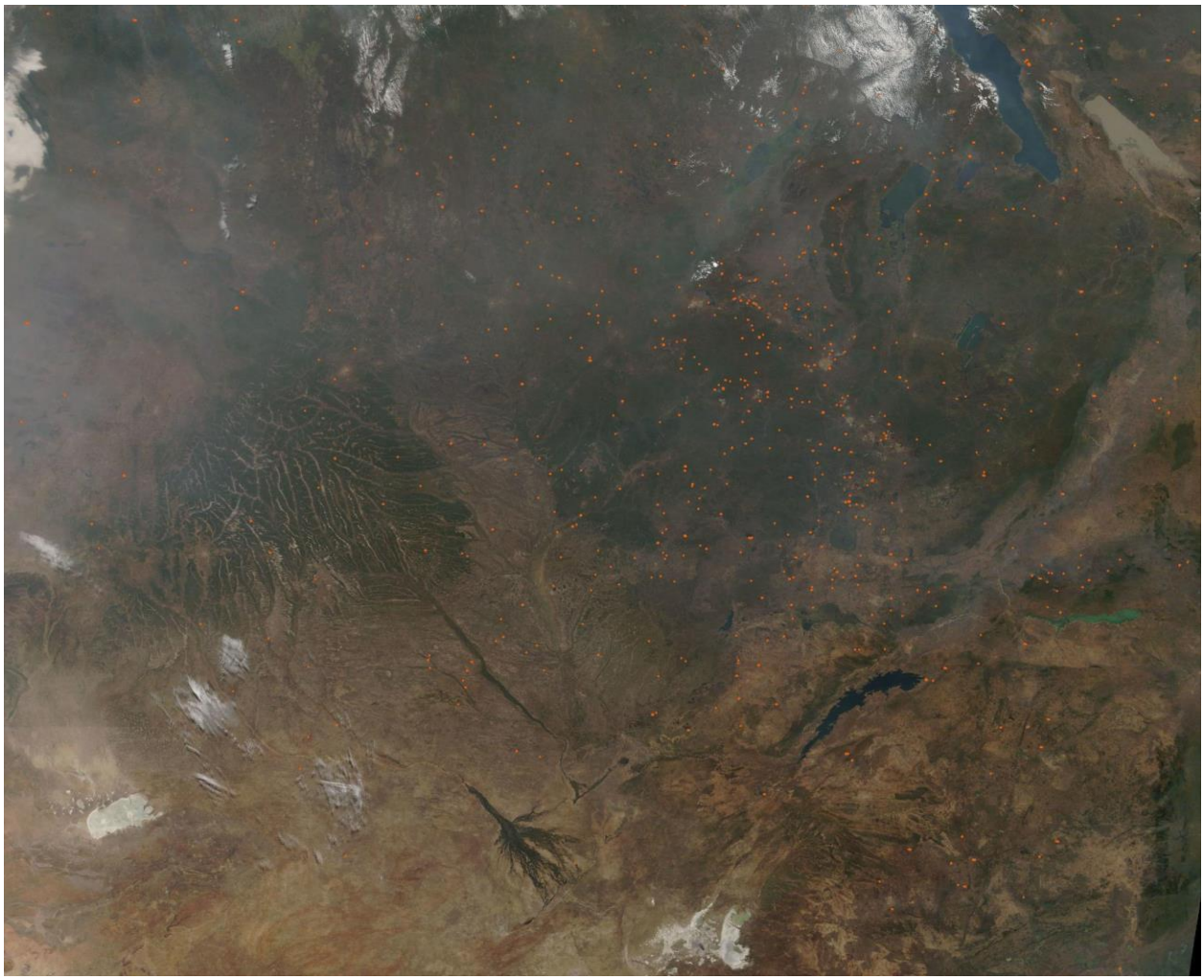

Figure 1.10 Satellite photo over sub-Saharan Africa showing the ubiquitous haze created by the thousands of fires scattered across the continent. Each small orange dot is a fire signature detected by the MODIS instrument. It is important to note that MODIS does not detect every fire event, only the larger ones, so there are many more smaller fires also burning in this photo. For reference, Lake Malawi is the large lake in the top right corner of the photo. (MODIS, NASA Worldview, 2018)

The results of crop burning in the US are the same as anywhere in the world - a ubiquitous pallor of smoke permeates throughout the mixed layer in the region in which the fires are being burned. The combined emissions from all of the burning fires linger in the boundary layer and settle with it at night, effectively concentrating the emissions from the fires close to the surface.

This will yield the same health consequences as in western fires, yet these hazards are not nearly as well quantified as for western wildfires.

This work will focus on the areas of fire science that are not well understood: VOC contributions in mixed fire- and urban-polluted areas, effects of agricultural and prescribed fires on VOC abundances especially in disenfranchised areas, and broader effects of fires on the continental US. In particular, the change in ozone concentrations as a result of biomass burning emissions entering an urban area will be analyzed. Theoretically, ozone should be enhanced following a smoke-impacted period in an urban area, as the influx of VOCs and NOx would improve the ozone-forming potential of the region. However, observations from very fresh biomass burning emissions show that NOx titration dominates in these regions, causing an overall decrease in ozone in very fresh smoke. Box modeling using inputs based on real observations of a smoke-impacted city will be used to analyze the trends in ozone concentration in a city following a biomass burning event. These results are compared to actual observations to determine if the modeling results are accurate, and what the results may mean for ozone enhancement across the US as a result of biomass burning.

2. Methods

2.1 NASA DC-8 & NSF C-130 Research Aircraft

The data used in this analysis were collected during two airborne field campaigns: the Fire Influence on Regional to Global Environments and Air Quality (FIREX-AQ) mission aboard the NASA DC-8 research aircraft, and the Western wildfire Experiment for Cloud chemistry, Aerosol absorption and Nitrogen (WE-CAN) mission aboard the NSF C-130 "Hercules" research aircraft. The overall goals of these missions - that apply to this research - were to better understand biomass burning emissions from forest fires in the western US. FIREX-AQ also had an additional goal of analyzing prescribed agricultural and brush burns in the southeastern US, which were not sampled during WE-CAN. The benefit of this was to collect data from fires consuming different fuels. Additionally, since the fires were planned, the fuels being burned were well constrained prior to the burn. This is difficult to do with wildfires, as they usually occur in remote areas where the fuels are not well known. To achieve the goals of the missions, the aircrafts used in each campaign were outfitted with a comprehensive suite of instruments designed to analyze a variety of aspects related to biomass burning. A detailed list of the instruments involved in each campaign, as well as a schematic of each aircraft as it was outfitted for each deployment are shown in Figures 2.1 and 2.2.

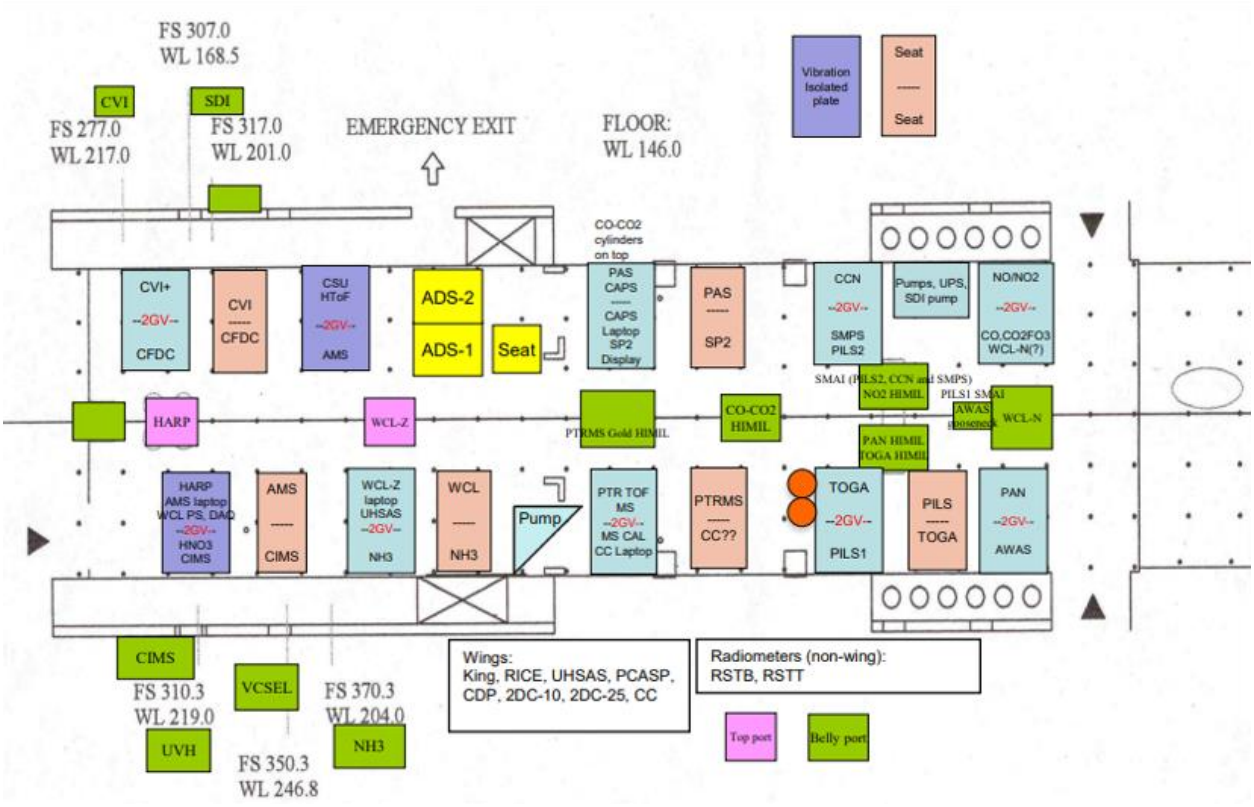

Figure 2.1 Seat and instrument layout for the C-130 cabin during the WE-CAN campaign (adapted from WE-CAN Overview, 2017).

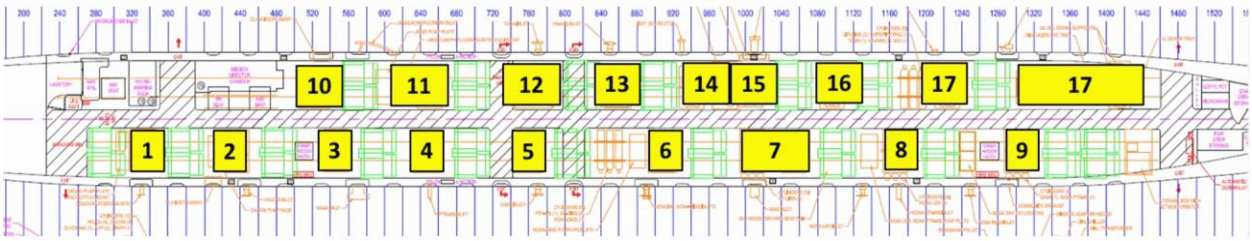

Figure 2.2 Seat and instrument layout for the DC-8 cabin during FIREX-AQ (Adapted from FIREX-AQ White Paper, 2018).

Gas Phase Measurements (Tracers and Reactive Nitrogen)			
Seat	**PI**	**Species Measured**	**Technique**
1	Tom Ryerson	O_3, NO, NO_2, NOy	Chemiluminescence
2	Glenn Diskin	CO_2, CO, CH_4, H_2O	Laser Absorption Spectroscopy
4	Armin Wisthaler	NH_3	PTR-ToF-MS
6	Greg Huey	PAN, PPN, other speciated PANs	CIMS
6	Patrick Veres	HNO_3, HONO, HO_2NO_2, HNCO	Iodide ToF-CIMS
8	Carsten Warneke	CH3CN	PTR-ToF-CIMS
8	Jeff Peischl	CO	Cavity Enhanced Absorption
9	Carrie Womack	NO_2, HONO	Airborne Cavity Enhanced Spectroscopy (ACES)
14	Andrew Rollins	SO_2	Laser Induced Fluorescence
15	Paul Wennberg	SO_2, HCN	CIMS
15	Mark Zondlo	NH_3	Laser Absorption Spectroscopy

Gas Phase Measurements (Hydrocarbons and Oxidation Products)			
Seat	**PI**	**Species Measured**	**Technique**
5	Dirk Richter	CH_2O, CH_3OH, C_2H_4, C_2H_6	Laser Absorption Spectroscopy
7	Don Blake	C_2-C_10 Alkanes, C_2-C_4 Alkenes, C_6-C_9 Aromatics, C_1-C_5 Alkylnitrates, etc.	Whole Air Sampling
8	Carsten Warneke	Speciated Hydrocarbons and OVOCs	PTR-ToF-CIMS
9	Jessica Gilman	C_2-C10 Alkanes, C_2-C_4 Alkenes, C_6-C_9 Aromatics, C_1-C_5 Alkylnitrates, etc.	Whole Air Sampling (WAS)
9	Carrie Womack	CHOCHO, CH_3COCHO	Airborne Cavity Enhanced Spectroscopy (ACES)
12	Eric Apel	C3-C10 Hydrocarbons, C_1-C_7 OVOCs, HCN, CH_3CN, C_1-C_2 Halocarbons, etc.	HR-ToF-GC/MS
14	Tom Hanisco	CH_2O	Laser Induced Fluorescence
15	Paul Wennberg	H_2O_2, Organic Peroxides, Organic Acids, Isoprene Oxidations Products, etc.	CIMS

Aerosol Measurements (Physical/Optical/Chemical)			
Seat	**PI**	**Species Measured**	**Technique**
3	Jack Dibb & Rodney Weber	Brown Carbon, Bulk Aerosol Composition, HNO3	Filter Sampling, Spectrophotometer, and Mist Chamber
10	Nick Wagner	Aerosol Absorption & Extinction, RH	Cavity Ringdown Extinction, Photoacoustic Absorption Spectrometry
10	Adam Ahern	Aerosol Scattering Phase Function - UV & Blue Wavelengths	Laser Imaging Nephelometer
11	Rich Moore	Aerosol Number, Volatility, Size Distribution, and Optical/Physical Properties, CCN	Particle Counters, Nephelometers, etc.
12	Joseph Katich	Black Carbon Concentration, Size, Mixing State	Single Particle Soot Photometer (SP2)
13	Jose Jimenez	Submicron Aerosol Composition	HR-ToF-AMS
11	Bernadett Weinzierl	Cloud and Coarse Mode Size Distribution	Optical Wing Probe Detectors
11	Kouji Adachi	Shape, Mixing State, Composition, of Individual Particles	Filter Sampling, Transmission Electron Microscopy (TEM)
12	Art Sedlacek	Aerosol Absorption/Scattering - 532 & 405 nm	Photothermal Interferometer (PTI)

Remote Sensing Measurements (Active & Passive) and Meteorology (T, P, Winds)			
Seat	**PI**	**Species Measured**	**Technique**
1 & 8	Sam Hall	CAFS (Zenith/Nadir Solar Actinic Flux & Photolysis Frequencies)	4π-sr Spectroradiometry
10	Jochen Stutz	Mini-DOAS (Trace Gas Columns)	Airborne MAX-DOAS
16	Jeff Myers	Active fires ($T \geq 850$ K) & Burn Scars (10-20 m resolution)	MODIS/ASTER Airborne Simulator (MASTER) Scanning Spectrometer
17	John Hair	Zenith & Nadir Active Remote Sensing of O3, Aerosol Backscatter, Extinction, Depolarization, etc.	Differential Absorption Lidar - High Spectral Resolution Lidar (DIAL-HSRL)
No Rack	Paul Bui	Temperature, Pressure, 3D Winds	Meteorological Measurement System (MMS)
No Rack	Van Gilst	Thermal Imaging for Flight Guidance	FLIR Camera

Table 2.1 List of PIs and Instruments according to their seat number, outlined in Figure 2.2.

2.2 Flight Plan Outline

Both campaigns followed similar flight plans. Unless there was a prescribed burn planned for the day, the general schedule was as follows. First, the instruments were prepared on the morning of the flight day. Takeoffs were scheduled for early afternoon, as fires would typically flare up around midday and therefore would be producing a large enough quantity of smoke to be sampled by the early afternoon. Prior to takeoff, there would be a preflight briefing to update the mission team (~50 people) on the target fires for the day. These target fires were fires that had been burning strongly on the previous day and where firefighting operations were limited. The specific target fires for the day were chosen based on their likelihood of producing adequate smoke for collecting good samples, their involvement in cloud formation, the ease of accessing the immediate area around the burn (which was often a no-fly zone due to firefighting operations), and any chance of producing unique meteorological conditions such as a pyrocumulonimbus (PyroCb) cloud. However, because of the uncertainty inherent in wildfires, the flight plan was designed to be changed with ease to target any unique opportunities. Prescribed burn days followed a similar preflight schedule, but with the added benefit of knowing exactly when and where the fires were going to be and therefore could be planned with much more specificity.

For the larger, western fires, after the aircraft arrived at the fire location the first track would be a long overhead run along the fire plume and directly over the fire (if possible). This was to allow the MASTER and DIAL instruments to make remote sensing measurements of the burn scar and fire plume. This pass also gave information into the height of the fire plume and its

structure based on the LIDAR imagery. This information is crucial to the next sampling stages as it showed the best altitude to fly through the plume at its core, yielding the freshest smoke.

Next, at least one pass was made upwind of the fire to sample the background air that was mixing with the fresh fire smoke. Any urban emissions or smoke from other fires would be detected in this pass. Following this, the sampling began by intersecting the plume orthogonally to the direction of the wind. As the fire burns, the smoke gets lofted and then carried along by the wind. It's along this trajectory that the smoke gets processed and "ages", an important aspect of biomass burning emissions that the project aimed to better understand. A perfectly orthogonal pass to the direction of smoke travel is ideal as it prevents integrating a sample across different ages of smoke. Since the aircraft traveled much faster than the local wind speed ($V_{plane} >> V_{plume}$), it can be assumed that the smoke plume is stationary compared to the aircraft. Therefore, the general sampling strategy was to conduct these orthogonal crossings at as many points as possible at different distances downwind of the fire, in a Lagrangian fashion. This would yield enough data to understand not only how the smoke processes as it ages, but would also give insight into the internal structure of the plume itself. However, in reality the smoke plume is moving at the same time the aircraft is moving, albeit much slower, so this sampling approach is technically be described as semi-Lagrangian (Figure 2.3).

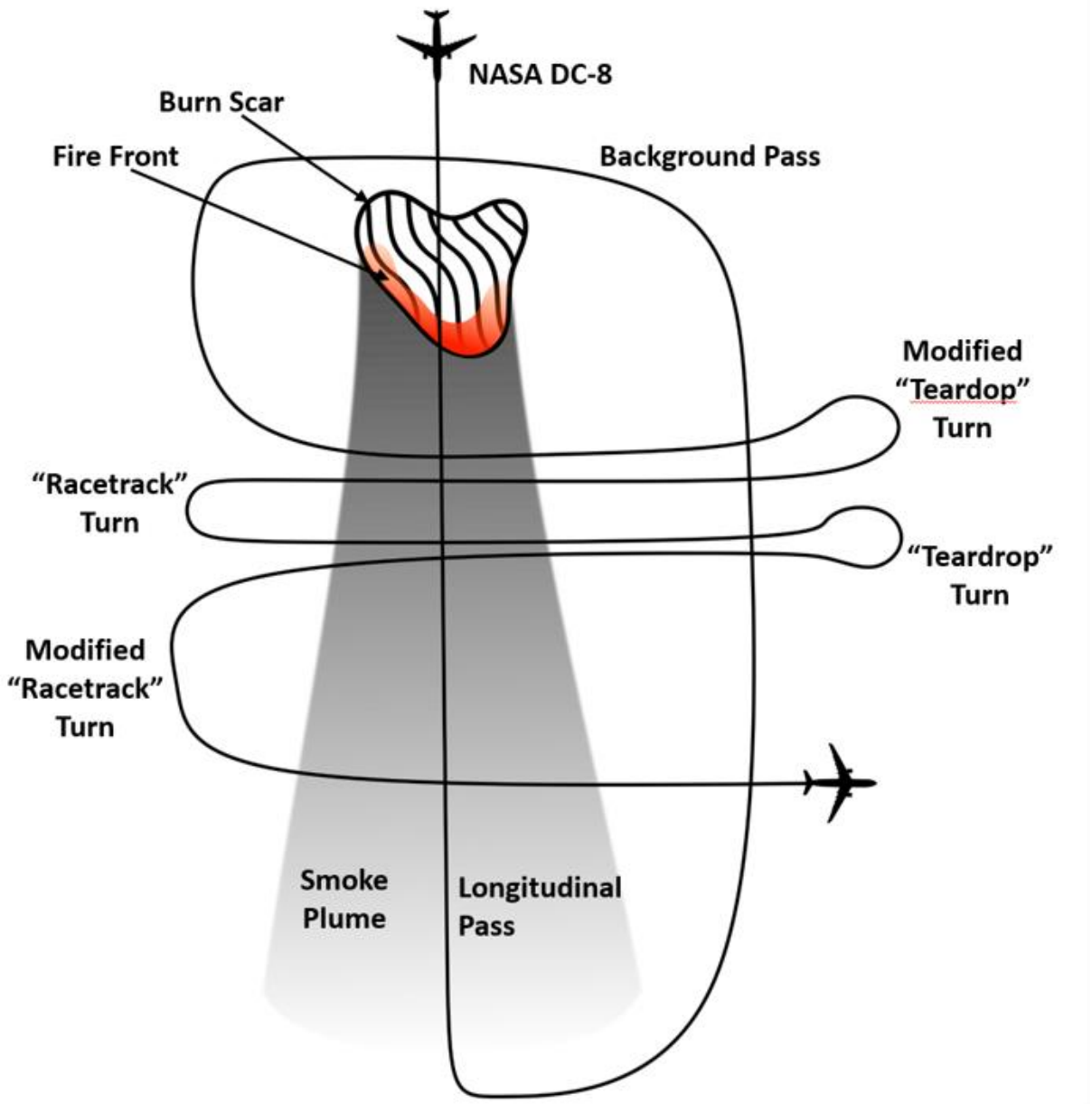

Figure 2.3 An overhead view of the different sampling passes performed during field campaigns to sample smoke plumes. Note that this is a representation of a large fire with a well-defined plume. Smaller fires or plumes that mixed quickly with the background were sampled by simply doing overhead passes as close to the burn area as possible.

The main constraints on the flight track were firefighting operations and the plume itself. When there was active firefighting in the area, often a cylindrical temporary flight restriction (TFR) would be placed around and above the fire to make room for water-dropping aircraft

trying to access the fire. Any flight into this area required special permission from air traffic control (ATC) and was frequently denied. This meant that it was often difficult or impossible to sample very close to the fire. However, even when the aircraft was able to sample close to the fire either due to ATC permission or because the fire wasn't being fought, the center of the plume directly above the fire was difficult to sample. This was due to the extreme upwelling caused by the heat of the large forest fire, which could interfere with the aircraft's flight and was therefore a major safety hazard.

The southeastern fires followed a similar sampling strategy, but generally with fewer restrictions. Almost all of the fires sampled in the southeastern US during the second half of the FIREX-AQ mission were prescribed burns. Therefore, there was never any airborne firefighting activity that required a TFR, so combined with the fact that these fires were relatively weak compared to the large western fires, the aircraft was able to sample directly over the fires at it's minimum altitude limit of 1000 feet. In most cases, however, the plumes were too weak to follow for more than a few miles. For these fires the plume crossings were altered to target the most intense portion of the plume. This was often limited to directly over the fire, as the weak plumes diluted quickly in the boundary layer, creating a ubiquitous haze that permeated throughout most of the southeastern US.

2.3 Western Wildfire Experiment for Cloud chemistry, Aerosol absorption and Nitrogen (WE-CAN)

The WE-CAN campaign was organized by the National Center for Atmospheric Research (NCAR), and was funded by the National Oceanic and Atmospheric Administration (NOAA) and the National Science Foundation (NSF). The science objectives for the campaign were to better understand: aerosol absorption and their properties, fixed nitrogen, and cloud activation and chemistry within wildfire plumes in the western US (WE-CAN Overview, 2017). To achieve these objectives, the campaign was designed as an airborne field deployment, utilizing the NSF "Hercules" C-130, and was stationed at Boise Airport (KBOI) in Boise, Idaho. The fixed-base operator (FBO) at KBOI was chosen because of its central location in the northwestern US, which has the highest propensity for wildfires during the summer months in the US. Freshly emitted smoke was the primary target, as the majority of the chemical and physical processing takes place within the first few hours after emission. In certain cases, such as the Mendocino Complex fire in the California Central Valley, aged background smoke was sampled because it presented an opportunity to examine the mixing of smoke with urban background emissions.

Understanding nitrogen chemistry and emissions from wildfire smoke is a crucial objective for understanding the effects of smoke on air quality and the environment. Biomass contains fixed nitrogen (e.g., NH_4), which is pyrolyzed during the combustion process to form small, nitrogen-based compounds such as HCN, CH_3CN, and NH_3. These compounds are then oxidized shortly afterward to form nitrogen oxides such as NO, NO_2, and HONO. NOx is then sequestered as PAN, which thermally decomposes back into NOx far downwind of the fire.

Another important objective for WE-CAN was to gain a better understanding of aerosol absorption and properties in smoke plumes. Aerosols are climate forcers, and contribute to an overall cooling of the climate. However, the degree to which aerosols from wildfires contribute to climate forcing is not well understood. Different particles have different properties, depending on their color and albedo. Fires emit black and brown carbon particles, which behave differently and have different implications for climate when emitted into the atmosphere. The WE-CAN campaign targeted black and brown carbon as well as other particles to study the properties of fire-emitted particles compared to those observed from other emission sources. The information gained from these observations help inform climate modelers and emissions inventories.

The final science objective was to study cloud activation and chemistry in smoke plumes. Aerosol particles also have the ability to seed cloud formation, and participate in aqueous chemistry as the particles accumulate water. The properties that define a particles ability to participate in cloud seeding are not well understood for wildfire particles, including black and brown carbon. Additionally, the aqueous chemistry that occurs in wildfire plumes had not been studied prior to WE-CAN. Several instruments including a particle-into-liquid sampler (PILS) focused specifically on measuring these properties to better understand these aspects of wildfire emissions (WE-CAN Overview, 2017).

2.4 Fire Influence on Regional to Global Environments Experiment - Air Quality (FIREX-AQ)

The FIREX-AQ campaign was organized and funded by the National Aeronautics and Space Administration (NASA) and the National Oceanic and Atmospheric Administration (NOAA). FIREX-AQ was essentially a follow-on to the WE-CAN campaign, with similar science objectives but with the addition of an agricultural fire study late in the campaign and a larger instrument payload. The campaign began with test flights out of the NASA DC-8's home base of operation at the Palmdale airport (PMD). The checkout flights were conducted throughout the LA basin and CA Central Valley. During the transit flight to KBOI, the FBO for the first portion of the campaign, the DC-8 conducted sampling runs in the boundary layer throughout the CA Central Valley. The data collected during this flight was given to the California Air Resources Board to aid in their air quality and policy-making decisions.

Once at KBOI, the campaign followed a similar weekly plan to the WE-CAN campaign. As fires cropped up throughout the western US, the planning and meteorology team would decide on the most promising sampling targets for the week, and the aircraft would fly to sample the best fires approximately 3-4 times per week. Weekends were designated no-fly days for instrument and aircraft maintenance. On August 19, 2019 the DC-8 transited to the Salina, Kansas FBO (KSLN) for the second half of the deployment. The goal of this part of the deployment was to sample southern agricultural fires and prescribed brush fires.

The science goals for FIREX-AQ were to determine emission factors for trace gases emitted from fires, effects of meteorology on fire plumes, plume chemistry and structure, nighttime chemistry, and effects of agricultural fires on local air quality and climate (NOAA-NASA

FIREX-AQ White Paper, 2018). Emission factors are quantitative estimates of the amount of a given type of trace gas that will be emitted from a fire. Emission factors for fires are one of the most important variables to calculate with respect to trace gases, as it provides information the chemical properties, air quality, and climate impacts of the smoke plume. Emission factors are used in modeling studies to predict air quality and climate impacts from fire smoke. Studying and understanding the development and structure of fire plumes was also a topic of interest for FIREX-AQ. The DC-8 was outfitted with the NASA Langley DIAL instrument, which is a downward and upward facing LIDAR instrument that is capable of measuring aerosol scattering properties. The sampling strategy specifically included longitudinal passes along the fire plume to gain information into its structure. FIREX-AQ also included a ground team of meteorologists and modeling experts that forecast fire activity, and also compared the smoke plume structure and formation to the meteorological conditions of the day they developed. This provided information on how smoke plumes develop given the prevailing conditions of the day they form. Having the team on site and cooperation between the ground and aircraft instrument teams led to the sampling of the first PyroCb plume to develop in the continental US in 2019, and the first time a PyroCb had been studied *in situ* with such a comprehensive suite of instruments (Thapa et al., 2020). The long-range capabilities of the DC-8 that were not available during WE-CAN because of the limited range of the C-130 allowed the aircraft to remain on site around fires much later into the day than was possible in WE-CAN. A few of the flights out of KBOI continued sampling fire smoke late into the evening. This provided the opportunity to begin to observe nighttime chemistry in action in a fire plume, which had never been done previously on such a highly instrumented aircraft. Finally, the agricultural burn focus of the campaign was one of the most important science goals. Agricultural fire emissions had not been studied *in situ* with

such a comprehensive suite of instruments prior to FIREX-AQ. In previous campaigns any sampling done of agricultural emissions were usually incidental, and never in any large quantities. FIREX-AQ collected data on hundreds of separate crop and brush burns, and on several different crop species. This wealth of data has already informed updates on emissions estimates from agricultural fires, which were previously poorly constrained.

2.5 NCAR Trace Organic Gas Analyzer (TOGA)

a. Aircraft Inlet

The TOGA uses a constant mass flow inlet designed to limit aerosol intrusion into the GC system. A key aspect of the inlet that differs from the WAS inlet is the capability to reroute the incoming air away, which allows for blanks and calibration (ACOM Website, 2021).

b. System Design

The NCAR ACOM Trace Organic Gas Analyzer (TOGA) is an online gas chromatography system. Two different versions were used between the WE-CAN and FIREX-AQ campaigns. Each configuration will be described briefly here.

The WE-CAN configuration utilized an Agilent HP 5973N quadrupole mass spectrometer as the detector, and a Restek MXT-634 polyimide capillary column (Figure 4). The TOGA operated on a 100 s sample cycle. During the first 28 seconds air was directed from the inlet into a liquid nitrogen-cooled cryotrap. The cryotrap preconcentrates the sample, allowing for a lower limit of detection and better instrument precision. After cryotrapping, the sample was revolatilized and

released into the separation column. The remaining 72 seconds of the sample cycle was dedicated to the separation time and subsequent VOC detection and quantification. This configuration was capable of quantifying 72 different VOCs (Permar et al., 2021). Figure 2.4 shows a schematic of the TOGA configuration used during WE-CAN.

The FIREX-AQ configuration was a modified version of TOGA, which utilized a time-of-flight (TOF) mass selective (MS) detector. The TOF configuration operated on a 105 second sampling cycle, but unlike the WE-CAN configuration was able to quantify over 80 different species - including fire-specific tracers and low molecular weight oxygenated VOCs, which were difficult to measure precisely on the previous configuration (Apel et al., 2020).

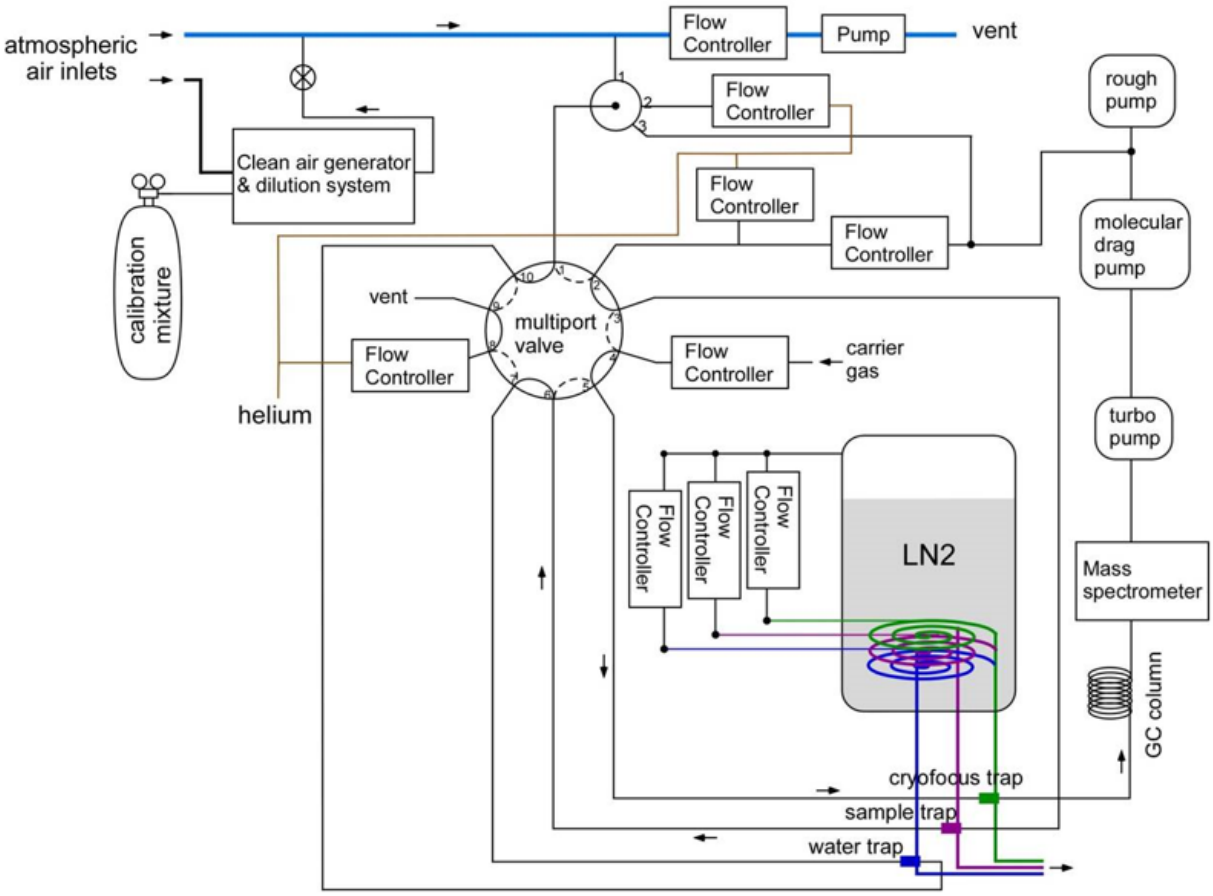

Figure 2.4 Schematic of the ACOM TOGA instrument as configured for the WE-CAN campaign. The FIREX-AQ configuration utilized a TOF-MS in place of a quadrupole MS (ACOM Website, 2021).

2.6 UCI Whole Air Sampler (WAS)

a. Aircraft Inlet

Mounted on the outside of the aircraft adjacent to the forward-most rack is a constant flow atmospheric inlet. The inlet is mounted to a specialized plate affixed into what used to be the

aircraft window. Figure 2.5 shows how the inlets are mounted in different manners to the DC-8 fuselage. The WAS inlet is mounted just behind the wing in the photo (Figure 2.5).

Figure 2.5 Picture of the outside of the fuselage of the DC-8, showing the inlets and ports mounted to the aircraft. The port side and underside also have inlets and ports for instruments (not pictured).

b. Bellows Pump

Air is pulled into the aircraft cabin through the UC-Irvine (UCI) whole air sampler (WAS) intake line using a Parker MB-602 bellows pump (Colman et al., 2001). The pump is necessary to pressurize the canisters to ensure that a specific amount of sample is collected. The model of

pump was selected because it is grease-free and all stainless steel, which limits the materials present in the pump that could outgas VOCs and contaminate the samples.

c. Snakes

The sample canisters are 2L stainless steel canisters which are prepared and evacuated as described in the next section. The canisters are set into foam inserts in three rows of eight for a total of twenty-four canisters per insert. Each canister was then connected in series using an Ultra-Torr T-connector which fits to the port connector on the canister. The T-connectors are then connected using degreased 1/4" stainless steel tubing which is cut to length. These inserts are then shipped in custom-made shipping boxes to the FOB for the field campaign. They can then be unpacked and brought onto the aircraft, where they are then set and locked into the rack and manifold. The connected canisters in the foam insert are colloquially referred to as a "snake" because of the winding tubing that connects the canisters. This configuration will here on be referred to as a snake.

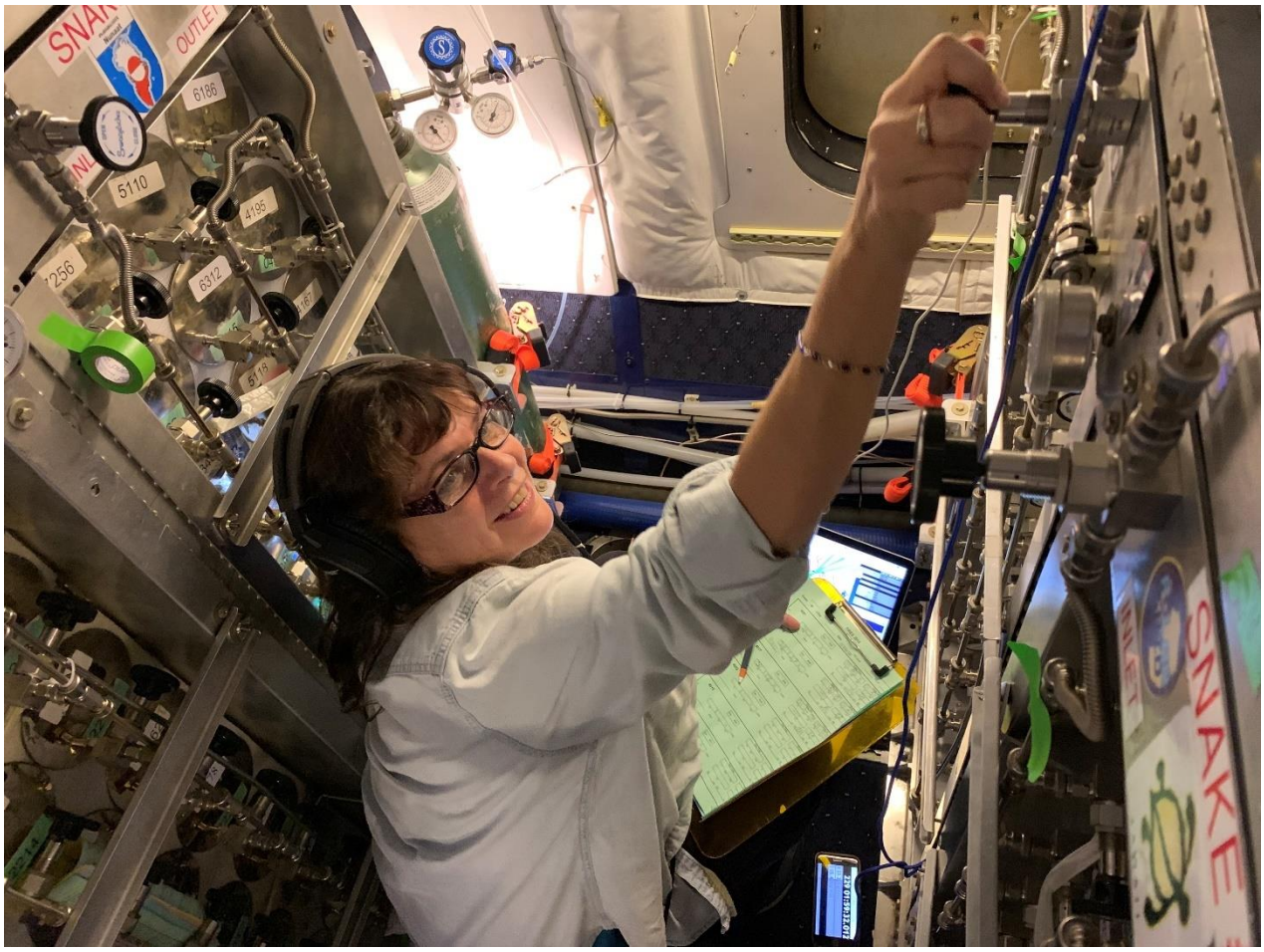

Figure 2.6 Dr. Nicola Blake collecting a whole air sample during the FIREX-AQ campaign. In this photo Dr. Blake has her hand on the outlet valve.

Figure 2.7 Photo taken during the 2019 FIREX-AQ campaign showing the location of the pontoon used for pressure testing on the fuselage side of the rearmost rack. To the right is a new snake loaded into the caddy, with the data collection sheets rolled and set in the snake for use.

Figure 2.8 Photo of myself (Alex Jarnot) recording data pertaining to a recently collected sample on data sheets exactly like those shown in Figure 22. Also pictured are the inlet and outlet valves for the caddies shown. I am sitting between the two racks facing the opposite direction of travel.

d. Snake Caddies & Aircraft Rack System

The rack and manifold system vary slightly depending on the aircraft being used (e.g., DC-8, P-3, Sherpa) for a field campaign. Given that the WAS system was installed on the NASA DC-8 for the FIREX-AQ campaign, a description of that configuration will be given here. The current DC-8 specific rack and manifold system was designed and constructed by former Rowland-Blake lab group members.

The space allocated for the WAS system on the NASA DC-8 gives enough room for seven can caddies - the steel housings in which the foam snake inserts are set and locked into place. The snakes are locked into place using two steel cross braces fixed in place across the front of the snake by wing nuts attached to the sides of the rack.

Above each can caddy is a simple manifold of tubing and two Swagelock valves (identical to those on the canisters). Stainless steel tubing from the inlet through the bellows pump to the first rack serves as the inlet tube and is connected to the first of the two Swagelock valves. The inlet valve allows the rack to be isolated from the inlet. 1/4" stainless steel flex tubing connects the valve to the snake in the rack to provide ease of installation. The end of the snake tube is then connected to another piece of 1/4" ribbed steel tubing which connects to the second Swagelock valve. This outlet valve allows the pressure to build in the snake lines and canisters. Each of the seven snakes are connected to the others in parallel, and ultimately connects to an outlet exhaust port which vents the air out of the cabin.

After the snakes are loaded into and connected to the caddies and inlet system, they have to be pressure tested to ensure the connections are good and so that cabin air won't leak into the snake lines. A pontoon is mounted to the fuselage side of the rearmost rack, which is connected to the inlet system. This pontoon is filled when the aircraft is near its peak altitude (~40 kft),

because there usually aren't many canister samples being collected at this time, and more importantly because the air at this altitude is very clean compared to the surface and cabin air that may leak into the snake line. When the snakes are first installed, air from this pontoon is released into the snake lines and pressurized to above ambient pressure. Each snake caddy is individually locked off, so if there are any leaks they are contained to the individual caddy, and therefore the leaky rack is easily found and fixed.

e. Sampling Operation

Prior to takeoff, the bellows pump is turned on to start the flow of air through the sample lines. The snake and manifold lines are then pumped and flushed with clean air that was collected above 40 kft and stored in a gas pontoon at the side of the rack. This clears out any possible remaining contaminants that may have seeped into the lines while the aircraft was on the ground. Air flows through the entirety of the system and snakes before exiting the aircraft. To take a sample, the outlet for the snake is shut, which builds pressure in the line. Then, the valve for the can the sample will be collected in is opened slowly, bleeding the pressure in the line (which is the sample air) into the canister. The valve has to be cracked slowly to prevent the line from being evacuated quickly and creating negative pressure in the line, which could draw air from the cabin into the line if there were a small leak, and thereby contaminating the sample. A way to tell when this happens is to look for elevated concentrations of H-1211 in later analysis, as halon fire extinguishers in the aircraft cabin leak small amounts of H-1211, which isn't found in the atmosphere in large concentrations. If a sample were to exhibit an enhancement in H-1211, it is likely that the canister was opened too quickly and the sample is contaminated. This serves as an extra check. Once the canister starts to fill the valve is opened completely. As the pressure

in the line and canister reaches 40 PSIg, the canister valve is shut and the outlet valve quickly opened to prevent excessive pressure buildup, which will damage the bellows pump.

f. Canisters

All samples analyzed by the Rowland-Blake lab are collected via whole air sampling. Samples are collected and contained in proprietary canisters. The canisters are constructed from 316 stainless steel and are equipped with a Swagelock SS-4BG valve (Figure 2.9, A), and the cans are approximately two liters in volume. The valve is connected to the canister body (Figure 2.9, B) via quarter-inch stainless steel port connector welded to the canister body and connected to the valve fittings. A port connector is swaged to both sides of the valve, which is used to connect the canister to the gas chromatography manifold (Figure 2.9, C). A vinyl tube end cap is fitted over the manifold connector when not in use, ensuring dust and debris does not enter the valve mechanism.

In order to assure canister cleanliness, the sample canisters must be thoroughly cleaned and evacuated prior to use. Otherwise, they may contain concentrations of residual ambient VOCs from the laboratory environment to influence the results of sampling.

The first step in canister preparation is to “bake” each canister in an oven for approximately twelve hours at 225 °C under humid conditions. The humidity inside the oven is created via an aspirator setup filled with distilled water fed into the top of the oven. The purpose is to help remove molecular impurities that may be stuck to the inside walls of the canister. A clean steel surface is essential as the heat promotes a passivated oxide layer to form over the surface of the stainless steel (Figure 2.9, E). This oxide layer prevents interactions between the VOCs in the sample and the free metal, mitigating wall losses.

Next, the canisters are flushed with clean air (Figure 2.9, D) to ensure each canister starts the evacuation process in as pristine a condition as possible. Each canister is flushed at least one dozen times, each time being pressurized to approximately 30 psi, and then allowed to vent and return to just above ambient pressure. This ensures no laboratory air is allowed to return to the canister, and only the clean air remains in the can. The air is collected from Aldrich Park in the center of the University of California - Irvine campus. This is because the park air is well characterized by the Rowland-Blake lab, and is composed of primarily biogenic VOCs.

The canisters are then placed under vacuum. Once the inside pressure reaches 10^{-2} torr the cans are flushed with cleaned ultrapure helium and pressurized to 1000 torr. Once the canisters are pressurized to 1000 torr with helium they are evacuated again, this time to a final internal pressure of 10^{-3} torr. Once this internal pressure is reached, the SS-4BG valves are closed tightly.

Before the canisters are sent out to the field for sampling, they are left to sit undisturbed for a period of time (usually overnight during field campaigns). This way, if any of the cans leak then the leakers are discovered before being shipped out to the field, which would be one less sample that could be collected. After the cans have sat, they are reconnected to the vacuum manifold and individually checked to see if they have held their vacuum. Any leakers are removed and noted, and replaced with known good canisters or replaced and rechecked.

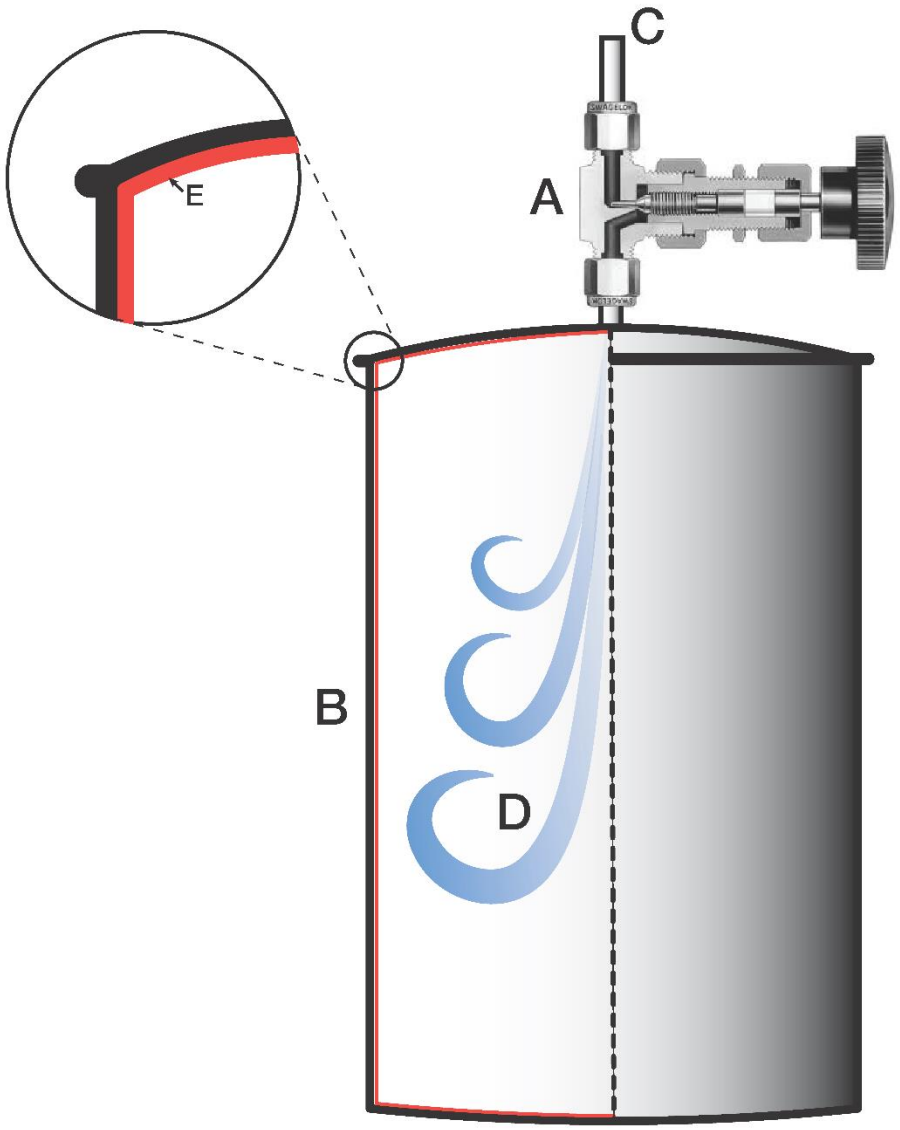

Figure 2.9 Schematic of a Rowland-Blake lab sample canister. The components are (A) a Swagelock SS-4BG valve, (B) the 2L stainless steel body, (C) ¼" diameter inlet, (D) shows air entering the evacuated canister, and (E) the passivated layer inside the canister.

2.7 UCI Rowland-Blake Laboratory Systems

a. Laboratory Gases

All nitrogen and air used in the analytical system is produced by the lab. First, house air is cleaned and dried using two prefilters (glass wool then 100-12 BX) leading to a Wattman 64-02 air dryer. The air stream is then split, one part passing on to a Praxair zero air generator, the other passing on to a Dominic-Hunter nitrogen generator. Hydrogen and helium are purchased in pressurized cylinders at ultra-high purity (UHP) grade.

All gases are further cleaned prior to use in the analytical systems. Each gas is passed through tubing packed with glass wool, graphite, then coarse and fine molecular sieve. Hydrogen and helium are passed through a secondary trap to remove any trace gas contaminants. This secondary trap is identical to the first trap but is continuously submersed in liquid nitrogen, causing any trace gases with vapor pressures lower than those of hydrogen or helium to be trapped in the filter, thereby purifying the desired gases further.

b. Methane System

The methane system utilizes a single Agilent HP 5890 gas chromatograph containing an FID to quantify methane concentrations in a canister sample. The detector outputs its signal to an analog integrator, which calculates the peak height and area under the peak, which are used to calculate the methane concentration.

Canisters are connected to an ultra-torr union that serves as an inlet into the manifold system, where the operator is able to precisely control the pressure of the sample that is released into the GC. For airborne samples which are pressurized on the plane, 400 torr of sample is injected into

the system. The sample is loaded into the manifold system which includes an eight-port Valco switching valve, with two homemade constant volume sample loops attached. The sample fills the vacuum manifold as well as the 5cc sample loop. When the operator is ready to inject, they turn the splitting valve, which closes the inlet of the sample loop and opens it to the GC. There is a constant draw of vacuum which removes any residual sample from the previous canister from the sample loop and injection line. This process allows for precise, repeatable injections of a known volume into the GC.

The carrier gas is nitrogen flowing at a rate of 30 mL/min. The column used in the GC is a 0.9m-long, 1/8" diameter column packed with 80/100 molecular sieve Spherocarb packing (Blake, 1984). Once the sample exits the column it is mixed with a hydrogen carrier gas which carries the sample to the FID. All the data are recorded on a Spectra-Physic Chromjet Integrator.

c. CO/CO_2 System

The Rowland-Blake CO/CO_2 system consists of two Agilent HP 5890 gas chromatographs connected to an inlet and manifold system, and uses helium for the carrier gas. The inlet is the same as on the methane system, and the manifold is similar, but has two sample loops connected to the splitter valve instead of one. Also, for aircraft samples the sample loop is pressurized to 500 torr of sample. After the sample is injected, it is split between two sample lines connected to each GC. The line going to the CO GC first passes through a nickel catalyst heated to 365 °C which converts carbon monoxide in the sample into methane. This fraction of the sample feeds into a GC equipped with an FID, and follows the same process from here as the methane system except the column is 3m long and 1/4" in diameter.

The second aliquot of sample travels to the other GC which is outfitted with a 2m long, 1/8" diameter column packed with 80/100 CarboSphere packing. After exiting the column, the eluents enter a thermal conductivity detector (TCD), which measures the CO_2 concentration. All the data are recorded automatically onto a computer connected to the GCs.

d. VOC System

The Rowland-Blake lab VOC analysis system, or "big system" and it is referred to by the analysis team, consists of a large inlet and manifold, a splitter box, three separate GCs with five capillary columns, and a computer data recording system. Figure 2.10 shows a simplified schematic of the Rowland-Blake lab VOC system.

Canisters are connected to an ultra-torr inlet on the manifold, which has been flushed with helium and evacuated prior to the sample being attached to prevent hold over. For FIREX-AQ, a short column packed with fiberglass wool was added between the canister and inlet to prevent dirt, ash, and large particles that may have been trapped in the canister while sampling in a smoke plume from entering into the manifold. The sample is then introduced into the evacuated manifold, which contains an evacuated canister (called the extra volume canister) to allow for equal volumes of air to be processed. A capacitance manometer reports the pressure inside the manifold and canister. Once the sample volume equilibrates with the manifold and the pressure stabilizes, the sample is passed through the mass flow controller and into the preconcentration loop. The preconcentration loop is a 5 cm^3 stainless steel tubing loop packed with glass beads that is immersed in liquid nitrogen and allowed to equilibrate prior to the sample introduction. The sample passes through a mass flow controller to prevent condensation from the Joules-Thompson effect which could produce liquid oxygen in the manifold line. As the gaseous sample

passes into the preconcentration loop, any gases with boiling points greater than -80 °C will condense onto the glass beads and remain in the loop while the bulk gases (e.g., nitrogen, oxygen) pass through the loop and on to the vacuum pump. This process condenses a 2033 cm^3 volume of sample into the 5 cm^3 volume of the loop. After 2033 cm^3 of sample has been trapped in the sample loop, the inlet is closed and the loop is left under vacuum to pull off any remaining bulk gas. To inject, the liquid nitrogen is removed and a flask of near-boiling water is placed under the preconcentration loop, immersing it. This re-volatilizes any gases that were condensed on the glass beads. The six-port switching valve is actuated, flushing the 5cc loop to the splitter. This reproducibly splits the sample into five separate aliquots, which then pass to the three GCs. GC #1 contains a DB-1 column connected to an FID for C_3-C_{10} compounds, and a PLOT column connected to an FID for C_2-C_7 compounds. GC #2 contains a Restek column, and a DB-5 column connected in series. Both columns are connected to ECDs, and are used for halocarbons and alkyl nitrates. GC #3 contains a DB-5MS column connected to an MSD, which quantifies a variety of compounds.

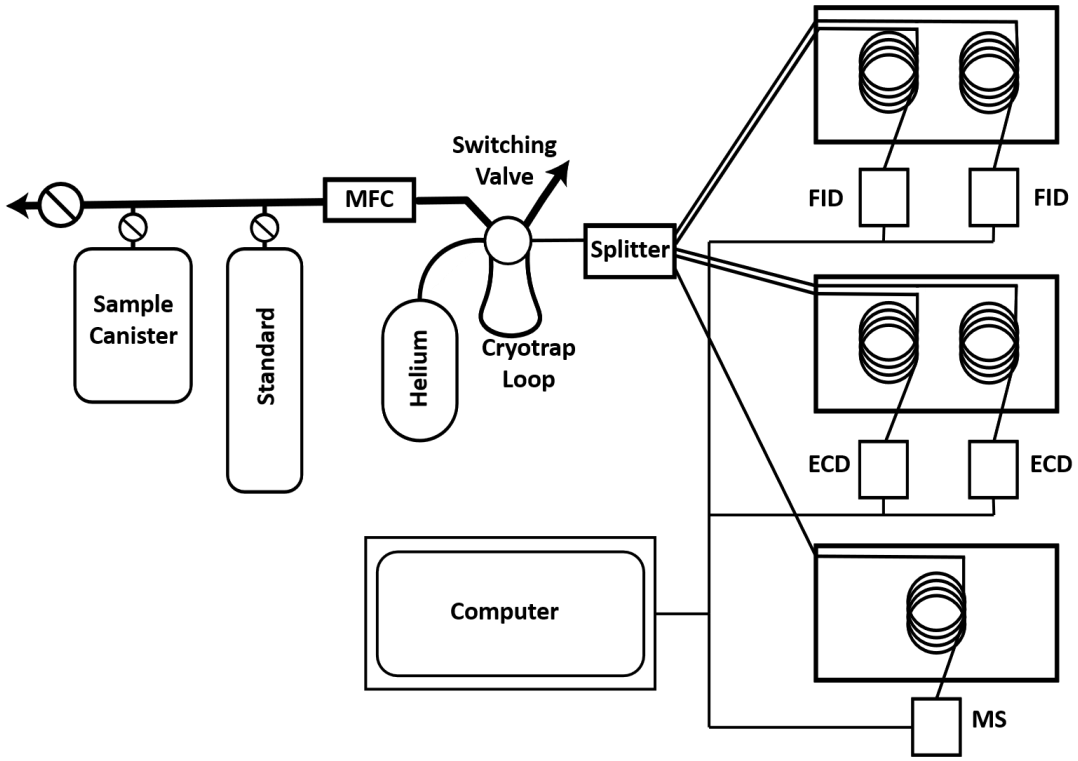

Figure 2.10 Simplified schematic of the Rowland-Blake lab VOC system.

The lower limit of detection (LLOD), precision, and accuracy associated with each trace gas measurement are reported in Tables 2.2 – 2.6. These values and gases are reported for the system configuration (i.e., MSD settings) used during the FIREX-AQ campaign.

C_2-C_5 Hydrocarbons			
Species	LLOD	Precision	Accuracy
Ethane	3	2%	5%
Ethene	3	2%	5%
Ethyne	3	2%	5%
Propene	3	2%	5%
Propane	3	2%	5%
Propadiene	3	3%	5%
Propyne	3	3%	5%
i-Butane	3	2%	5%
n-Butane	3	2%	5%
1-Butene	3	5%	5%
i-Butene	3	5%	5%
trans-2-Butene	3	5%	5%
cis-2-Butene	3	5%	5%
1,3-Butadiene	3	5%	5%
1,2-Butadiene	3	5%	5%
1-Buten-3-yne	3	5%	5%
1,3-Butadyine	3	5%	5%
1-Butyne	3	5%	5%
2-Butyne	3	5%	5%
i-Pentane	3	2%	5%
n-Pentane	3	2%	5%
1-Pentene	3	5%	5%
trans-2-Pentene	3	5%	5%
cis-2-Pentene	3	5%	5%
3-Methyl-1-butene	3	5%	5%
2-Methyl-1-butene	3	5%	5%
2-Methyl-2-butene	3	5%	5%
1,3-Pentadiene	3	5%	5%
3-Methyl-1-pentene & 4-Methyl-1-pentene	3	5%	5%

Table 2.2 Specifications for the Rowland-Blake lab C_2-C_5 measurements.

C_6-C_{10} Hydrocarbons			
Species	LLOD	Precision	Accuracy
1-Hexene	3	5%	5%
1-Heptene	3	5%	5%
1-Octene	3	5%	5%
1-Nonene	3	5%	5%
1-Decene	3	5%	5%
n-Hexane	3	3%	5%
n-Heptane	3	3%	5%
n-Octane	3	5%	5%
n-Nonane	3	5%	5%
n-Decane	3	5%	5%
n-Undecane	3	5%	5%
2,2-Dimethylbutane	3	5%	5%
2,3-Dimethylbutane	3	5%	5%
2-Methylpentane	3	5%	5%
3-Methylpentane	3	5%	5%
2-Methylhexane	3	5%	5%
3-Methylhexane	3	5%	5%
2,3-Dimethylpentane	3	5%	5%
2,2,4-Trimethylpentane	3	5%	5%
2,3,4-Trimethylpentane	3	5%	5%
Cyclopentane	3	5%	5%
Methylcyclopentane	3	5%	5%
Cyclohexane	3	5%	5%
Methylcyclohexane	3	5%	5%
Cyclopentene	3	5%	5%

Table 2.3 Specifications for the Rowland-Blake lab C_6-C_{10} measurements.

Halocarbons & Organosulfur			
Species	LLOD	Precision	Accuracy
CH_3CCl_3	0.05	2%	5%
CCl_4	0.1	2%	5%
$CHCl_3$	0.05	5%	10%
CH_2Cl_2	0.1	10%	10%
C_2HCl_3	0.01	10%	20%
C_2Cl_4	0.005	5%	10%
CH_3Cl	30	2%	5%
CH_3Br	0.1	3%	10%
CH_3I	0.005	3%	10%
CH_2Br_2	0.01	5%	20%
$CHBrCl_2$	0.005	5%	20%
$CHBr_2Cl$	0.005	5%	20%
$CHBr_3$	0.005	5%	20%
CH_2ClCH_2Cl	0.2	5%	20%
C_2H_5Cl	0.1	10%	20%

Chlorofluorocarbons			
Species	LLOD	Precision	Accuracy
Carbonyl sulfide	10	3%	10%
Dimethyl sulfide	0.1	10%	20%
CFC-12	10	1%	2%
CFC-11	10	1%	2%
CFC-113	1	2%	2%
CFC-114	1	2%	2%
HFC-152a	0.1	5%	10%
HFC-134a	0.5	3%	5%
HFC-365mfc	0.2	5%	15%
HCFC-22	1	3%	5%
HCFC-142b	1	3%	5%
HCFC-141b	1	3%	5%
H-1301	0.01	2%	5%
H-2402	0.01	3%	5%
H-1211	0.01	2%	5%

Table 2.4 Specifications for the Rowland-Blake lab halocarbon, chlorofluorocarbon, and organic sulfur measurements.

Alkyl Nitrates			
Species	LLOD	Precision	Accuracy
Methyl nitrate	0.01	3%	10%
Ethyl nitrate	0.01	3%	10%
i-Propyl nitrate	0.01	5%	10%
n-Propyl nitrate	0.01	8%	10%
2-Butyl nitrate	0.01	5%	10%
3-Pentyl nitrate	0.01	5%	10%
2-Pentyl nitrate	0.01	5%	10%
3-Methyl-2-butyl nitrate	0.01	5%	10%

Aromatics			
Species	LLOD	Precision	Accuracy
Benzene	3	3%	5%
Toluene	3	3%	5%
Ethylbenzene	3	3%	5%
m,p-Xylene	3	3%	5%
o-Xylene	3	3%	5%
Styrene	3	5%	5%
Ethynylbenzene	3	5%	5%
i-Propylbenzene	3	5%	5%
n-Propylbenzene	3	5%	5%
3-Ethyltoluene	3	5%	5%
4-Ethyltoluene	3	5%	5%
2-Ethyltoluene	3	5%	5%
1,3,5-Trimethylbenzene	3	5%	5%
1,2,4-Trimethylbenzene	3	5%	5%
Chlorobenzene	3	25%	25%

Table 2.5 Specifications for the Rowland-Blake lab alkyl nitrate and aromatic compound measurements.

Terpenes, Alcohols & Nitriles			
Species	LLOD	Precision	Accuracy
alpha-Pinene	3	10%	35%
beta-Pinene	3	10%	35%
Tricyclene	3	25%	35%
Camphene	3	25%	35%
Myrcene	3	25%	35%
Limonene	3	10%	35%
Furan	3	25%	25%
2-Methylfuran	3	25%	25%
3-Methylfuran	3	25%	25%
Benzylfuran	3	25%	50%
i-Butanal	3	40%	40%
Butanal	3	40%	40%
Acetone & Propanal	3	30%	30%
Methyl ethyl ketone	3	30%	30%
Methacrolein	3	30%	30%
Methyl vinyl ketone	3	30%	30%
Acrolein	3	30%	30%
i-Propanol	3	30%	20%
Nitromethane	3	40%	30%
Acrylonitrile	3	40%	40%
Propylnitrile	3	40%	40%
Methyl acetate	3	40%	40%
Isoprene	3	3%	5%

Table 2.6 Specifications for the Rowland-Blake lab terpenes, alcohols, and nitrile measurements.

2.9 Rowland-Blake Laboratory Standards

Standards are analyzed twice prior to starting sample analysis for the day, and twice at the end of the analysis. Standards are also analyzed after every eight canister samples, and are used to quantify the concentrations of trace gases in each sample. A separate standard is used for each of the three systems, specific to the gas or gases analyzed on that system. The methane system standard is a whole air standard collected in a gas cylinder, and pressurized to 2000 psi in Aldrich Park at UCI. It was then calibrated against the Rowland-Blake lab's primary standard, which was mixed in 1977. The area under the methane peak allows for the calculation of the methane concentration in each sample given the known concentration of methane in the standard. The CO/CO_2 system standard is a 192 ppbv CO and 364 ppmv CO_2 whole air standard collected in the same way as the methane standard. The primary standard for this system was mixed in 1986.

For FIREX-AQ, a standard was created that included some fire-specific trace gases, which allowed for greater precision when quantifying those specific gases on the VOC system. The dopants included in the fire-specific standard (PONT-BC) are listed below in Table 2.7.

Functional Type	Compounds			
Alkene	1-heptene	1-nonene	1-octene	1,4-pentadiene
Nitrile	valeronitrile	allyl cyanide		
Furan	2,3-benzofuran	2-acetylfuran	2-furaldehyde	2-ethylfuran
Terpene	alpha-pinene	3-carene		

Table 2.7 Compounds, grouped by functional type, added as dopants to the PONT-BC laboratory standard. The PONT-BC standard was used to calibrate the Rowland-Blake NMHC system during FIREX-AQ.

These compounds were chosen to dope into the standards because they span different retention times when run through the DB-1 column using the Rowland-Blake lab temperature profiles. The standard is first doped with a known amount of a compound. Then the standard and a sample canister that is known to contain the compound are analyzed on column B, which is the DB-1 column paired with an FID. The key characteristics of an FID are that is a carbon counter, and has a wide range of linearity. Knowing the number of carbons in the dopant (in this case an alkane), the approximate retention time of the dopant compound will be known. Once the peak is found, the response factor is calculated given the height and area of the peak. However, the FID cannot distinguish between coeluted compounds, so if another compound in the sample coeluted with the dopant then the response factor would be inaccurate. To correct for this, the standard is also run on the MSD operating in single ion mode (SIM). Operating in SIM means that the peaks can be positively identified without much worry of coelution unless they have the same mass. However, the MSD suffers from nonlinearity issues. So, the response factor is calculated based on the FID peak, and then used to calculate the concentration of the dopant based on the MSD peak. If the concentration is too great then it means there is a coelution issue in column B.

A fundamental problem that will affect any electron ionization mass spectrometers is the issue of filament degradation, causing a drift in the system response. After field campaigns when thousands of canisters are being analyzed continuously on the NMHC system, the loss of signal response is noticeable as the electron ionization filament degrades, and may need to be replaced during the analysis. To account for this, standards are analyzed every eight samples. The area under the curve for each standard is plotted against the time they were analyzed, and the resulting plot is fitted with a polynomial best fit equation. The response factor for each sample can then be calculated by finding the Y value on the equation at the time (X) that the sample was

analyzed. This corresponds to the area under the curve for a standard collected at that time. Dividing the absolute amount of standard by that area yields the response factor of the detector at that time.

Figure 2.11 shows a sample plot for CFC-11 as measured during the FIREX-AQ deployment. A clear decline in signal (area under curve) is observed as the MSD filament degraded over the course of the sustained, 24/7 use as the thousands of samples collected in the field were analyzed on the system continuously.

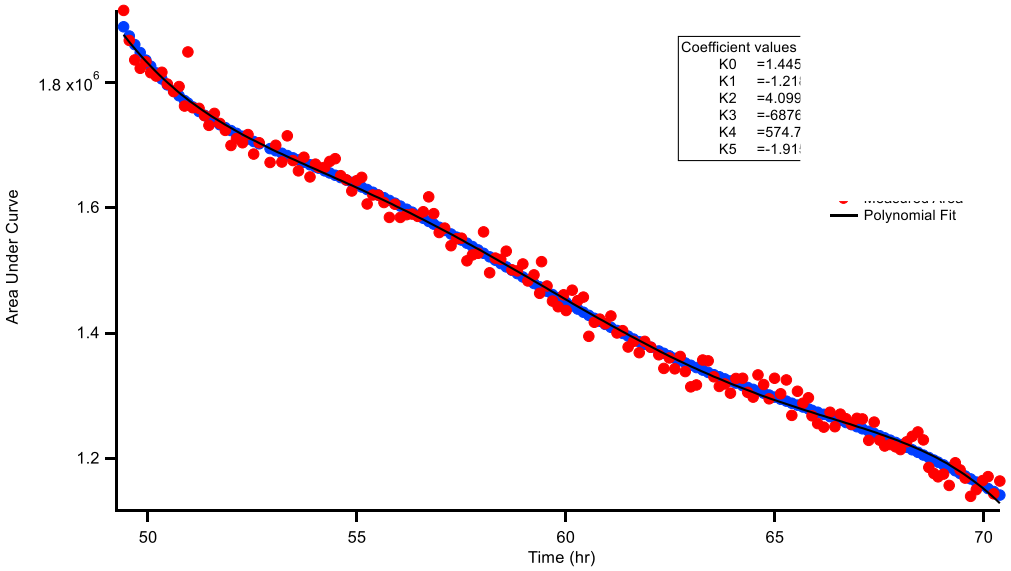

Figure 2.11 Plot of area under the curve for CFC-11 signal in the whole air standard over time. Note the decrease in signal as the filament in the MSD degrades. A sixth-order polynomial equation was used to calculate the best fit, which was used to calculate the response factors given the known concentration of CFC-11 in the standard. This process is repeated for all gases quantified on the MSD.

The response factor (RF) is used to calculate the concentration of the gases present in the sample. To calculate the response factor, the concentration of the gas of interest in the standard,

which is known, is divided by the area under the curve for the gas (Eq. 2.1). The response factor is multiplied by the area under the curve of the peak corresponding to the gas of interest in the sample, which yields the concentration of the gas (Eq. 2.2).

$$RF = \frac{Area_{Calculated}}{[X]_{Standard}} \quad \text{Eq. 2.1}$$

$$[X] = \frac{Area_{Measured}}{RF} \quad \text{Eq. 2.2}$$

3. Smoke Plume Structure

The collective emissions from a fire — VOCs, aerosols, ash, particulates — together is what we know as smoke. Smoke is carried up vertically into the atmosphere via convection from the heat of the fire. Depending on the fire radiative power (FRP), this upward convection can carry smoke all the way to the top of the boundary layer where it is trapped beneath the capping inversion (Wooster et al., 2005). Particularly strong and hot fires can have enough upward convective energy to disrupt and break through this capping inversion, injecting smoke directly into the free troposphere where it can remain for weeks.

Prevailing winds will catch a rising smoke plume and carry it horizontally away from the fire source. As the air parcel containing the smoke equilibrates with the surrounding air temperature its upward momentum will slow and the horizontal component of its velocity will dominate. If the smoke has been injected into the free troposphere, the prevailing winds can carry smoke for thousands of miles from the fire source before it will start to descend. In the boundary layer, geostrophic wind carries the smoke miles downwind of the fire. As the smoke travels it mixes with background air, diluting the plume. The rate of dilution is dependent on the longitudinal wind speed and degree of turbulence in the boundary layer.

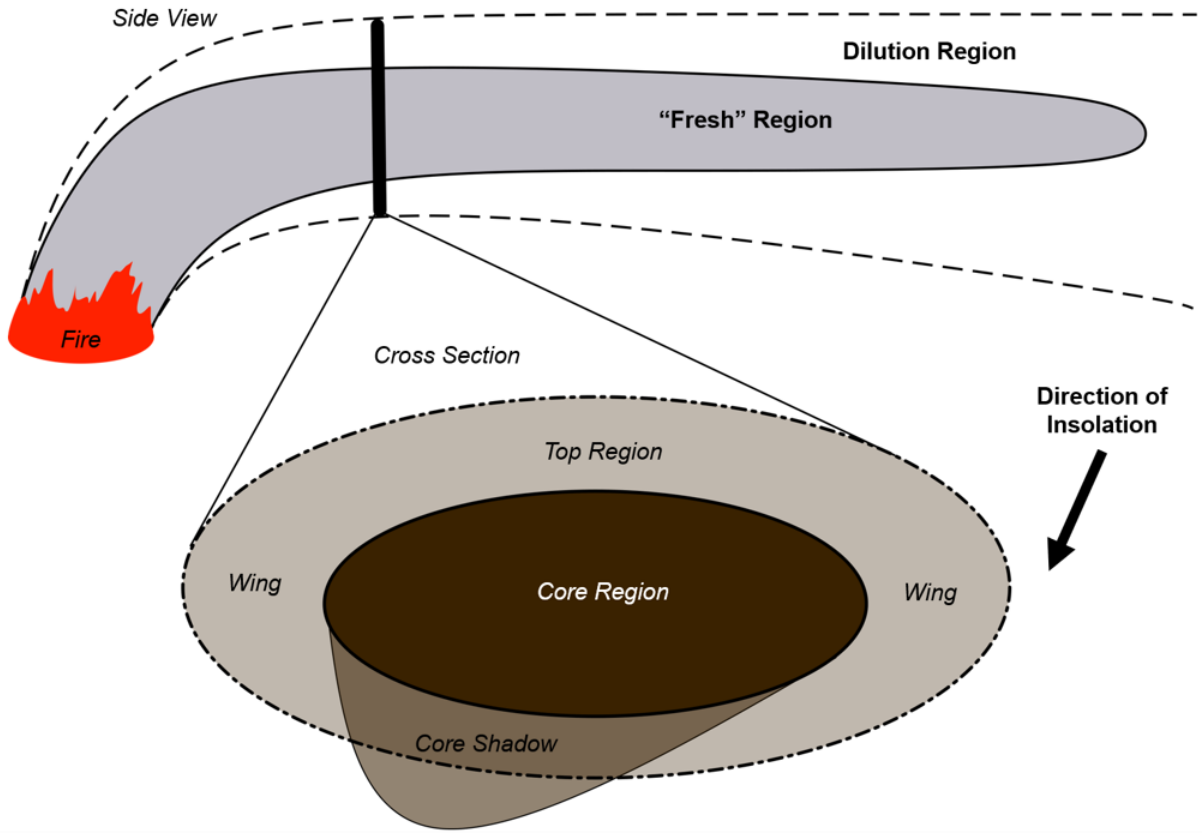

Figure 3.1 Diagram of a typical wildfire smoke plume. Note the heterogeneity of the smoke, and that the particles that make up the plume will block out sunlight, creating the shadow seen in the bottom of the diagram.

The result of the combined effects of meteorology on a smoke plume is shown in Figure 3.1. The structure of a smoke plume is relatively heterogeneous compared to the structure of the atmosphere, and therefore can vary greatly (Wang et al., 2021). There are four key regions of interest with respect to chemistry within a smoke plume.

The center of the smoke plume is interesting from a chemical perspective, as this region contains greatly enhanced NO_x concentrations alongside a plethora of VOCs. In addition, there is little to no photochemical reactions taking place as the particulate matter component of the smoke often nearly or entirely occludes incoming sunlight. The consequence of this is that there is almost no OH formation in the center of the plume. Therefore, the dominant oxidant in this

region is ozone, which is formed via reactions between NO_x and VOCs and can be transported to the center of the plume. However, an interesting phenomenon occurs in the center of the plume where ozone concentrations drop significantly, likely because of the enhanced NO_x concentrations from combustion and the lack of sunlight.

Figure 3.2 shows the flight track for the 8/8/2019 flight to the Williams Flats fire in eastern Washington state. The DC-8 took off from KBOI and intercepted the smoke plume in northern Idaho, and proceeded to follow the plume eastward into Montana. The DC-8 then turned and followed the plume upwind west to the fire source, where it spent several hours sampling a fresh PyroCb that had formed that afternoon above the fire.

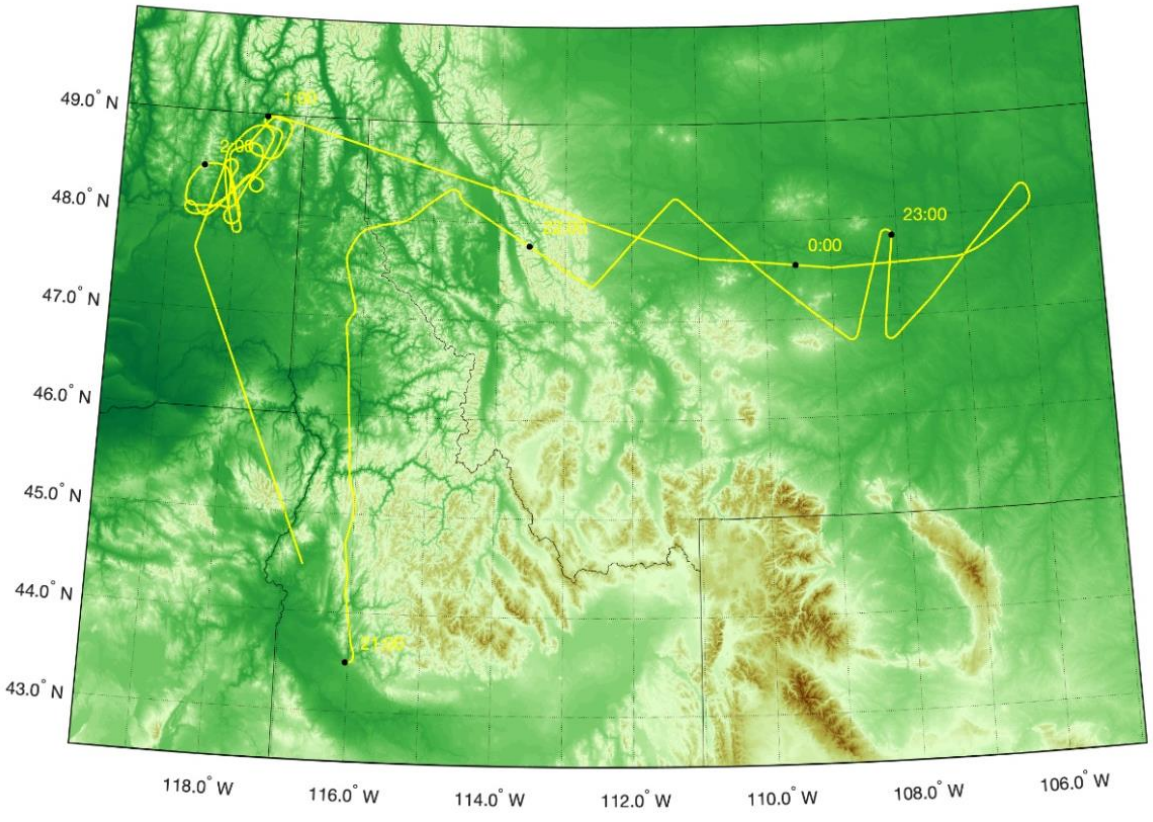

Figure 3.2 Flight track of the 8/8/2019 flight to sample the Williams Flats fire, on the day that a PyroCb formed and was sampled.

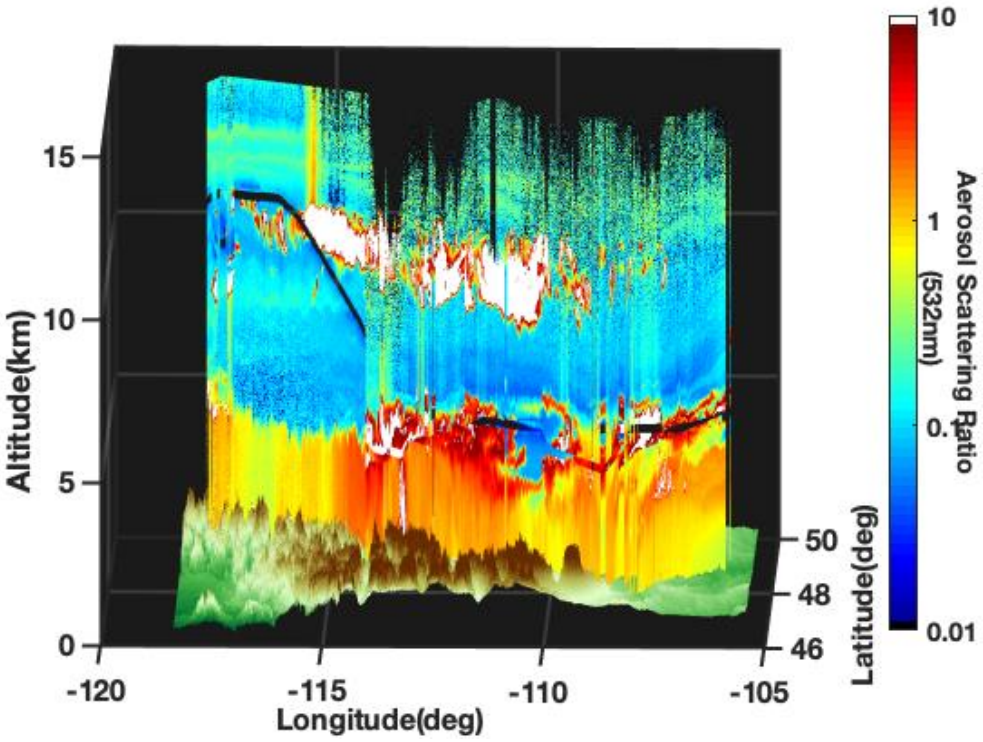

Figure 3.3 3D recreation of the Williams Flats fire smoke plume created using data collected from the NASA Langley DIAL LIDAR instrument. Shown is a section of the 8/8/2019 flight track (black line) through the PyroCb cloud.

Figure 3.3 shows a 3D reconstruction of the Williams Flats fire as it was observed on 8/8/2019 by the NASA Langley Differential Absorption Lidar (DIAL) (operated by Johnathan Hair and Tayler Shingler) aboard the NASA DC-8. The black line through the image shows the DC-8's flight path through the fire plume, which is the red and white blobs which correspond to intense aerosol scattering from the particulate matter in the smoke.

Figure 3.4 shows a section of the flight track from 8/8/2019 and a collection of the images collected by the DIAL instrument as the DC-8 traveled along and through the smoke plume. The pink line through the center of the image represents the DC-8's path. Again, areas of red and white correspond to the smoke plume which has high aerosol backscattering from the particulate matter in the smoke. Note the symmetry in the plume between times 23 and 24, where

the DC-8 did some perpendicular transects through the smoke plume. In this region, the plume appears mirrored where the aircraft turned and repeated a transect, showing the structure of the plume.

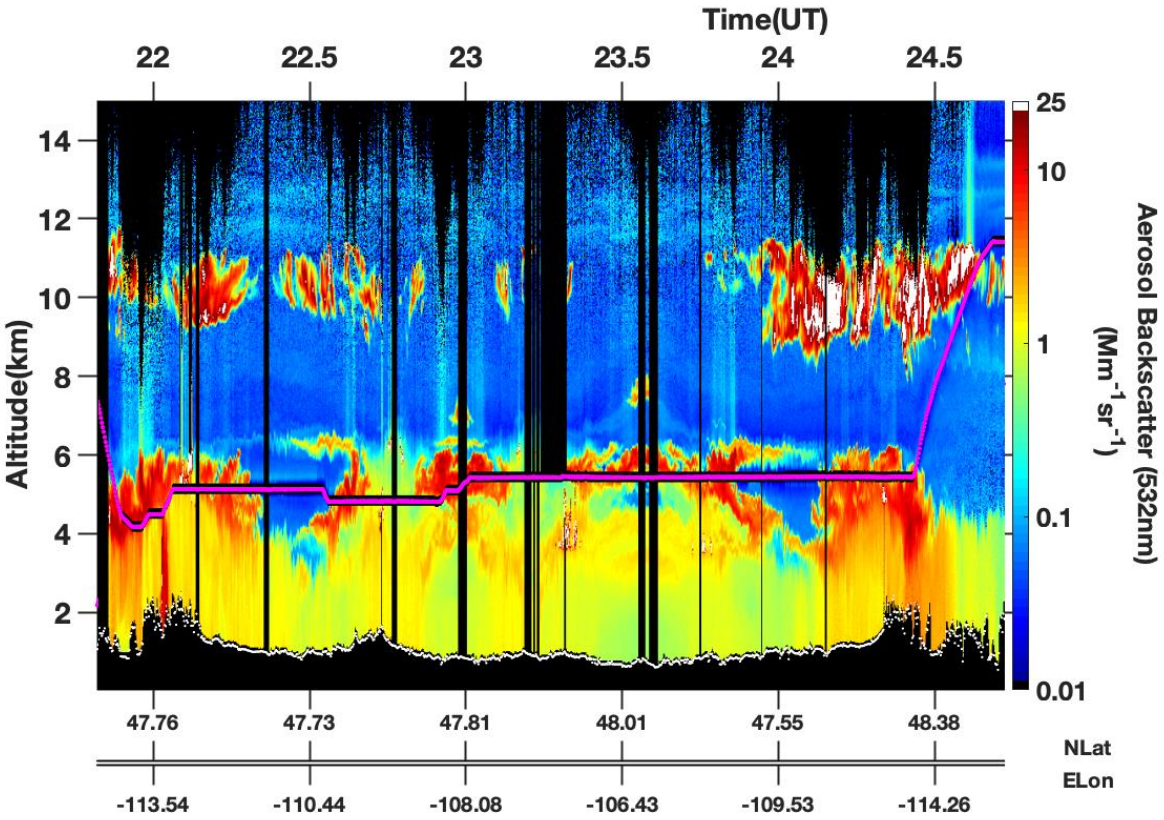

Figure 3.4 A section of the flight track with images collected from the NASA Langley DIAL LIDAR instrument. The DC-8's path is shown as the pink line in the image. The red blobs along the flight track are places where the DC-8 intersected with the smoke plume. Note that the DC-8 was turning and traveling into and out of the plume during this flight, and shown is a compilation of the images collected during the flight.

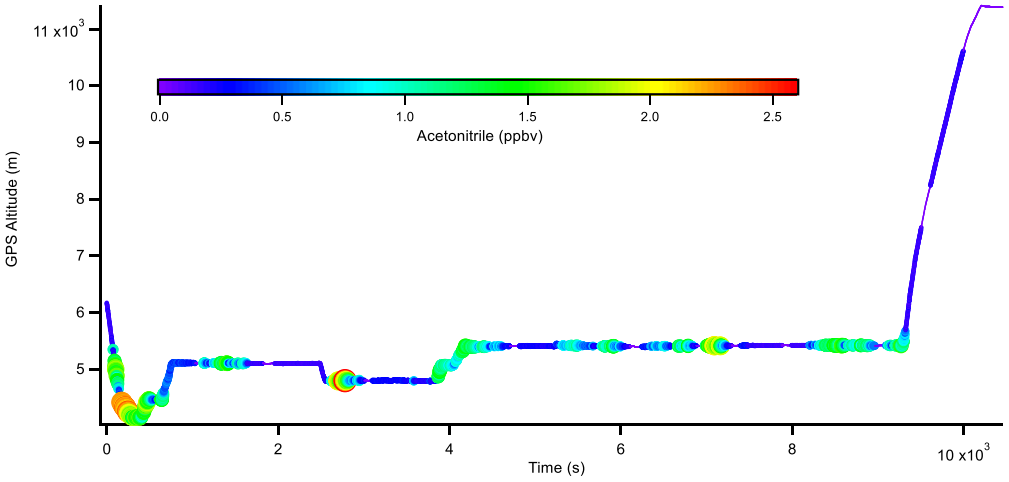

Figure 3.5 A section of the flight track for the 8/8/2019 flight to the Williams Flats fire. The track has been concatenated to show the same section as seen in Figure 3.4. The points are colored and sized by acetonitrile concentration to show where the plane intersected with the smoke plume along the path. Note that where the path in Figure 3.4 intersects with the plume corresponds to areas of enhanced acetonitrile in this figure.

Figure 3.5 shows the same section of the flight track from Figure 3.4, but the points, collected by the onboard PTR-MS every second, have been sized and colored by acetonitrile concentration as it is a fire tracer. The areas of enhanced acetonitrile correspond to the areas in Figure 3.4 where the aircraft passes through the smoke plume. For example, around 23:00 UTC in Figure 3.4 the aircraft passed through a section of the plume, and at the same time in Figure 3.5 there is an enhancement in acetonitrile.

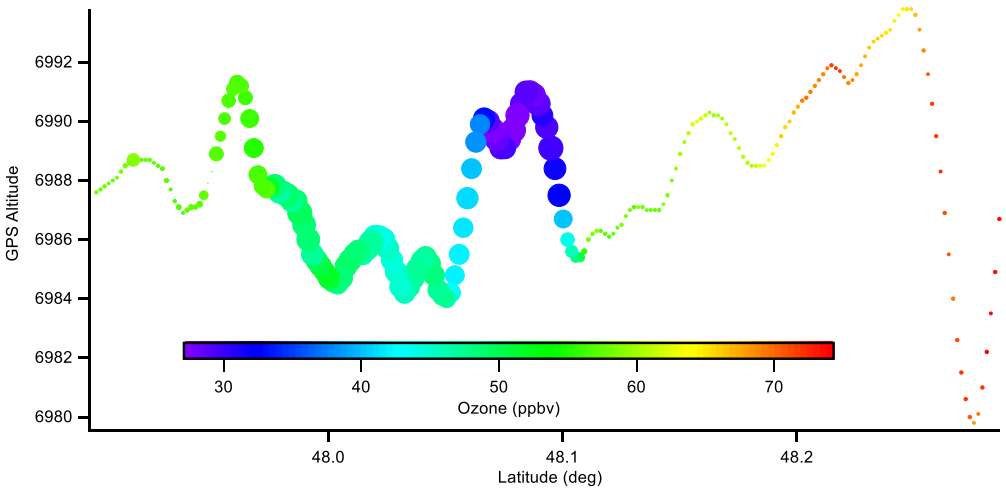

Figure 3.6 A section of the flight path from the 8/8/2019 Williams Flats fire flight that intersected the plume directly. The points are colored by ozone concentration and sized by acetonitrile concentration, so the larger points correspond to the center areas of the plume while smaller points correspond to edges of the plume.

Figure 3.6 shows a small section of the flight path where the DC-8 passed directly through the fire plume. This same section is used in Figures 3.7 and 3.8. The points in Figure 3.6 are sized by acetonitrile concentration, but are colored by ozone concentration. Note that the area where the points are largest (center of the plume) yield a local minimum in ozone concentration, while the edges of the plume denoted by smaller points have much higher ozone concentrations.

In regions of enhanced NO_x, ozone will titrate out from reactions with NO seen in Equation 2.1, which quenches the ozone forming NO_2 and O_2 (Stedman et al., 1972).

$$NO + O_3 \rightarrow NO_2 + O_2 \qquad \text{Eq. 2.1}$$

This means that the two most important oxidants - OH and ozone - aren't present in the centers of very large smoke plumes, with good occlusion of sunlight and enhanced NO_x concentrations. Figure 3.7 shows the plume transect shown in Figure 3.6, and tracks the concentrations in ozone, NO, and NO_2 as the DC-8 passes through the plume. Note that as the aircraft enters the center of the plume the ozone and NO concentrations decrease while NO_2 concentration increases. Note that there is a point where the NO_2 concentration decreases as the ozone and NO concentrations decrease. This is likely an area where the DC-8 exited the plume from underneath but was still occluded from the Sun. This phenomenon will be explored in detail in later chapters.

VOCs in these types of plumes can be transported without being oxidized as long as the plume remains thick enough to block out sunlight and the NO concentration remains enhanced. This phenomenon can effectively extend the life of VOCs that would otherwise react quickly.

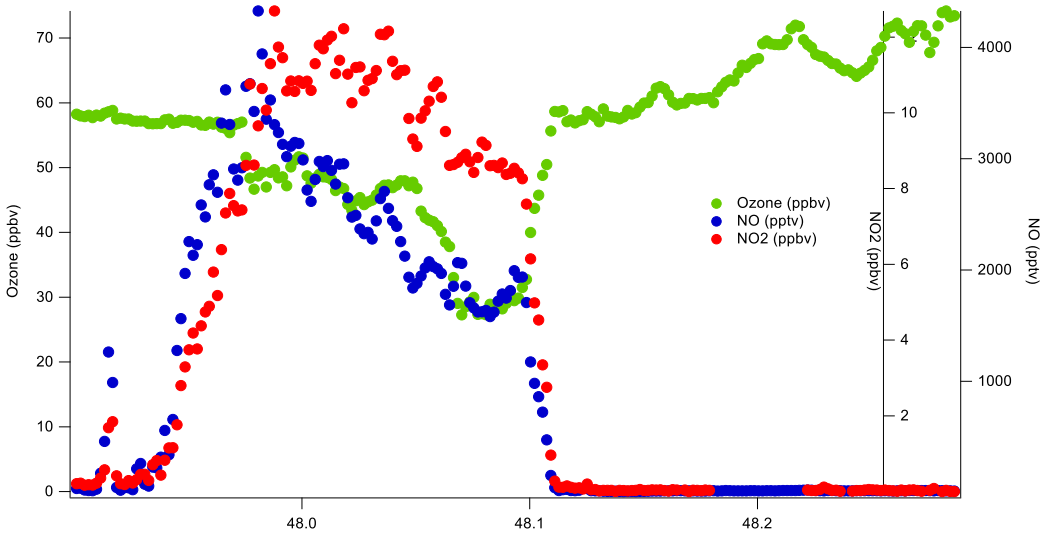

Figure 3.7 A single pass through the heart of the Williams Flats smoke plume. Ozone titration is observed as the aircraft passes through the center of the plume, where ozone and NO decrease concurrently and NO_2 remains enhanced.

The edges, or wings, or the plume are highly variable with respect to chemistry as this region of the plume is the front for smoke dilution into background air. Here, chemical gradients of VOCs form as the plume dilutes and exposes the freshly emitted VOCs to insolation and background oxidants. Ozone is also formed quickly in this region because of the insolation and high NO_x content of the fire plume. Because of the enhanced ozone concentrations, highly reactive compounds such as terpenes will react away quickly, forming a gradient. Figure 3.8 shows this well. Figure 3.8 shows the same section of the 8/8/2019 flight as Figures 3.6 and 3.7. Plotted are the concentrations of ozone with ethane and propene, respectively, as the DC-8 transected the plume. Note that both ethane (lifetime of ~2 months) and NO_2 show enhancements in the center of the plume where ozone is lacking, but go away quickly at the edges of the plume (wings), and are present at background levels outside of the plume. Like in Figure 3.7, there is an

interesting phenomenon where at about 48.1 degrees in latitude, where ozone is at a minimum, there is a significant enhancement in ethane while propene goes away to a local minimum very suddenly. This is likely an area where the DC-8 may have exited the plume from underneath yet was still occluded from insolent solar radiation. Therefore, ozone formation would be limited, but the air would still be exposed to background oxidants.

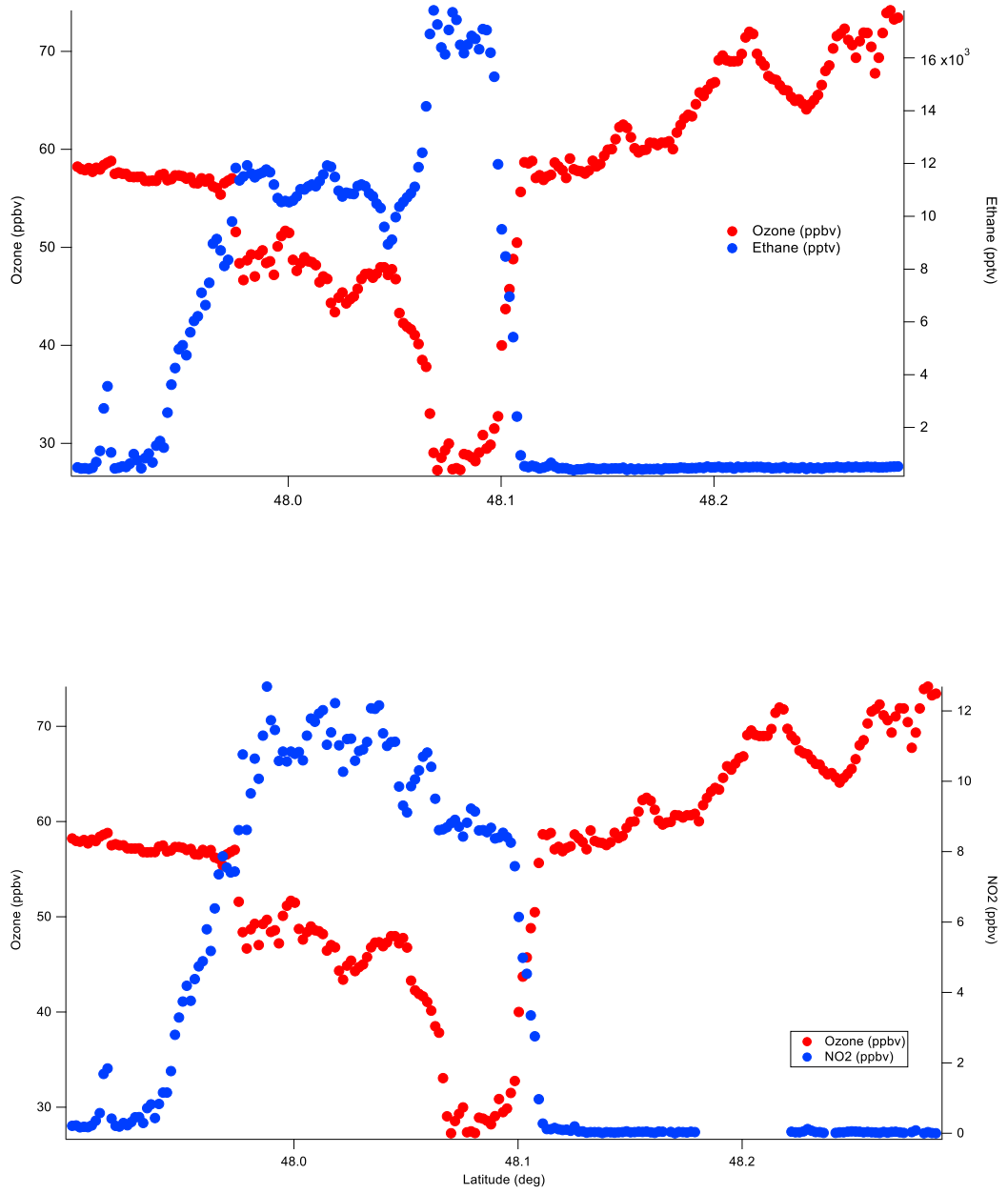

Figure 3.8 Figure showing the lack of ozone in the centermost region of the plume, and how a species that typically reacts away very quickly can survive several hours in the atmosphere. Note the gradient in ethane on the edges of the plume where ozone is enhanced.

The region of the plume with arguably the simplest chemistry is the top of the plume. In this region the smoke is directly exposed to insolation which drives photochemistry with the freshly

emitted VOCs. Typically, in this region there isn't as much dilution as compared to the edges of the plume. If a fire is large enough to break through the capping inversion, then it will mix somewhat with the free troposphere, however because the free troposphere is not nearly as turbulent as the boundary layer this mixing will be minimal. Most western wildfires get large and hot enough to inject a smoke plume right up to the capping inversion layer. However, only very large and hot fires have the convective energy to break through this inversion. The rest will reach this inversion but not break through. The result is a flat-topped plume with almost no vertical dilution with the background atmosphere.

Agricultural fires do not get large or hot enough for their plumes to reach the capping inversion before they start to travel horizontally. These plumes dilute much quicker than those of the larger western fires, and therefore do not have the same well-defined structure. A particularly large or smoky agricultural fire or brush burn may exhibit some fine plume structure close to the fire source, yet this will dissipate quickly in the turbulence of the mixed layer.

The underside of the plume is very similar chemically to the top of the plume. However, there will understandably be significantly less photochemistry from the lack of sunlight reaching the underside of the plume, save for reflection from the surface and scattering from the atmosphere.

The finding that large smoke plumes are heterogenous has implications for local air quality. Typically, very short-lived compounds such as propene will not survive long enough in the atmosphere to travel far from where they were emitted. Therefore, unless the emission source is very close, then these short-lived compounds will not have a direct effect on the local air quality, only an indirect one in the form of the products of chemical reactions or secondary organic aerosol formation. However, it has been shown here that these same very short-lived compounds

can survive in sizeable concentrations much farther downwind, even in sunny environments like the western US, than they normally would if emitted by other means. However, this effect is not likely to play a major role in sourcing very short-lived trace gases to places such as local towns or cities unless they are very close to the fire itself, as eventually the smoke will dilute enough with the background air to allow sufficient sunlight to pass through and contribute to photolytic chemistry in the plume. However, the homogeneity of the smoke plume does offer some interesting chemistry in the form of NOx titration, and the rapid formation of ozone and the resulting gradient at the edges of the plume. These regions provide insight into the different relationships between ozone, NOx, and VOCs within a very small region of space. While these interactions have been studied in depth previously, biomass burning emissions provide a way of observing a wide range of ozone formation dynamics in a short period of time, repeatedly (e.g., Stedman et al., 1972; Sillman, 2002).

4. Results of Positive Matrix Factorization Analysis

Biomass burning is a major source of particulate matter and trace gases in the boundary layer. Particulate matter has been shown to be harmful when breathed, and many of the gases emitted by fires are designated as hazardous air pollutants (HAPs) by the US EPA (Strum et al., 2016). Depending on the meteorological conditions of the area, the smoke from fires can linger for days to weeks as the fire burns, and even after it has died out. This phenomenon is especially obvious in California's Central Valley. The Central Valley is a prime location for poor air quality because of several factors. First, the valley is bordered on the eastern side by the Sierra Nevada Mountain range, which is the tallest, unbroken range in the contiguous US. The western side of the valley is bordered by the coastal range, the Diablo range, and the Klamath mountains. A prevailing ocean breeze from the west means that air masses enter the valley on the western side through gaps in the mountains. The base of the valley is typified by relatively flat, low terrain, and is very dry. This combination means that the boundary layer in the valley is very stable and low, much lower than the western mountain ranges. This creates a "lid" over the entirety of the Central Valley, and air masses that enter the valley are trapped within the mixed layer. Because of these conditions, the Central Valley has consistently recorded some of the worst air quality days in the US, as emissions from cities like San Francisco, Stockton, Merced, and Sacramento are trapped in the mixed layer, which quickly form photochemical smog in the heat and sunlight.

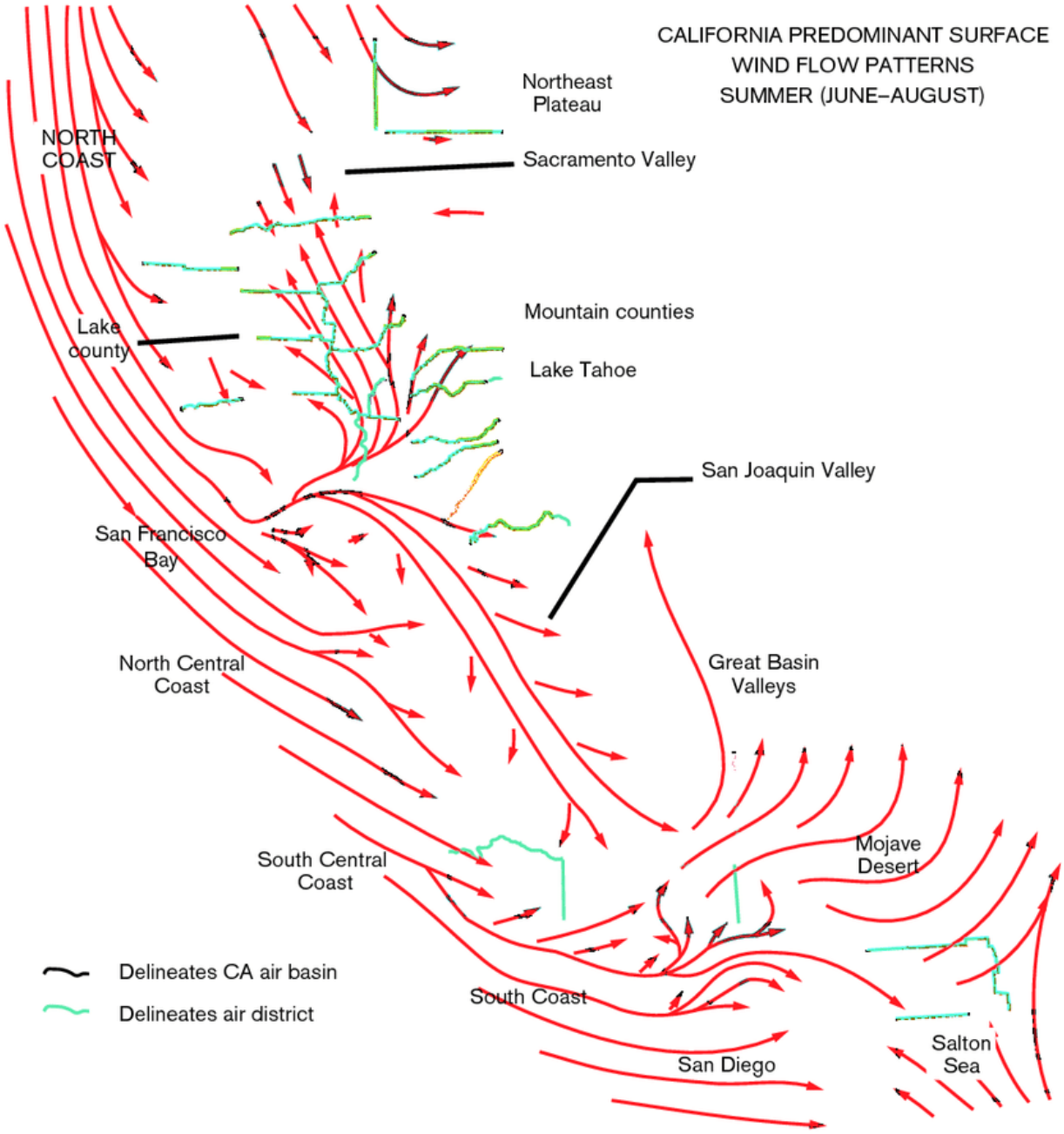

Figure 4.1 Overview of the general air flow patterns in the Central Valley and LA Basin. Note that the overall trend in air flow is from north to south within the valley, with some northerly flow meeting southern flow from the mountains at the north end of the valley (adapted from Bytnerowicz et al., 2015).

Figure 4.1 shows the general trends in air flow coming into and around the Central Valley. In general, air enters the valley through San Francisco Bay and the Sacramento Valley in the north. After entering the valley, the air circulates and ultimately flows southeastwards towards Bakersfield. Local air quality boards have been working to combat conditions that lead to poor air quality by placing restrictions on emitters in the valley, and the restrictions have had some success. Ozone exceedance days in the San Joaquin basin are down from 70 in 1988 to less than 5 in 2012 (San Joaquin Valley Unified Air Pollution Control District, 2013). However, another intrinsic aspect of California and the western US is the presence of wildfires. While air quality boards may be able to control emissions from most sources in the Valley, wildfires are completely out of the control of any regulations. As stated in the introduction, wildfires have been increasing in frequency and severity in the past decades, and the Klamath mountains and Sierra Nevada range see their fair share of fire activity. Smoke from fires spills into the Valley and permeates throughout the valley's mixed layer, where it can remain for weeks. The influx of nitrogen oxides and trace gases significantly degrades local air quality. Also, as the emissions from wildfires vary and are not yet well constrained, the effects of these emissions on local and regional air quality are not well understood as the interactions of urban air with fire smoke can change the atmospheric chemical balances. Therefore, it is critical to gain an understanding of the types and quantities of trace gases that are being introduced into the valley from biomass burning.

The NASA DC-8 is based at the NASA Armstrong Building 703 in Palmdale, CA. The aircraft is used for a variety of campaigns, which also includes flights for the NASA Student Airborne Research Program (SARP). Campaign checkout flights and SARP flights are conducted throughout the LA Basin and Central Valley. Also, typically the first flight or transit for a field

campaign includes a thorough sampling run throughout these air basins. The data collected during these flights is shared with the California Air Resources Board. Any data collected during a NASA funded campaign (SARP included) are publicly available. There is an archive of public data spanning over a decade of measurements of air quality in the Central Valley.

In 2008, the NASA ARCTAS campaign was conducted aboard the DC-8 to study wildfire emissions in boreal Canada. However, as stated earlier, flights were conducted throughout the Central Valley prior to the transit to the Edmonton, Canada FBO. Coincidentally, the Klamath Complex Fire was actively burning during these flights, and the Central Valley was filled with fresh and aged smoke mixing with urban emissions, similar to the conditions observed during the WE-CAN flight. Figure 4.2 outlines the five flights that were conducted in and around the Central Valley and LA Basin regions of California. In particular, flights thirteen and sixteen spent a great deal of time in the Central Valley within the boundary layer during the height of the Klamath Complex fires.

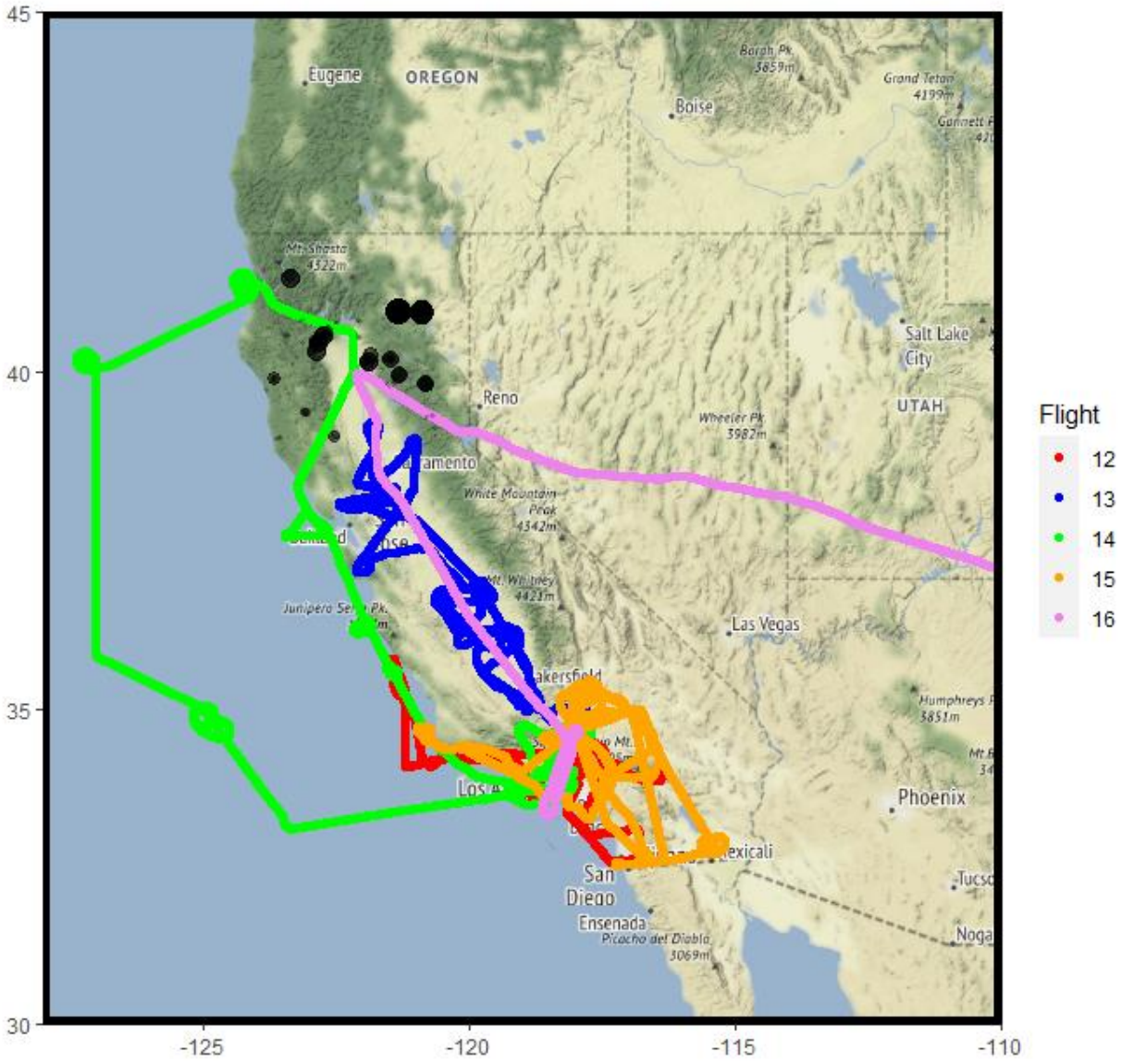

Figure 4.2 Flight tracks during the summer 2008 ARCTAS flights through the CA Central Valley. Note that flight 16 was the transit flight to the Edmonton, Canada FBO.

Also, in 2016 NASA flew the KORUS-AQ campaign, which utilized a full suite of instruments aboard the DC-8 to study air quality in Korea. Immediately following the campaign, the DC-8 was used for two SARP flights with the full instrument payload. The difference between these flights and those of WE-CAN and ARCTAS is that only one fire was actively burning during the 2016 SARP flights. The fire was a relatively small (compared to the Klamath and Mendocino complex fires) brush fire north of Santa Barbara, and the prevailing winds for the day carried the smoke out over the ocean. So, the Central Valley was nearly completely devoid of smoke during the flights. Figure 4.3 outlines the two flight tracks for the 2016 NASA SARP flights. The first flight was conducted around the LA Air Basin with many missed approaches, while the second flight was conducted throughout the Central Valley, with a few missed approaches. The second SARP flight offered an opportunity to use the data as a background for emissions in the Central Valley. The data collected on this flight could then be compared to the data collected during WE-CAN and ARCTAS to examine how emissions from fires affect air quality in the Central Valley, and how they interact with urban emissions.

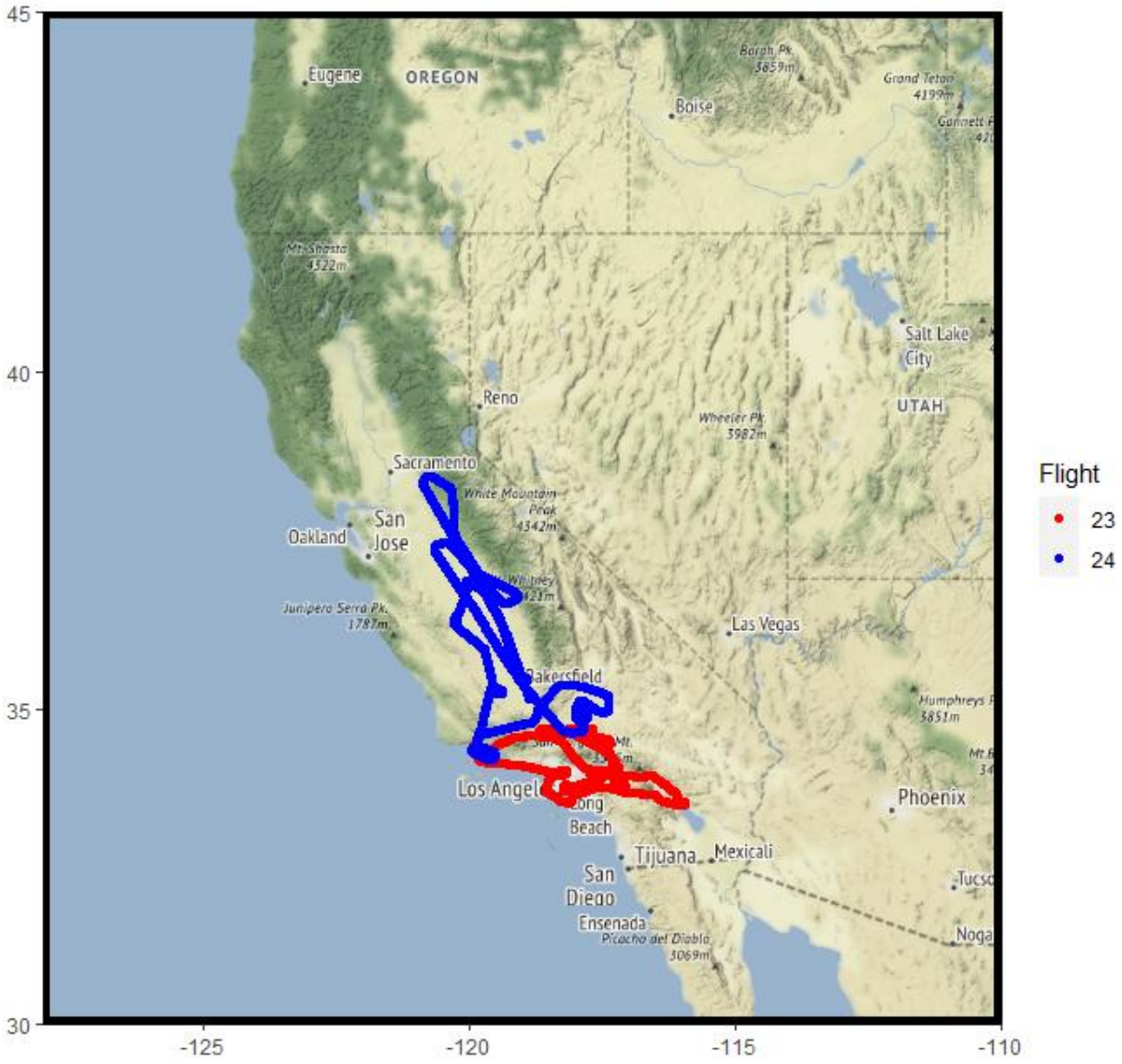

Figure 4.3 Flight tracks for the 2016 NASA SARP flights in the LA Basin and Central Valley.

The instrument suites between all three campaigns contained a few compatible measurements. For trace gas analysis, the compatible instruments of use are the NCAR TOGA and UCI WAS systems, which have been shown to have good agreement between both the ARCTAS and SARP flights. The NCAR TOGA was present on WE-CAN and SARP, while WAS was present on ARCTAS and SARP.

Figure 4.4 Flight tracks for the 2019 FIREX-AQ flight in the LA Basin and Central Valley before the transit to Boise, ID.

Finally, in 2019 the FIREX-AQ was launched to study fire emissions in the western and southeastern US. On July 7th, 2019, the DC-8 departed Palmdale airport and conducted a research flight around the LA Basin and throughout the Central Valley to collect air quality data that would be passed on to the California Air Resources Board. Fortunately, the conditions during this flight were comparable to those observed during the 2016 SARP flights, and therefore the FIREX-AQ samples serve as an excellent comparison of background Central Valley emissions during a non-smoke-impacted period to the smoke-impacted periods observed during ARCTAS and WE-CAN. Figure 4.4 shows the flight track for the transit flight as the DC-8 traveled through the LA Basin and Central Valley before transiting to Boise, ID.

Figure 4.5 shows the locations of samples collected by the WAS and TOGA instruments that were used in the PMF analysis. Only samples collected inside the Central Valley Air Basin and within the boundary layer (calculated for each flight day) were included in this analysis.

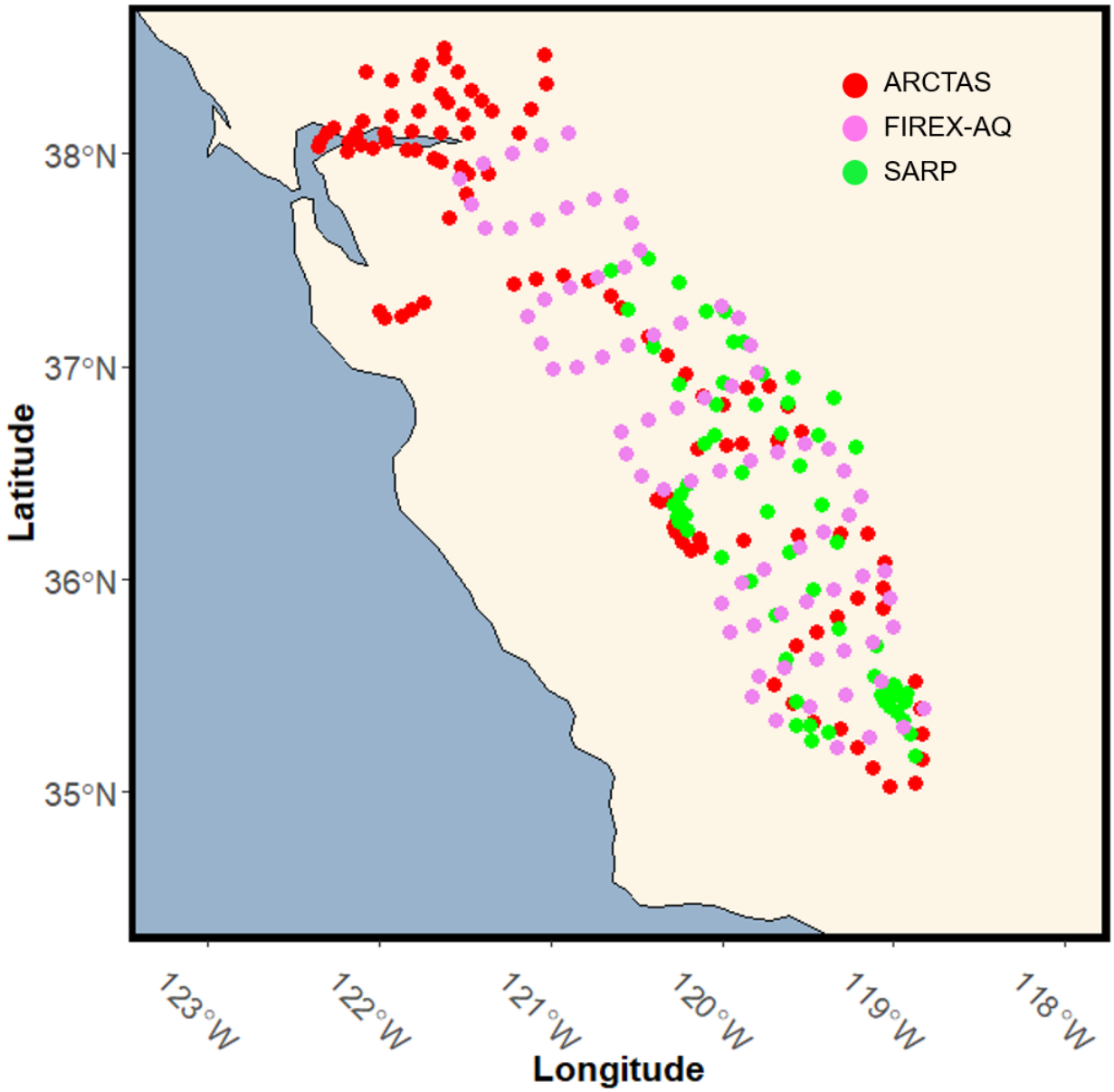

Figure 4.5 Map of the CA Central Valley region. Plotted are the locations of each sample collected during each campaign that was within the central valley, and within the boundary layer calculated for each flight day.

Figure 4.6 shows the NASA Worldview satellite imagery on the days the Central Valley was sampled during 2008, 2016, and 2019. The images from 2016 and 2019 show that the Central Valley was visually clear of any smoke influence, and there were no MODIS hotspots or fires

detected in or around the Central Valley on those days. In 2008, however, the Central Valley was heavily impacted by smoke from large wildfires in the northernmost end of the valley. The smoke from these fires drifted south following the prevailing air currents (Figure 4.1), bringing smoke into the southern end of the valley. Here the smoke would have mixed with local anthropogenic emissions, and given the time it would have taken to reach the south end of the valley the smoke would have photochemically aged to form secondary organic aerosol and trace gases.

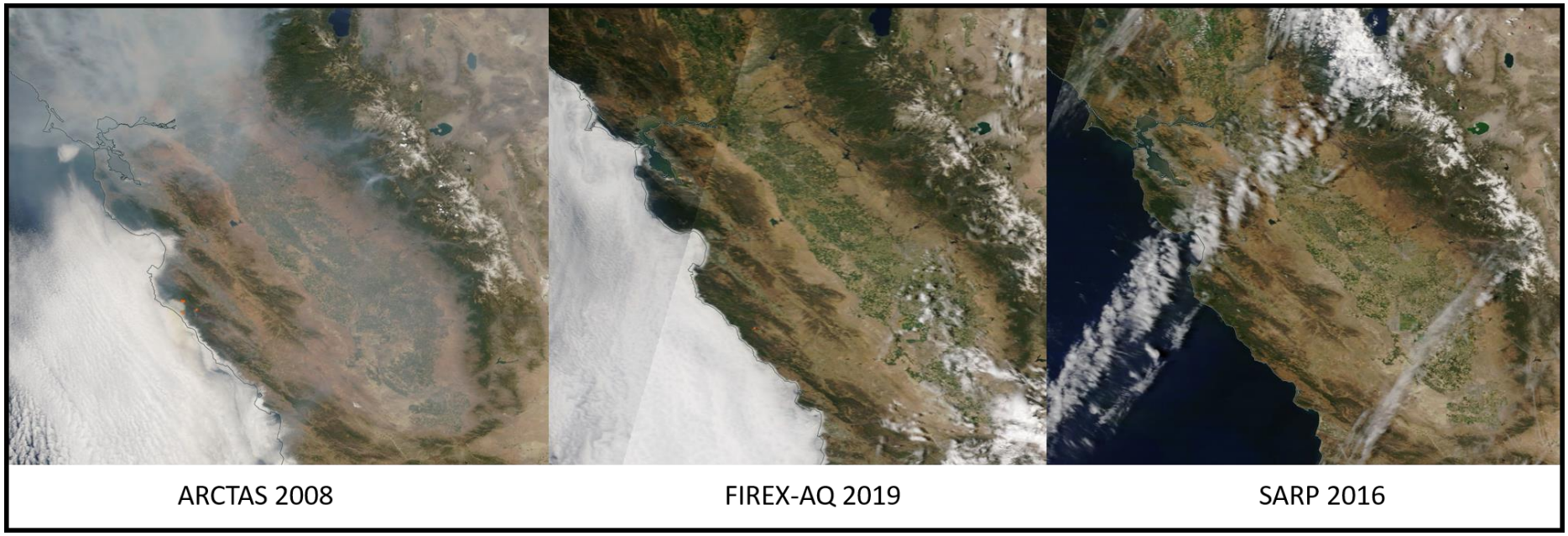

Figure 4.6 NASA Worldview Satellite images of the California Central Valley in summer 2008, 2016, and 2019. The small orange dots in the 2008 image are fires detected by the MODIS instrument. Note that the Central Valley is heavily impacted by smoke in 2008, and is not impacted in 2016 or 2019.

Figure 4.7 shows the ambient trace gas concentrations observed in the Central Valley during each campaign. Here the general trend in air flow within the valley is clear, as the majority of emissions are present in the southeastern edge of the valley. Note that there are also major emission sources in this area – Bakersfield, Oildale, Visalia, Tulare, and Fresno are all located in this area and are home to petroleum and oil and natural gas sources. However, given the lifetime of some of the anthropogenic tracers one would expect to see these tracers prevalent everywhere in the valley if there were no prevailing winds. Dichloromethane does exhibit this trend during FIREX-AQ, which suggests that the winds may have been weaker on that day, since during ARCTAS and SARP dichloromethane enhancements are observed in the southeastern edge despite dichloromethanes relatively long lifetime in the boundary layer (~5 months). Fire tracers such as carbon monoxide and ethyne were significantly enhanced during ARCTAS at the northernmost end of the sample area, which was likely caused by very fresh fire emissions being sampled there as a fire was actively burning just west of Sacramento. Benzene was also enhanced in this area, suggesting that fires may be a large source of benzene in the Central Valley.

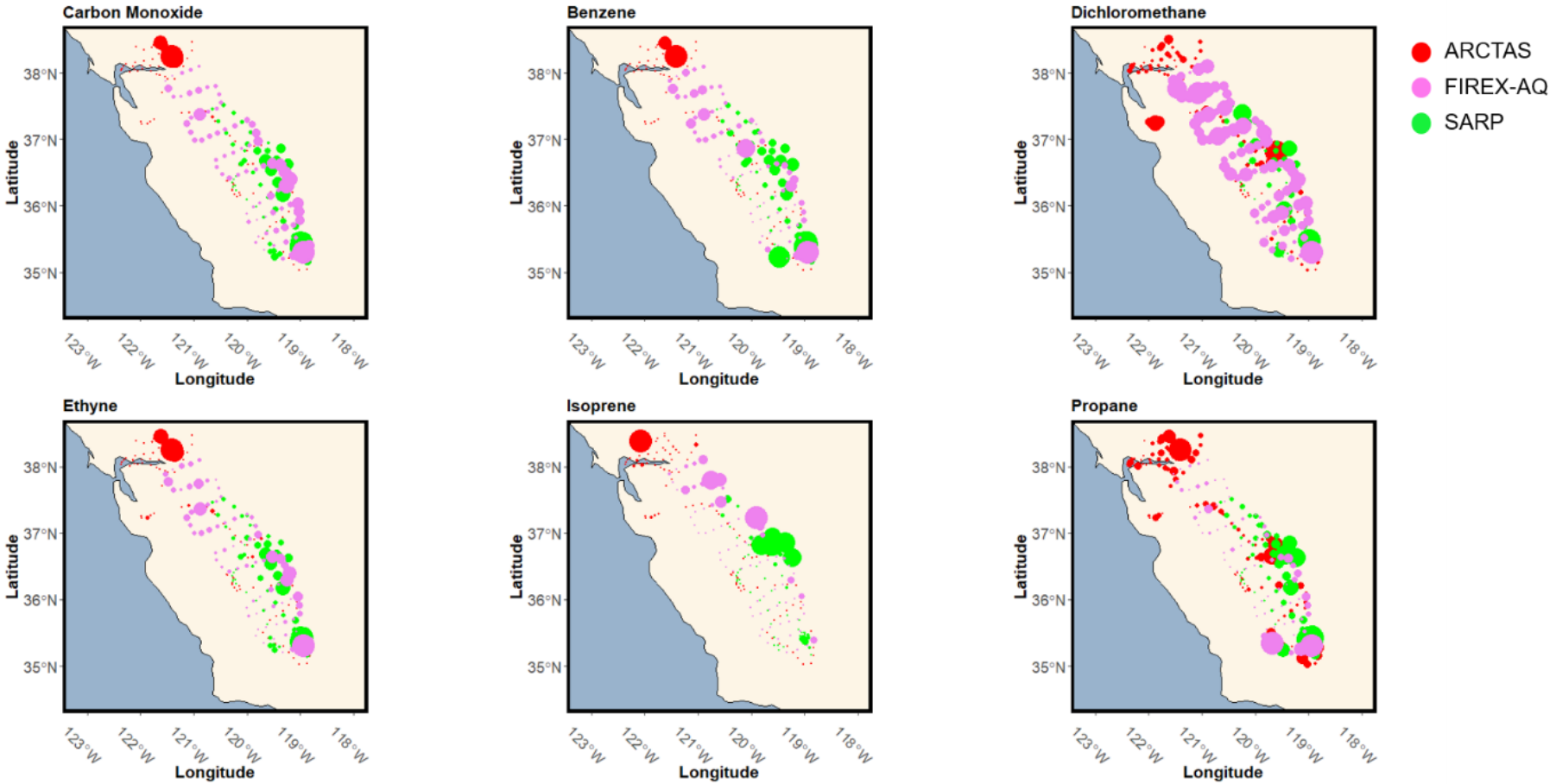

Figure 4.7 Maps showing the flight tracks for each campaign. The points are sized according to the observed trace gas concentration.

4.1 Positive Matrix Factorization Theory

As trace gases are emitted and mix with ambient air, it can be difficult to determine the initial amount released from the emission source. And, unless the trace gas is emitted from a specific source it can be even more difficult to attribute a species to a specific source. For example, dimethyl sulfide (DMS) is almost exclusively emitted from oceanic sources. Therefore, if enhanced DMS concentrations are observed near the ocean then it is safe to assume that the ocean is the source of the DMS. However, benzene for example can be emitted from a variety of sources - car exhaust, petroleum refining, and fires. So, if a well-mixed air mass is sampled and found to contain enhanced concentrations of benzene, then it is difficult to know the benzene source. In the case of studying fire emissions, it can be difficult to determine exactly the amounts of trace gases emitted from a fire versus from nearby sources, unless the smoke being sampled is very fresh. This makes studying the mixed emissions from fires and urban sources like those observed in the Central Valley difficult.

One approach to this issue is a process called positive matrix factorization. In essence, positive matrix factorization (PMF) is a receptor model - a mathematical technique which can deconvolute a mixed system into its original sources and attribute the correct amount of each constituent to each source. So, given a mixed air mass, positive matrix factorization is able to attribute concentrations of each species in the air mass to a given source. The key word there is "given" sources. PMF is not magic, and cannot define the sources, or even the number of sources that contributed to the air mass. Like any tool, proper use and knowledge of the tool influences how well it functions.

The dataset that goes into the PMF model is essentially a two-dimensional matrix of j by k dimensions, representing the number of species measured and the number of observations (in this case, number of trace gases quantified by the number of samples collected). The model deconvolutes this matrix by first solving chemical mass balance equations based on the measured concentrations of each species and the number of factors, or sources, that contributed to the mixing in the dataset. By definition this makes PMF a receptor model, as mass conservation is assumed and the contributions from the sources are non-negative (Paatero 1997; Hopke et al., 2000). The chemical mass balance equation is shown in Equation 4.1 (Norris et al., 2014):

$$X_{j,k} = \sum_{i=1}^{p} g_{j,i} * f_{i,k} + e_{j,k} \qquad \text{Eq. 4.1}$$

A function called the objective function, Q, represents how well the model fits to the measured observations (Norris et al., 2014). The objective function is shown in Equation 4.2:

$$Q = \sum_{j=1}^{n} \sum_{k=1}^{m} \left[\frac{e_{j,k}}{u_{j,k}} \right]^2 \qquad \text{Eq. 4.2}$$

The PMF model reports two types of Q, Q(robust) and Q(true). Q(true) is simply the result of calculating the objective function for all points. Q(robust) is the result of calculating the objective function excluding points with residuals with values greater than four. Additionally, there is the expected Q value (Qexp) which is the result of calculating the objective function for an ideal case. PMF defines Qexp as (# of strong species * # of observations) - ((# of factors * # of strong species) + (# of factors * # of observations)) (Norris et al., 2014). A representation of

how well the model fits the observations can be gained by dividing Q(true) by Qexp. If the model fits perfectly then Q(true)/Qexp should equal one. However, there is uncertainty inherent in any measurement, and therefore Q(true)/Qexp should always be slightly greater than one. If Q(true)/Qexp is much larger than one, it indicates that the uncertainties have been underestimated, and/or there aren't enough factors included in the model (Norris et al., 2014; Polissar et al., 2001). Conversely, if Q(true)/Qexp is less than one that indicates that the uncertainties given in the original data are likely overestimated (Zhang et al., 2011).

The PMF model relies on an iterative step process called the multilinear engine (ME) (Norris et al., 2014). The ME solves the objective function in an attempt to minimize Q. Each time it performs an iteration and solves the objective function, the result is analyzed to determine if it is greater or less than the previous result (Paatero 1999). The process follows the minimization of Q along the path towards a global minimum. Typically, the model is run many times (100 times is recommended for final results) to give the ME the best chance of finding the global minimum (Norris et al., 2014).

4.2 Model Configuration

The first step prior to running the PMF model is to prepare the data for entry into the model. Ideally, because the PMF model relies on matrix transformations, the input data will be close to a square matrix (j ~= k; i.e., the number of species is relatively equal to the number of measurements, and there are not an overwhelming number in favor of either). The raw datasets

from the archive contain some missing data as a result of instrument malfunctions, calibrations, and measurements below the limit of detection, for example. The model cannot handle missing values, so these must be replaced with an appropriate substitute that won't skew the data. Rows in the dataset that contained only missing values for any reason were removed so that they did not influence later preprocessing methods. Any species that were missing more than 25% of their observations for any reason were removed from the dataset. According to the PMF handbook's recommendations, any missing values caused by calibrations or instrument malfunctions (-999 values) were replaced with the species mean (Norris et al., 2014). Data points which had missing values because a gas was below the LLOD (-888 values) were replaced with one-half of the reported LLOD value. In addition to the observations data set, the PMF model requires a dataset containing the uncertainties for each measurement, which it uses to calculate and scale the residuals later.

When calculating the uncertainty values, it is important to keep track of missing values in the original data, and why they were missing (i.e., calibration vs LLOD value). Missing values caused by calibrations or malfunctions (-999 values) in the observations were assigned an uncertainty of four times the calculated uncertainty, and missing values caused by measurements below the LLOD were assigned an uncertainty value of $5/6^{th}$ of the LOD. The uncertainty values for the rest of the dataset (valid observations) were calculated using the uncertainty values provided in the archived data, and the uncertainty equation from Polissar et al., 2001 as recommended in the PMF handbook (Norris et al., 2014).

The datasets are then fed into the model. The model used for this analysis is the EPA PMF v5.0, which uses the second development of the ME, and is often referred to as PMF-2. The EPA PMF v5.0 will hereon be referred to simply as PMF or the PMF model. When entering data into

the model program there are options to assign ‘weak’ or ‘bad’ labels to certain compounds, which tells the program to assign a greater uncertainty to these compounds when interpreting the model (Norris et al., 2014). Any compounds that had a signal-to-noise ratio less than two were designated ‘weak’, compounds with a signal-to-noise ratio less than one were designated as ‘bad’. Compounds designated as ‘bad’ were not included in the final data as per the model. Any compounds with residuals greater than five were also designated as ‘weak’.

4.3 *In Situ* Observations & Positive Matrix Factorization Results

As described in the introduction, data from three airborne campaigns were compared to analyze the effects of biomass burning emissions on regional air quality in the California Central Valley. The datasets were first limited to observations collected within the boundary layer, for which the height was calculated for each flight day. Trace gas measurements taken within the boundary layer across the three campaigns show enhancements in certain trace gases during biomass burning events, while other gases remain consistent across the campaigns.

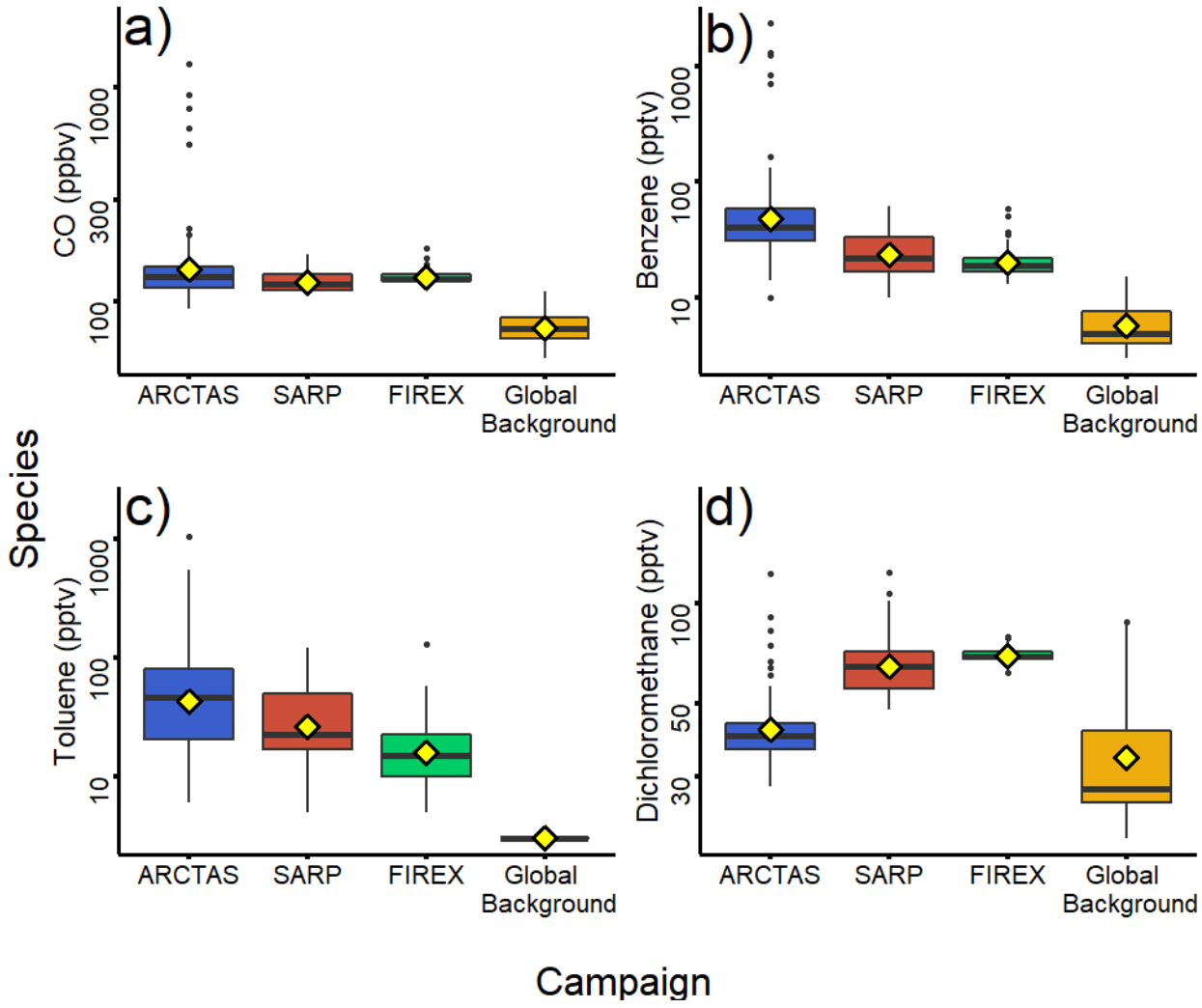

Figure 4.8 Ambient concentrations of trace gases measured throughout the CA Central Valley within the boundary layer during ARCTAS, WE-CAN, and SARP. The "global background" is represented by measurements collected during the summer ATom-1 campaign within the boundary layer in the northern hemisphere.

Figure 4.8 shows enhancements in trace gases observed during the three campaigns. Carbon monoxide, benzene, toluene, and dichloromethane were chosen because carbon monoxide is emitted heavily during biomass burning, benzene and toluene have multiple different sources including biomass burning, and dichloromethane is recognized as an exclusively anthropogenic tracer. The measurements from the four campaigns are compared to measurements taken during the NASA Atmospheric Tomography-1 (ATom-1) campaign, which

reports trace gas measurements from remote areas around the Earth during the summer months (July - August 2016) which is consistent with the peak of biomass burning events in the northern hemisphere. The data from ATom-1 are included as a reference for baseline concentrations of the trace gases, while the SARP and FIREX-AQ data act as a reference for the background concentrations of the trace gases in the Central Valley. Figure 4.8 shows that carbon monoxide, benzene, and toluene are enhanced during the biomass burning year (ARCTAS 2008), while dichloromethane, an urban tracer, shows only mild enhancement during non-biomass burning years (SARP 2016 and FIREX-AQ 2019). Therefore, fires appear to be contributing to the enhancement of HAPs and other trace gases in the Central Valley. However, the exact amount of each species that the fires are contributing is difficult to determine. PMF will be used to find the number of factors contributing to the enhancement of HAPs in the Central Valley, and the degree to which fires influence the ambient trace gas concentrations.

The PMF model was run under several different conditions for each campaign to find the ideal model configuration that would produce the most accurate results. The final results were gathered after performing one hundred model runs to give the model the best chance of finding the global minimum in the objective function. The final model results were also analyzed using the bootstrapping and displacement methods included in the EPA PMF program. The error estimation methods show that there are two results to the model, a mathematically robust result and a physically reasonable result (Simpson et al., 2011). The PMF model tends to favor fewer factors as they will provide more mathematically robust results. However, fewer factors may not be physically reasonable given the context in which the samples were collected, and some reasonable scientific intuition is necessary to interpret the data. The final results indicate that the Central Valley air mass is composed of four factors when impacted by smoke, and two factors

when not impacted by smoke. In the case of smoke-impacted years, a four-factor solution was the most reasonable solution given emission sources in the Central Valley, and because it showed the best error estimation results. The two-factor solution for the non-smoke years was the more mathematically robust result, whereas a three-factor solution may seem to be more reasonable given the number of potential emission sources present in the Central Valley. However, in the three-factor solutions there was significant (> 40%) factor splitting observed, and no reasonable new factors were observed. Therefore, the two-factor solution was chosen for these results. Reported here are the results of the four-factor solution for the smoke-impacted years and the two-factor solution for the non-smoke-impacted years. The identities of each factor were determined in two parts: first, by examining the composition of each factor's trace gases, and second by examining where the trace gas enhancements occurred geospatially for each factor.

For biomass burning-impacted years, the four factors were found to represent fresh smoke, mixed smoke, oil and natural gas emissions, and the regional anthropogenic background which includes long-lived anthropogenic gases and traffic emissions. Figure 4.9 shows maps of the calculated contributions from each factor for each year. The oil and natural gas factor was designated as such because of the enhancements in contributions to the factor located near oil fields like Oildale, CA and large urban areas where natural gas processing take place.

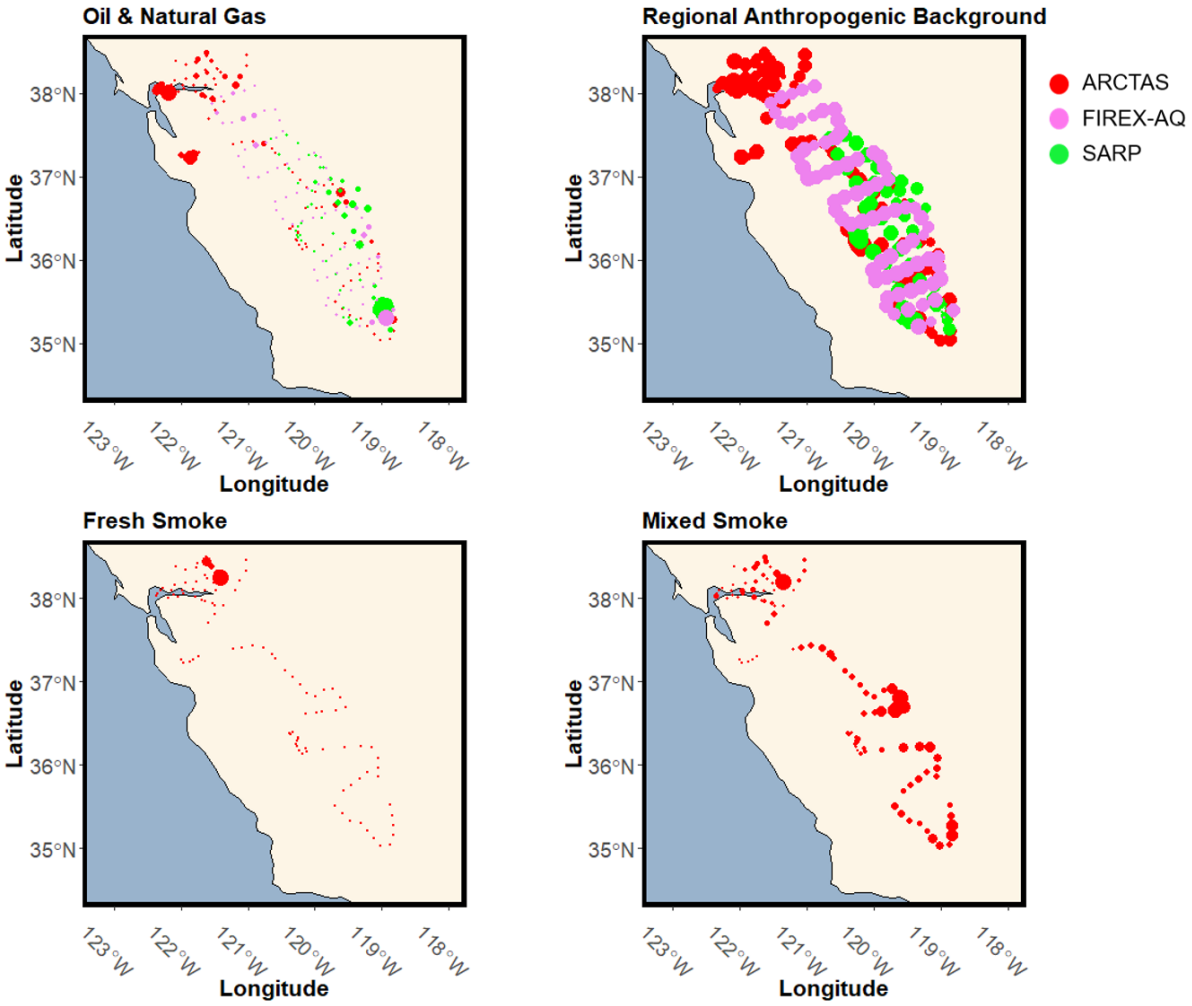

Figure 4.9 Maps of the flight tracks from each campaign, where the points have been sized by the relative contribution from the factor. Larger points indicate a greater contribution in that area.

The background factor showed contributions along the entire flight path, and was primarily composed of very long-lived gases such as CFCs, as well as carbon monoxide and gasoline emissions which indicate that vehicular exhaust may also be included in the background factor. Finally, the two biomass burning factors were designated as such because they exhibited significant enhancements in the factor contributions when the aircraft was in close proximity to fires in the northern section of the Central Valley, and because biomass burning tracers such as carbon monoxide, ethyne, and propyne were loaded predominantly into these factors. Exactly

what each factor physically represents is difficult to determine because the factors have very similar sources. However, it does not appear that these two factors are a result of factor splitting, because there was no factor swapping in the bootstrapping results. It appears that the fresh smoke factor represents very fresh biomass burning emissions and distillation from the surrounding biomass, while the mixed smoke factor likely represents chemically aged smoke because of the loading of secondary products such as methacrolein. In Figure 4.8 the fresh smoke factor shows the only significant enhancement when in close proximity to an active fire that was burning just west of Sacramento, CA. The mixed smoke factor, however, showed enhancements just downwind of the active fire and in the southeastern section of the valley where emissions accumulate. This factor also showed a small amount of loading from some oil and natural gas tracers, which indicates that the smoke was likely mixing with these emissions as it aged.

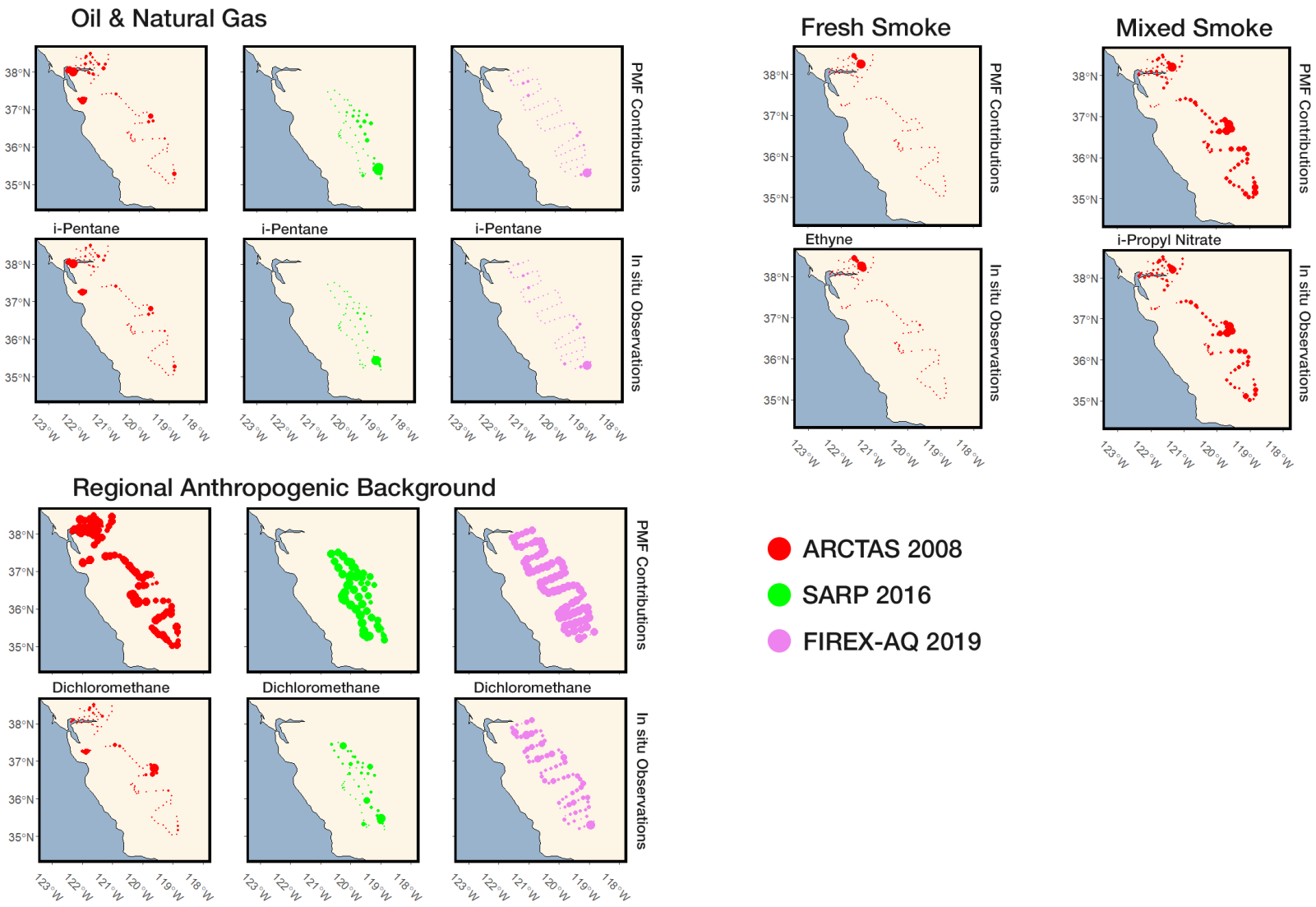

Figure 4.10 Contributions from each factor reported in the PMF results (top rows in each section) compared to real-world *in situ* observations of a corresponding tracer for each source (bottom row of each section).

As a final confirmation of the identity of each factor, the model output factor contributions were compared geospatially to *in situ* observations of trace gases with well-known emission sources. Figure 4.10 shows four sections of gridded maps, one for each of the factors observed in each PMF model run. The top left section shows the maps pertaining to oil and natural gas emissions. The top row shows the modeled contributions from this factor according to the PMF model, and the bottom row shows the points sized by the observed i-pentane concentration from each campaign year. Note the enhancements in i-pentane and correlating enhancements in the model contribution over Oildale and Bakersfield, near San Francisco (Phillips 66 refinery). The grid below shows maps with the modeled contributions from the regional anthropogenic background factor in the top row, and the observed concentrations of dichloromethane – an industrial tracer gas with a long lifetime – in the bottom row. The contribution maps show an enhancement in contributions to the factor nearly ubiquitously across the entire flight track, which makes sense for the long-lived background factor. In the *in situ* observations, however, there are some spikes in enhancements observed over cities such as Bakersfield and Fresno. These areas contain industries that emit dichloromethane, and therefore enhancements around these areas are expected. In the fresh smoke section, only data from the 2008 ARCTAS campaign are shown because that dataset was the only one of the three to report four factors, which makes sense as it is the only dataset collected during active biomass burning. The only major enhancement in this fresh smoke factor was observed near Sacramento, which makes sense because a wildfire had begun just outside of the city in 2008 a few days prior to this flight. Significant enhancements (2.8 ppbv) in ethyne – a combustion tracer (lifetime of ~3 weeks) - were also observed on this flight. The calculated contributions from the fresh biomass burning emissions correspond well to the observed biomass burning emissions during this

campaign. Finally, the mixed smoke factor (Figure 4.10, top right) was named as such because it showed contributions from just downwind of the fire, and also in the eastern side of the Central Valley where the smoke collected. The smoke also contained photochemical aging tracers in the form of the C_1-C_5 alkyl nitrates, which are also emitted during biomass burning (Simpson et al., 2002). However, the PMF results loaded a percentage of some oil and natural gas tracers into this factor as well, which makes sense as the smoke had mixed well with the background environment by the time it reached the southeastern tip of the valley. Therefore, this factor most likely represents aged smoke mixed with some of the anthropogenic background air of the valley.

An important note is that the model was run several times in different configurations, and each time the model iterated to the final results discussed here. This is key because it shows that the qualitative results are rigid and not susceptible to factor swapping. The final results presented here represent the most reasonable results while maintaining mathematical rigor as shown in the error estimation routines. The base model displacement summary showed at most a minimal drop in the Q value, indicating the results are already as close as possible to the minimum value in Q. Additionally, there were no factor swaps at the dQmax = 4 level, indicating the results are robust and have no rotational ambiguity. The bootstrapping results showed greater than 80% mapping of the boot factor to the corresponding base factor with up to 100% mapping for almost all factors in each data set, which indicates the number of factors is appropriate and that the results can be interpreted without danger of misidentification of factors.

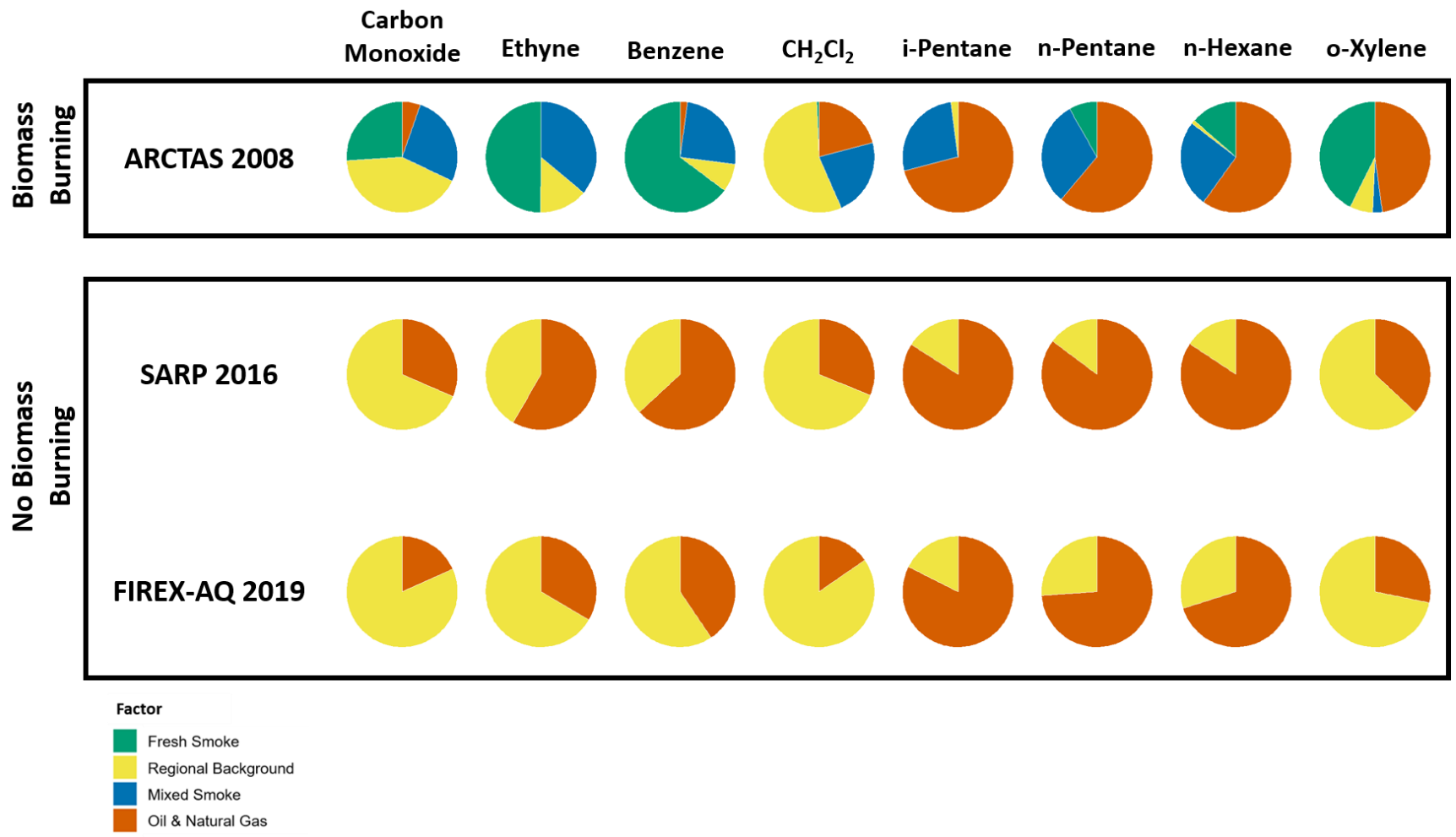

Figure 4.11 Factor compositions (% of factor total) for selected compounds for each campaign.

The results of the PMF analysis yielded some interesting discoveries. Figure 4.11 shows the percentage of the contribution from each factor to the total amount observed of selected gases. Notably, the results indicate that 88% of the benzene observed in the Central Valley during smoke-impacted periods can be attributed to wildfire emissions. Also, 52% of the carbon monoxide present in the Central Valley was attributed to fire smoke, whereas it was mainly attributed to the regional anthropogenic background (likely traffic and oil and natural gas processing) in non-smoke-impacted years. These values do not necessarily indicate that this much of the benzene present in the Central Valley came directly from fires, because the samples were preferentially collected in fire smoke. However, it does indicate that biomass burning is a major source of these gases to the mixed layer in the region. When compared to the observed enhancements collected during the campaign, the PMF results are reasonably accurate. The average benzene concentrations observed during ARCTAS was 108 pptv, while the observed concentration was 21 pptv and 26 pptv during FIREX-AQ and SARP, respectively. The value of 108 pptv is a factor of four enhancement compared to the average of the non-smoke-impacted years, which is within 10% of the enhancement predicted by the PMF model. The carbon monoxide enhancement only shows a 23% enhancement from non-smoke-impacted to smoke-impacted years (167 ppbv in 2008; 132 ppbv and 135 ppbv in 2019 and 2016, respectively) which is just under half of the enhancement predicted by the model.

These results also show the degree to which the Central Valley is impacted by oil, natural gas, and petrochemical processing emissions. Factors corresponding to these emissions were present in each data set, and in non-smoke-impacted years these factors were responsible for at least one-third of the benzene present in the sample. There appears to be some variation in the modeled factor contributions between the two non-smoke-impacted years. Also, there was some

loading of o-xylene into the background factor, and HCFC-142b into the oil and natural gas factor. This is likely caused by the prevalence of oil and natural gas, traffic, and gasoline emissions in the background environment in the Central Valley. When a third factor was added to the model, these gases were expected to split into a third factor likely representing traffic or gasoline evaporation. However, the factor simply split into two unreasonable results, and the xylene and other similar gases remained in the background factor. Therefore, it appears that these emissions sources are well-established in the background air of the Central Valley.

The results of this study show that wildfires are major trace gas emissions sources to the Central Valley environment. Based on the WAS measurements collected across the three campaigns, the Central Valley saw a significant increase in benzene, toluene, and reactive gas concentrations such as propane, which is typically considered a coal and oil tracer, compared to non-smoke-impacted years. This enhancement in trace gases is detrimental to human health in the region, as many of the gases like benzene and toluene are carcinogenic, or are toxic in their own right. The enhancement in reactive gases especially is significant for local air quality management districts. The excess of reactive VOCs is conducive to ozone formation in the region. This enhancement in ozone formation as a result of biomass burning emissions will be explored further in chapter six.

5. Trace Gas Emissions from Biomass Burning

While regions such as the western US, Greece, and Australia may garner the most attention for their wildfires (and rightfully so), there are also other parts of the world that are just as badly affected by the emissions from fires that go relatively unnoticed. For example, the southern and southeastern US are also impacted by smoke not only from western fires, but from hundreds of small agricultural fires that are intentionally ignited after the harvest season. As described in the introduction, these fires are intentionally started for a variety of reasons. The majority are done to clear crop lands from the detritus and stubble left over from the harvest. These fires are also believed to kill pests living in the field that might harm the future crop, and to return nutrients left in the crop residue back to the soil. This practice has been performed for thousands of years; however, recent findings have shown that burning crop fields is not as beneficial as once believed, and may in fact be more harmful to future crops than simply leaving the residue as is. Other fires are started to clear land of trees, brush, and cuttings for land use development or to remove gathered detritus from the development. In short - if it can be burned and is taking up space, history has seen it burn. While the EPA is trying to limit the number of agricultural burns taking place, there are many areas of the southern US where this practice still happens frequently. Figure 5.1 shows a NASA Worldview satellite image from 9/13/2019 with a MODIS fire and thermal anomaly overlay. Each small orange point represents a fire, and while there may not seem to be very many in the region, the MODIS thermal anomaly threshold is too high to pick up smaller fires. So, there are likely many more smaller fires that are not present in the image. Even so, there are a significant number of fires that did get picked up by MODIS present in the region.

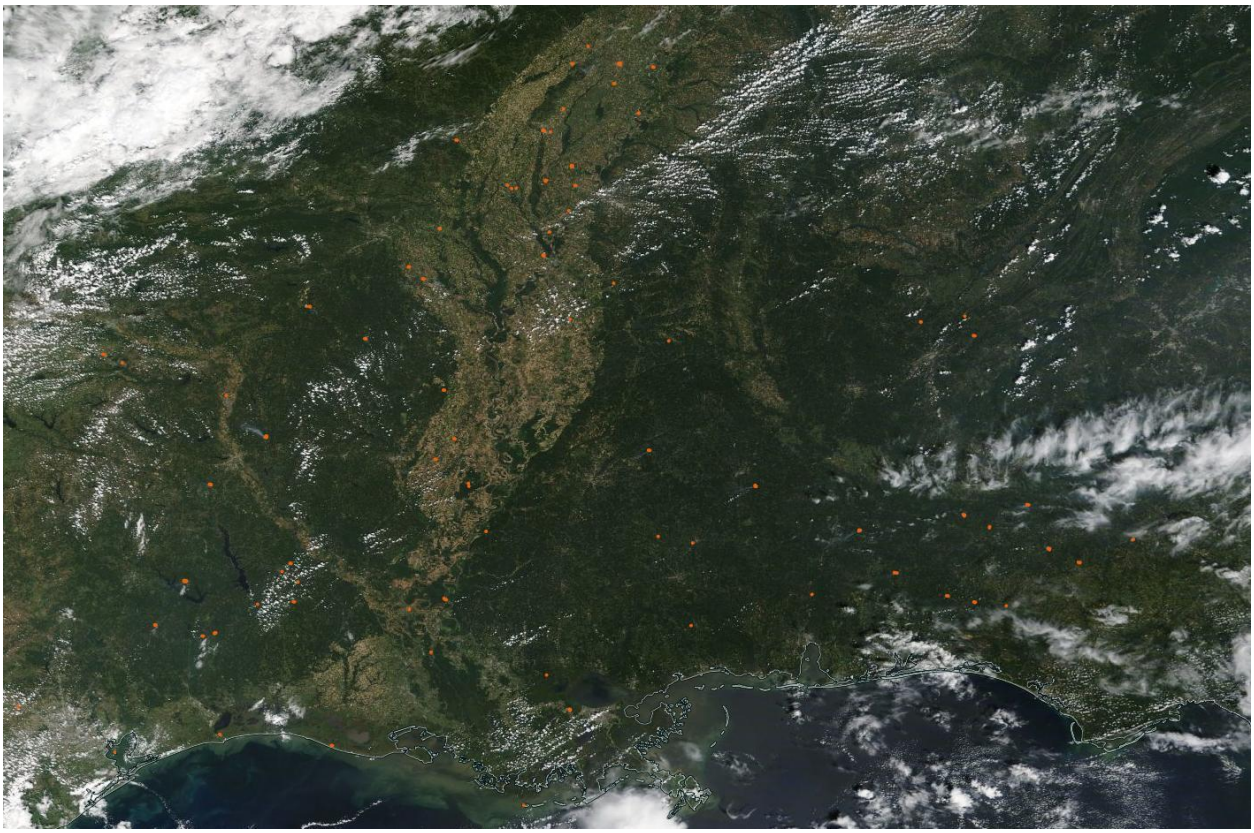

Figure 5.1 NASA Worldview satellite image from 9/13/2019 with the MODIS fire and thermal anomaly overlay showing fire activity in the region (orange points). The image was taken over Louisiana and the Mississippi Delta area.

Crop fires and prescribed burns produce smoke like any other fire, and therefore will contribute HAPs to the local environment. However, unlike larger wildfires, these small crop fires and land use burns have not been studied to nearly the same degree and therefore their impact on local and regional air quality and climate are poorly understood.

The 2019 NASA FIREX-AQ campaign allocated the second half of the field deployment schedule to address this issue specifically. While the first half of the campaign was based out of the FBO at KBOI, the DC-8 transited to the new FBO, Salina Airport (SLN), in Salina, Kansas for the remainder of the campaign. SLN was chosen as the FBO as it is a central location to the largest portion of the contiguous US, and therefore the DC-8 would have the best chance of

reaching the most fires that sprang up in the midwestern and southern US. This portion of the deployment took place from late August through mid-September, which is the peak of the agricultural burning season, and several prescribed burns were scheduled to take place at this time. Agricultural fires and the scheduled burns were targeted during this portion of the deployment, but two large wildfires in Utah and a structure fire that occurred during this time were also opportunistically sampled.

Here measurements from the NCAR Trace Organic Gas Analyzer will be reported to examine the effects of trace gas enhancements from biomass burning on the regional air quality of the areas studied during FIREX-AQ. The results presented here are compared to box modeling results calculated by the NCAR Cheyenne supercomputer using the Master Chemical Mechanism (MCM) base model.

5.1 Ambient Trace Gas Ratios & Possible Sources

The first step in this analysis was to use ratios of trace gases to determine sources of the trace gas enhancements. This simple yet effective method for determining the source of an air mass is to examine the ratio of two co-emitted species to one another. Different emission sources will emit different amounts of trace gases, and so by looking at a common ratio of two gases it is possible to identify the emission source based heavily on the ratio.

An excellent example of one of these ratios, and one that will be used heavily in this analysis, is the ratio of i-pentane to n-pentane. Isopentane and n-pentane are isomers of one another. They have the same chemical formula, the same mass, and similar physical properties like vapor

pressure and atmospheric lifetime. The only major difference between the two is their physical structure. Isopentane has a methyl group branch on the second carbon, while n-pentane is a straight carbon chain. This structural difference is what allows the ratio of these co-emitted species to be identified.

The key to this phenomenon occurs when the compounds are formed and how they are subsequently released into the atmosphere. The main sources of pentane isomers are oil and natural gas processing, gasoline evaporation, urban emissions, and wildfires (Simpson et al., 2010). During oil and natural gas processing, pentane isomers are formed during the thermogenic cracking of the crude petroleum (Gilman et al., 2013). Natural gas contains a relatively equal mix of both the n-pentane and i-pentane conformations. Observed ratios of i-pentane to n-pentane emitted from natural gas are typically about 1.2 to one (Pétron et al., 2012). Natural gas contains an abundance of the i-pentane isomer over the n-pentane configuration. Vehicular gasoline evaporation, however, yields an observed i-pentane to n-pentane ratio of ~3.9 to one (Gilman et al., 2013). Biomass burning also emits i-pentane and n-pentane, which are formed during the combustion process, yet in a very different ratio of the two gases. Typical values of i-pentane to n-pentane ratios observed during sampling of large western wildfires during ARCTAS were typically 0.5 to one (Simpson et al., 2011)). However, values observed during the WE-CAN campaign were as low as 0.35 to one.

Benzene and toluene are also co-emitted gases that can be used to identify emission sources. Benzene and toluene are aromatic compounds that differ only by a single methyl group. They are commonly emitted from combustion processes and petroleum refining, so common sources include traffic exhaust, gasoline evaporation, petrochemical processing, and also fires (Gelencsér et al., 1997).

Typical values for trace gas ratios are reported in Table 5.1. Isopentane, i-butane, n-pentane, and n-butane are typically used as urban, oil and natural gas, and biomass burning indicators (Gilman et al., 2013). Benzene to toluene has been almost exclusively used as a traffic tracer, and has been used as a biomass burning indicator (Gelencsér et al., 1997).

Ratio	Gasoline Evaporation	Urban	Raw Natural Gas	Oil & Natural Gas	Vehicle Exhaust	Biomass Burning
isoPentane/n-Pentane	3.9[1]	2.00 ±0.03[2]	1.18[3]	0.92 ±0.01[4]		0.51 ±0.03[5]
isoButane/n-Butane			0.6 - 1.0[6]	0.35 ±0.03[4]	0.2 - 0.3[7]	0.27 ±0.01[5]
Benzene/Toluene					1.48 - 1.70[8]	2.03 - 2.27[9]

[1] Gilman et al., 2013
[2] Baker et al., 2008
[3] Pétron et al., 2012
[4] Simpson et al., 2010
[5] Simpson et al., 2011
[6] Russo et al., 2010
[7] Simpson et al., 2013
[8] Gelencsér et al., 1997
[9] Baker et al., 2008

Table 5.1 Literature values for three common trace gas ratios from different emission sources.

Emission ratios can be used for more than just identification of emission sources. Trace gas emissions are often compared to the enhancements in certain gases as a way of determining the magnitude of the emissions of the trace gas for a given source. When studying fire emissions, trace gas enhancements from fires are often compared to the enhancement in carbon monoxide or acetonitrile – as both are biomass burning tracers – because the ratio of the trace gas to the tracer is consistent and can yield information into the fire's condition. More importantly, they yield insight into the mass of the different trace gases being emitted into the atmosphere, as the mass of the emissions can be back-calculated given the mass of the fuel burned which is a value that can be determined using satellite and ground truth data.

Another important piece of information that trace gas ratios can provide is the approximate age of an air mass. Trace gases have intrinsically different lifetimes as each compound has a different reactivity with oxidants. The average amount of time a gas remains in

the atmosphere before the ambient concentration of it decays to 1/e (37%) of the initial amount is defined as its atmospheric lifetime. When two or more compounds are emitted simultaneously from the same source, yet have different atmospheric lifetimes, then the approximate time since emission can be determined by taking the ratio of two of the gases. For example, benzene and toluene are co-emitted gases whose sources include traffic exhaust and fires (Gelencsér et al., 1997). But toluene is approximately five time more reactive with OH than benzene, and therefore has a much shorter lifetime in the atmosphere (Gelencsér et al., 1997). So, since benzene and toluene are emitted at very similar concentrations yet have such different lifetimes, the age of the air mass can be estimated by the ratio. A ratio close to one indicates relatively fresh emissions, while a ratio more in favor of benzene means some time has passed since the gases entered the atmosphere. However, caution must be taken when interpreting results, as remote or "clean" air will have a ratio of benzene to toluene, but the value will be meaningless as the concentrations of both gases will be close to the LLOD.

Figure 5.2 shows the ratios of i-pentane to n-pentane as measured by the TOGA instrument during the 2019 NASA FIREX-AQ campaign. An enhancement in the i/n-pentane ratio was observed during the southeastern US segment of FIREX-AQ that was not observed during the western US segment. Typical i/n-pentane ratios for boreal forest fires are ~0.5 (Simpson et al., 2002). Ratios observed during WE-CAN and FIREX-AQ were on the order of 0.35 – 0.29. However, a ratio of 0.82 (Figure 5.2) is significantly different than previously observed ratios.

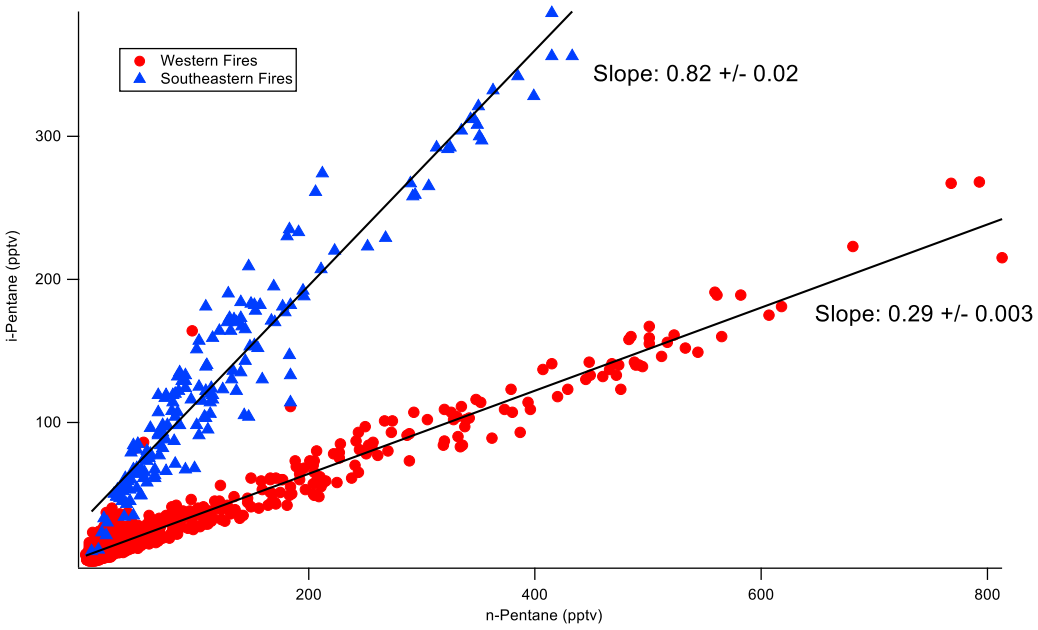

Figure 5.2 Example graph of i-pentane to n-pentane as observed over western and southeastern fires.

This is enhancement in the i/n-pentane ratio is likely caused by the prevalence in oil, natural gas, and coal processing in this area, and the meteorology of the region. This area of the southeastern US experiences weak prevailing winds, which allows emissions to remain in the area and mix into the background atmospheric environment. Figure 5.3 shows the ratio of ethane to methane observed in both the western and southeastern US during FIREX-AQ. Large ethane to methane ratios indicate the presence of oil and natural gas processing. However, there wasn't a significant enhancement in processing emissions observed as one might expect. Therefore, the likely explanation for the large difference in i/n-pentane ratios is that the southeastern fire plumes do not get large enough to be sampled when the emissions are at the freshest, or in the "core" of the smoke. By the time the aircraft samples the plume, it has already diluted heavily

with the background air, which is not the case in western wildfires. Therefore, even if the petrochemical processing emissions are not as intense in the southeast as elsewhere in the country, the smoke will be affected by these emissions very quickly after release, which may be skewing the ratio.

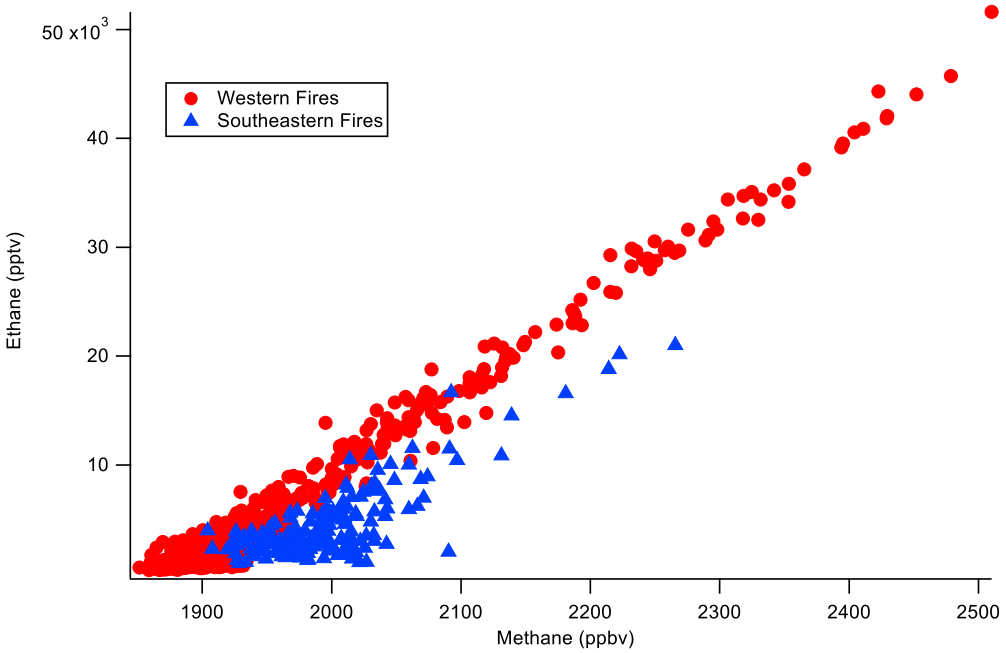

Figure 5.3 Ratio of ethane to methane observed during the FIREX-AQ campaign. The ratio was fairly consistent between the western and southeastern US, indicating similar contributions from oil and natural gas processing and other sources.

Figure 5.4 shows emission ratios of VOCs as measured by the NCAR TOGA vs carbon monoxide observed during the 2019 NASA FIREX-AQ campaign.

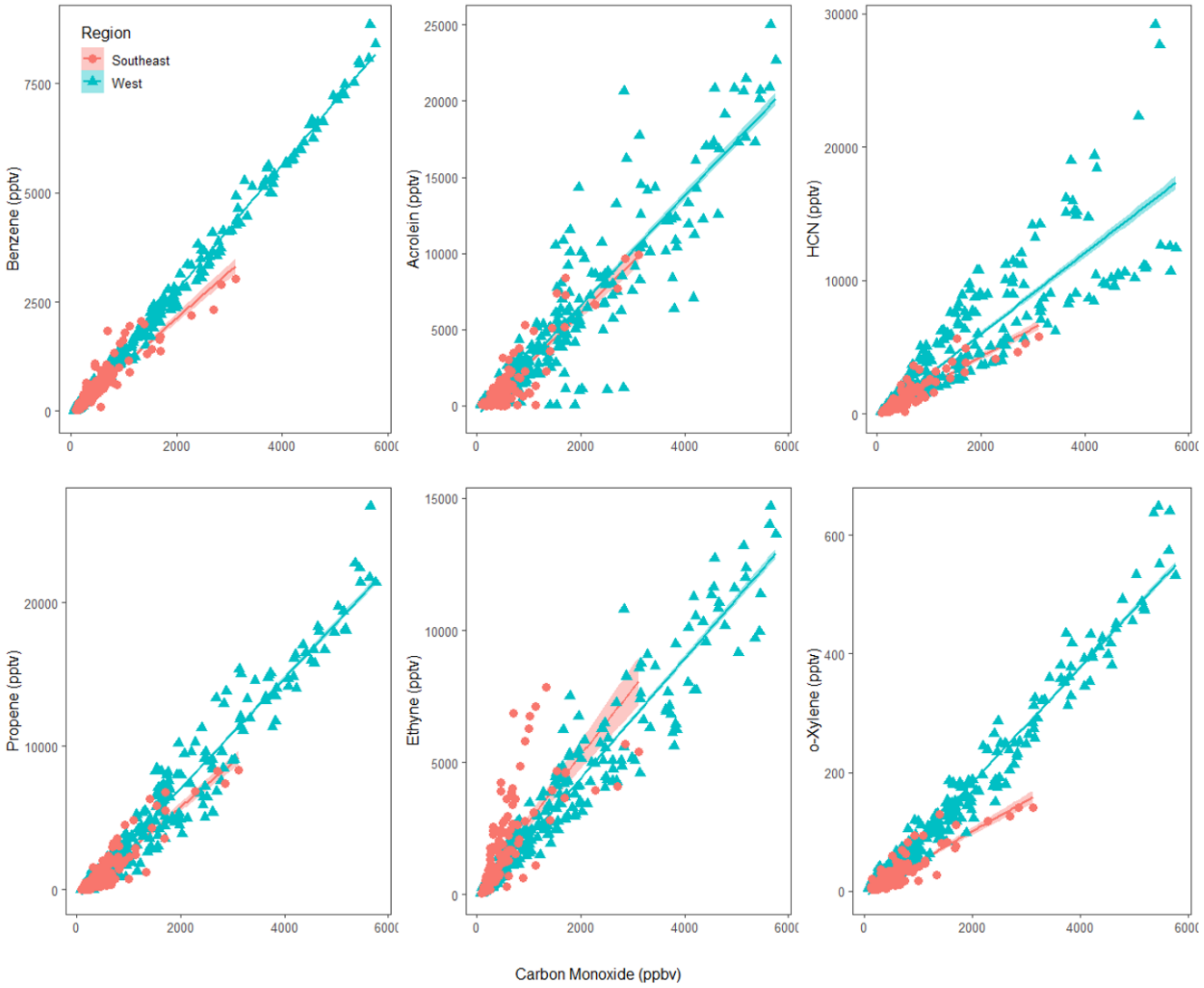

Figure 5.4 Emission ratios observed during FIREX-AQ.

The results of the trace gas analysis indicate that, in general, western fires and southeastern fires have similar emission ratios for most trace gases. This indicates that fuel type and fuel condition (e.g., wet or dry) don't have a significant affect the emission ratios for most trace gases except for a few such as ethyne (Figure 5.5) and methyl chloride (Figure 5.6).

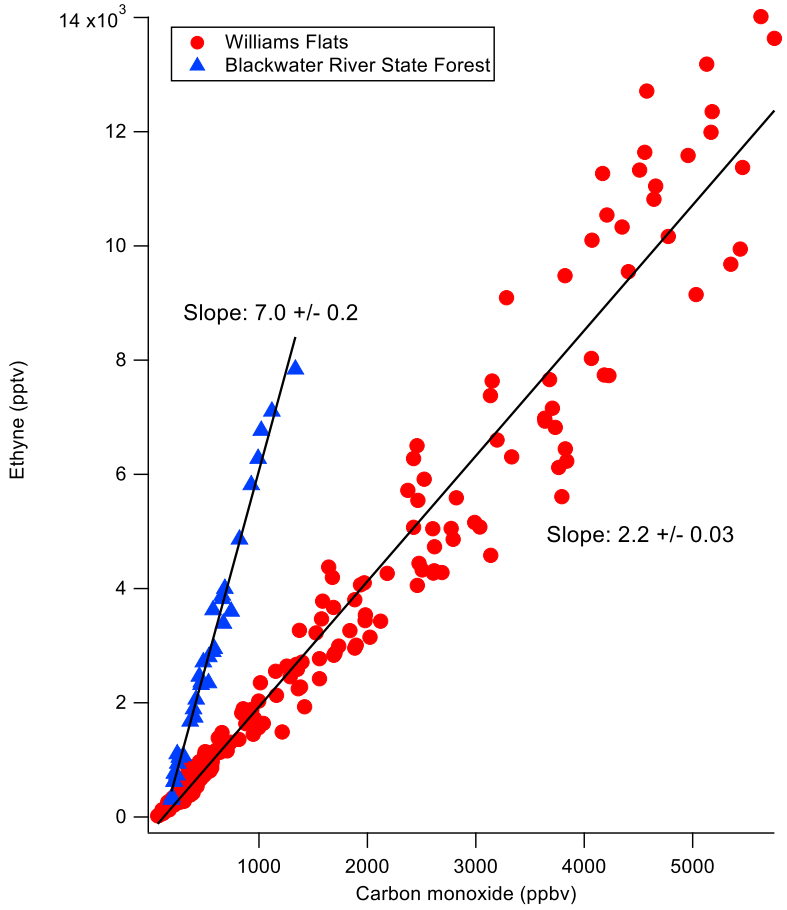

Figure 5.5 Ethyne to carbon monoxide ratio observed over the Williams Flats fire (large western fire) and the Blackwater River State Forest fire (prescribed forestry burn in western Florida).

Ethyne, however, showed a marked difference in emissions between the Williams Flats fire in eastern Washington compared to the Blackwater River State Forest (BRSF) fire in western Florida. While the Williams Flats fire was considerably larger than the BRSF fire, both fires consisted of similar sized fuels (logs and timber slash), and both burned pine fuels. The Williams flats fire fuel consisted of primarily ponderosa pine, while the BRSF fire consisted primarily of loblolly pine and mesic shrub with some oak. The primary difference between the Williams Flats and BRSF fires are the size (44,500 acres vs 674 acres burned, respectively) and the burn conditions. The Williams Flats fuel was the typical western wildfire fuel – dry ponderosa pine and grasslands, while the BRSF fire, being in Florida, burned in a wetland area. The difference in wetness between the two fuel types is likely an explanation for the different ethyne emission ratios, as a similar difference in emission ratios was observed by Lee et al., 2021 between Senegalese and Ugandan savannah fires. Lee et al. observed that ethyne emission ratios were enhanced in Ugandan fires than what was observed in the Senegalese fires. A likely explanation for this difference is the MCE. Lee et al. note that the Ugandan fires exhibited a much lower MCE than the Senegalese fires. The Williams Flats and BRSF fires both exhibited similar MCE values (0.92 and 0.93, respectively; calculated using transect-averaged MCE reported in the FIREX-AQ dataset), so it is likely that another factor such as fuel moisture may be playing a role in causing incomplete combustion to form ethyne.

The formation of ethyne in fires is important to understand as ethyne is a reactive VOC, and as such plays a role in ozone formation. The variation in ethyne emissions from fires is not well understood (Lee et al., 2021). Gaining a better understanding of variations in emissions of trace gases such as ethyne is important for modelers and air quality management districts to predict poor air quality events as a result of local biomass burning.

Methyl chloride also showed significant differences in the western versus southeastern biomass burning emissions, as shown in Figure 5.6.

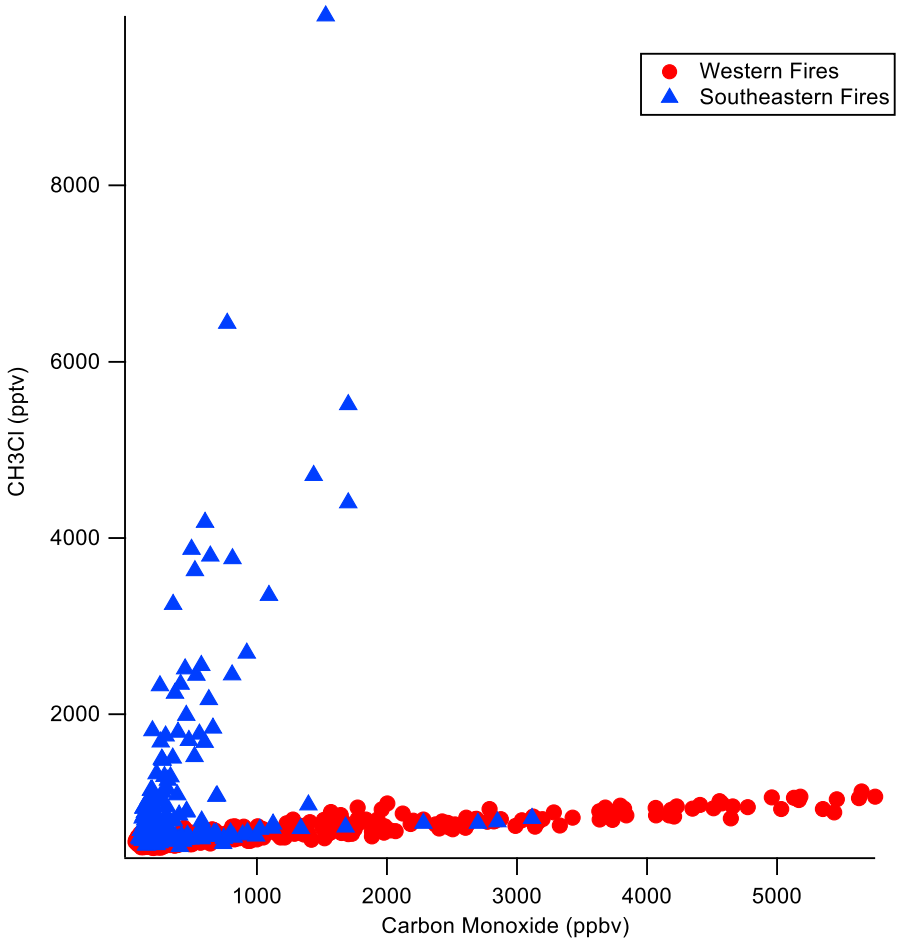

Figure 5.6 Methyl chloride enhancement observed in southeastern fires

It has been shown that methyl chloride is emitted during biomass burning, and emitted in large amounts from agricultural fires as shown in Figure 5.6. These enhancements are

investigated further in the following chapter. Figure 5.7 shows the time series of methyl chloride measurements during the FIREX-AQ campaign in 2019.

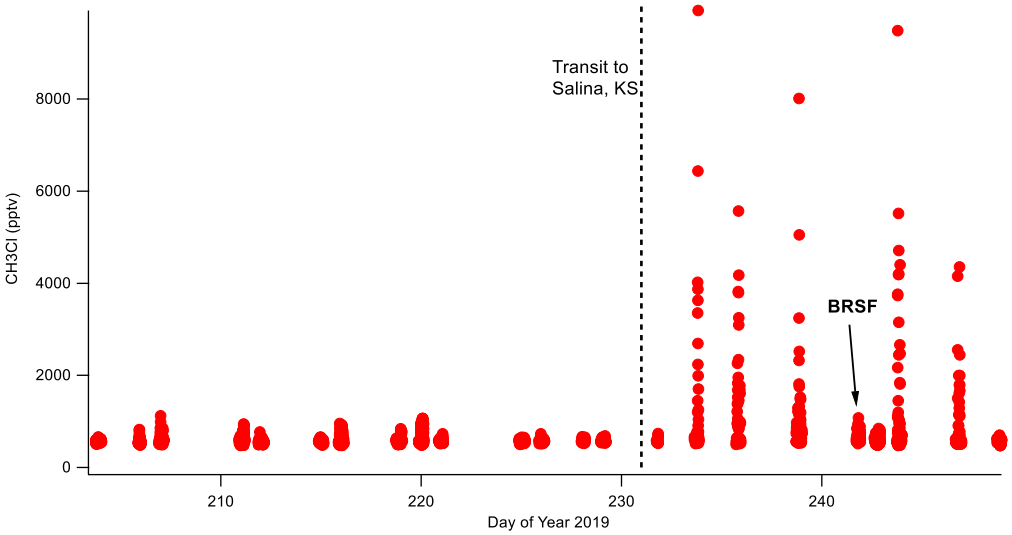

Figure 5.7 Time series of methyl chloride measurements during FIREX-AQ 2019. Note the significant enhancement in methyl chloride during the agricultural-fire-focused portion of the campaign (after transit to Salina), and lack of enhancements in forestry burns (Blackwater River State Forest fire).

The first half of the campaign (before the transit to Salina) was focused on collecting data from western wildfire emissions. During this portion, the maximum CH_3Cl concentration observed was 1123 pptv. The transit to Salina marked a shift in the campaign's focus, as after this transit emissions from crop fires and land use burns became the primary target for sampling. Figure 5.6 shows the stark difference in CH_3Cl emissions between the two types of fires. Note that forestry fires like the Blackwater River State Forest (BRSF) fire did not yield the same enhancements in CH_3Cl that the crop fires did (Figure 5.7 annotation).

6. Methyl Halide Enhancements from Biomass Burning

Methyl chloride (CH_3Cl) is a naturally occurring halocarbon trace gas, and is one of the few biogenic halocarbons that is released to the atmosphere. The reason this is important is because CH_3Cl has a relatively long lifetime (~1 year), therefore it is able to survive in the atmosphere long enough to be transported to the upper troposphere and even into the lower stratosphere (Crutzen & Andreae, 1990). Methyl chloride is the largest biogenic source of chlorine to the stratosphere, so understanding the sources and sinks are important for predicting its effect on climate. (Blake et al., 1996). The primary fate of CH_3Cl in the atmosphere is reaction with OH (Crutzen & Gidel, 1983). The reaction scheme is shown below in Equations 6.1 through 6.4 (Crutzen & Gidel, 1983).

$$CH_3Cl + \cdot OH \rightarrow CH_2Cl\cdot + H_2O \qquad \text{Eq. 6.1}$$

$$CH_2Cl\cdot + O_2 \rightarrow CH_2ClO_2\cdot \qquad \text{Eq. 6.2}$$

$$CH_2ClO_2\cdot + NO \rightarrow CH_2ClO\cdot + NO_2 \qquad \text{Eq. 6.3}$$

$$CH_2ClO\cdot \rightarrow HCOH + \cdot Cl \qquad \text{Eq. 6.4}$$

CH_3Cl can also form hydrochloric acid (HCl) in the atmosphere via reactions with diatomic oxygen and HO_2. The end result is that CH_3Cl acts as a transport mechanism and reservoir for chlorine radicals to reach the stratosphere, where they will go on to catalytically destroy ozone via reactions first proposed by Rowland and Molina in 1974 (Equations 6.5 and 6.6) (Molina & Rowland, 1974).

$$Cl + O_3 \rightarrow ClO + O_2 \quad \text{Eq. 6.5}$$

$$ClO + O \rightarrow Cl + O_2 \quad \text{Eq. 6.6}$$

CH_3Cl has been used in the past for industrial processes and as a substitute for CFCs as a refrigerant. However, the vast majority of CH_3Cl is biogenic (Tsai, 2017). Certain species of phytoplankton, marshes, and biomass burning are all sources of CH_3Cl (Tsai, 2017). However, the magnitude of these sources and therefore the global CH_3Cl budget is not well constrained. Research has been done in the past to gain a better understanding of the magnitude of CH_3Cl emissions from biomass burning, and the amount of CH_3Cl emitted from fires has been better understood. However, as stated in the introduction, emissions from agricultural fires are not well understood, and therefore the emissions of CH_3Cl from agricultural burns are not well constrained. Presented here are data collected by the UCI Whole Air Sampler (WAS) instrument during the 2019 FIREX-AQ campaign.

Enhancements in methyl bromide were also observed in agricultural burn emissions in the southeastern US. It has been shown in the literature that biomass burning is a minor source of methyl bromide, however the magnitude of these emissions is not well understood. With a lifetime of approximately two years in the atmosphere, methyl bromide is able to survive long enough to be transported to the stratosphere (Penkett et al., 2007). It has been shown that methyl bromide emission ratios are much less than methyl chloride emission ratios (Blake et al., 1996). But bromide is much more effective at catalytically destroying ozone, so even though methyl bromide is emitted in smaller quantities, it's impact on ozone depletion is disproportionately greater (Blake et al., 1996).

The magnitude of CH_3Cl and CH_3Br emitted from agricultural burns sampled during FIREX-AQ will be examined, and the climate implications of these emissions will be investigated in the following section.

6.1 Methyl Halide Emissions from Agricultural Burns

Calculating an emission ratio is a method of determining the quantity of a trace gas emitted from a source by comparing to a known, stable gas that is co-emitted with the trace gas of interest. This is done because simply examining the concentrations of the trace gas is often not enough to gain any meaningful information, especially when analyzing biomass burning plumes. This is because any dilution in the plume will affect the apparent concentration of gases in the sample (Andreae & Merlet, 2001). Therefore, comparing ratios of co-emitted gases provides much more meaningful information into the amounts of gases emitted from the source. In the case of biomass burning emissions, carbon monoxide is usually used as the stable comparison gas because it is consistently emitted from all types of fires, and because of its two-to-three-month lifetime in the troposphere. Emission ratios are calculated using Equation 6.7, and can also be calculated via linear regression calculated from the trace gas of interest plotted on the y-axis and carbon monoxide plotted on the x-axis (Blake et al., 1996).

$$ER = \frac{\Delta[Trace\ Gas]}{\Delta[CO]} = \frac{[X]_{Smoke} - [X]_{Ambient}}{[CO]_{Smoke} - [CO]_{Ambient}} \qquad \text{Eq. 6.7}$$

Upon review of the preliminary data collected by the WAS instrument during FIREX-AQ, it was discovered that there were enhancements in methyl chloride and methyl bromide in biomass burning emissions from crop burns specifically that were not present in western wildfires. Figure 6.1 shows data from samples collected by the WAS instrument over western wildfires and southeastern crop fires and brush burns. The points in Figure 6.1 are shaped by the region in which the sample was collected (western vs southeastern US). Western fires show a consistent emission ratio of 0.088 ± 0.0015. However, the southeastern fires exhibit a significant enhancement in CH_3Cl compared to western fires, and have a much greater variability in the measurements than was observed in western fires.

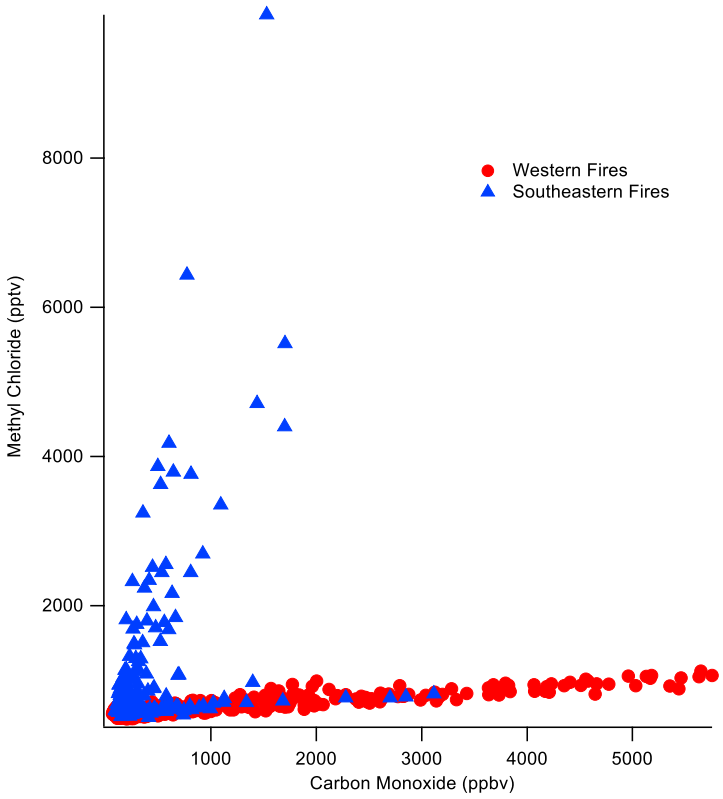

Figure 6.1 Methyl chloride and carbon monoxide observed in biomass burning emissions in the western and southeastern US.

This drastic difference in emission ratios between the types of fires sampled indicates that certain fuels may be contributing to the methyl halide enhancements observed in the biomass burning emissions.

Figure 6.2 shows emission ratios of CH_3Cl and CH_3Br to carbon monoxide observed in smoke plumes from southeastern US fires. Each point shown was identified as a sample collected in the smoke plume, so each point is representative of biomass burning emissions. Also shown are reference lines with slopes which correspond to the associated emission ratios. Note that the southeastern fire samples exhibit a wide range of emission ratios, yet seem to fall into

narrow “lobes” with defined emission ratios. This is likely because many different fires with different fuels were sampled during FIREX-AQ, indicating that it is likely the fuel which affects the emission ratios of certain gases – in this case CH_3Cl and CH_3Br.

Figure 6.3 displays a map of the area covered by the DC-8 during the second portion of the FIREX-AQ campaign. The primary regions of interest were the Mississippi Delta Valley in Louisiana, Mississippi, and Arkansas, western Florida, eastern Texas, and parts of Tennessee and Missouri. The points plotted over the map are samples that were identified as being collected in the smoke plume. Each point is then sized and colored by the associated CH_3Cl/CO emission ratio to easily identify fires that exhibited noteworthy ratios. The fires with the greatest emission ratios compared to the other fires sampled were notably all crop fires contained within the Mississippi Delta Valley.

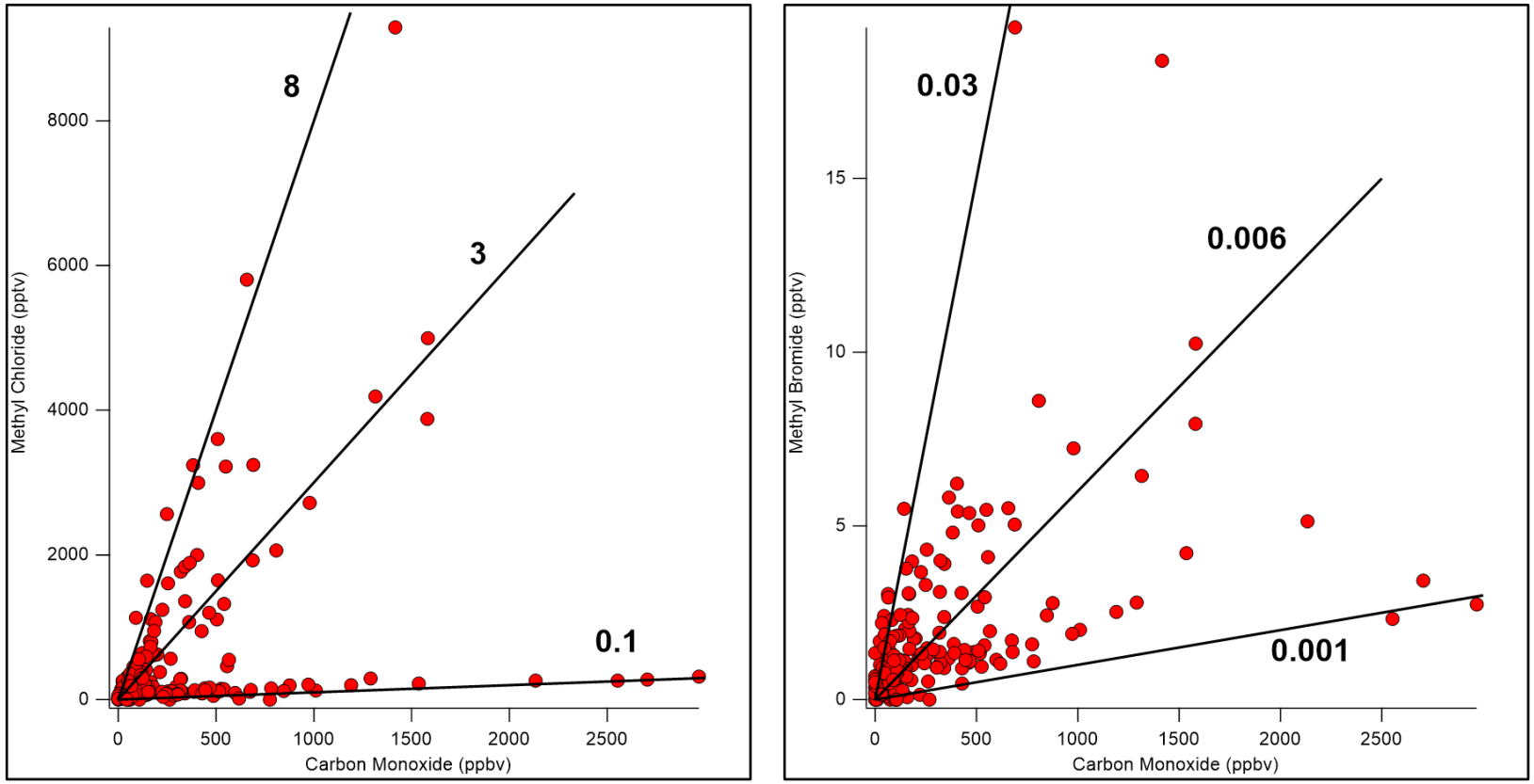

Figure 6.2 Emission ratio plots for CH_3Cl and CH_3Br to carbon monoxide in the southeastern US.

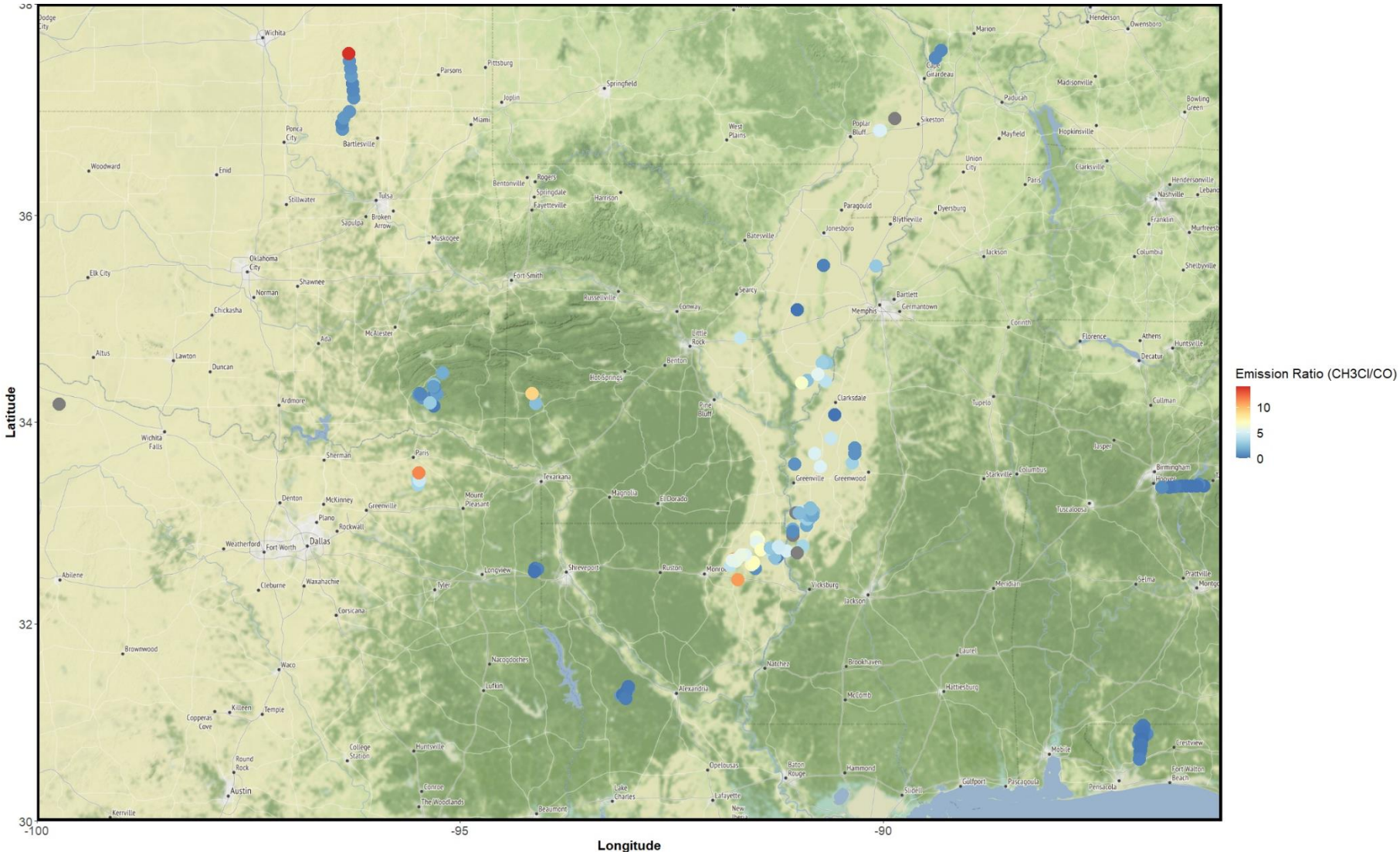

Figure 6.3 Map of the area covered by the DC-8 in the southeastern US. The plotted points are all samples collected in a smoke plume, and have bee sized and colored by their associated methyl chloride emission ratio.

Emission ratios of CH_3Cl and CH_3Br to CO were calculated for FIREX-AQ flights in the southeastern US. Literature values for this emission ratio are reported as 0.85 ± 0.06 for Brazilian biomass burning emissions, 0.57 ± 0.03 for African biomass burning emissions (Blake et al., 1996). In the dataset for the southeastern fires sampled during FIREX-AQ are numerous crop residue burns, timber slash burns, and a large prescribed forestry burn in the Blackwater River State Forest. Emission ratios of CH_3Cl and CH_3Br to CO were calculated for each day of sampling and are reported below.

CH_3Cl		CH_3Br				
Emission Ratio (pptv/ppbv)	R^2	Emission Ratio (pptv/ppbv)	R^2	Fire	Fuel	# of Measurements
9.0	1.0	0.014	0.99	Deadpool	Corn	3
6.5	1.0	0.012	1.0	Crawdaddy	Corn	3
5.3	1.0			Guacamole	Rice	3
5.1	0.99	0.005	0.98	Fargo	Corn	5
5.0	0.99	0.013	0.77	Rice-a-Roni	Corn	3
4.8	0.99	0.028	0.99	Jaws	Rice	3
4.6	0.91	0.012	0.80	Hellboy	Corn	5
4.6	0.99	0.011	0.95	Goonies	Corn	3
4.0	1.0	0.0090	0.66	Crouton	Corn	4
3.9	0.99	0.0034	0.74	Kingpin	Corn	3
3.5	1.0	0.0052	0.78	Psycho	Corn	3
2.7	0.89	0.0160	0.76	Bambi	Corn	4
2.2	1.0	0.0051	0.91	Chip	Corn	3
1.7	0.91	0.0028	0.97	Escargot	Corn	3
1.1	0.96			Dingo	Grass	4
0.74	0.83	0.0059	0.93	Elkhound	Grass	7
0.67	0.95	0.0052	0.80	Tallgrass	Grass	4
0.52	0.62			Hickory Ridge	Grass	6
0.15	0.84	0.0015	0.84	Pushmataha	Timber Slash	9
0.14	0.70	0.0019	0.68	Blackwater River	Timber Slash	34
0.075	0.92			Supertramp	Timber Slash	10
		0.0015	0.97	Land Clear	Timber Slash	4

Table 6.1 Observed emission ratios for southeastern US fires during the summer of 2019.

Table 6.1 shows emission ratios of CH_3Cl and CH_3Br to carbon monoxide. The halocarbon concentrations are reported in pptv, carbon monoxide is reported in ppbv. The

emission ratios were calculated using samples designated as in-plume and that had a specific fire assigned to them. The ambient concentrations were calculated using the minimal concentration measured just outside of the plume, which were determined using the background sample flag included in the final reported data. The ratios were calculated using linear regression methods. The data were split into separate sets for each fire, and the CH_3Cl and CH_3Br concentrations were plotted against the carbon monoxide measurements for each fire. Linear regressions were then calculated for each fire to determine the emission ratio. Any fires with fewer than three data points associated with it were not included in the final results, nor were fires with an R^2 value less than 0.6. The fuels for each fire were determined by Dr. Amber Soja and her team at NASA Langley Research Center using *in situ* observations, land use data, and MASTER data, which are reported in the final data archive.

Results indicate that crop residue burns are significant sources of both CH_3Cl and CH_3Br. The fires in Table 6.1 are sorted by their CH_3Cl emission ratio. Corn and rice fires consistently yielded significantly greater emission ratios than grassland fires, which exhibited greater emission ratios than timber slash fires (including the Blackwater River State Forest fire – a woodland fire). Emission ratios for CH_3Cl and CH_3Br from a biomass burning study in 1992 (0.85 ± 0.06 and 0.011 ± 0.0008, respectively) are significantly less than those observed during FIREX-AQ (Blake et al., 1996).

For chlorine to be emitted from biomass burning requires chlorine to be present in the biomass prior to the burn (Rudolph et al., 1995). The logical question is then: how did chlorine get into the biomass? A likely source lies in the pesticides and herbicides administered to crops during the growing season that are leftover in the biomass, and on the crop residue that is then burned.

Methyl halides are likely formed during the combustion process. For example, methanol reacts with hydrochloric acid (created during combustion) to form methyl chloride when catalyzed over burning (glowing) charcoal surfaces (Equation 6.8) (Andreae & Merlet, 2001).

$$CH_3OH + HCl \rightarrow CH_3Cl + H_2O \qquad \text{Eq. 6.8}$$

The source of the chlorine to supply this reaction still must be located within the biomass fuel. This is evidenced by the enhancement in chloride present in particulate matter emitted from biomass burning.

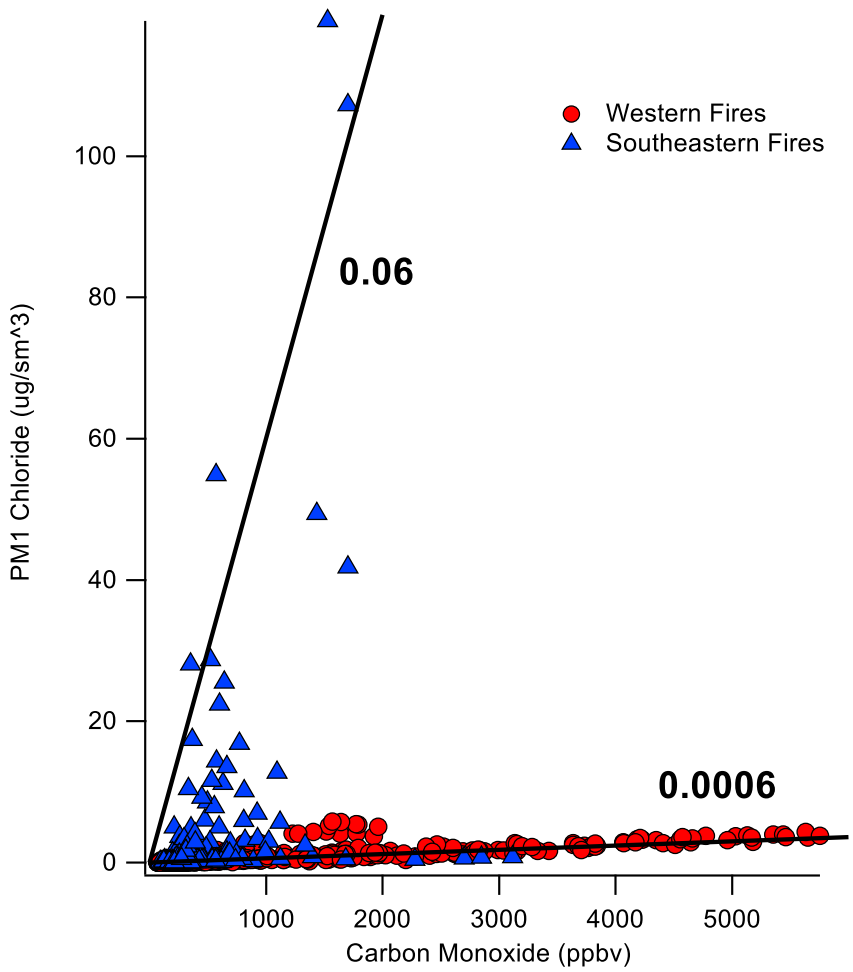

Figure 6.4 Standard mass concentration of chloride in non-refractory, sub-micron particulate matter plotted against the observed carbon monoxide concentration.

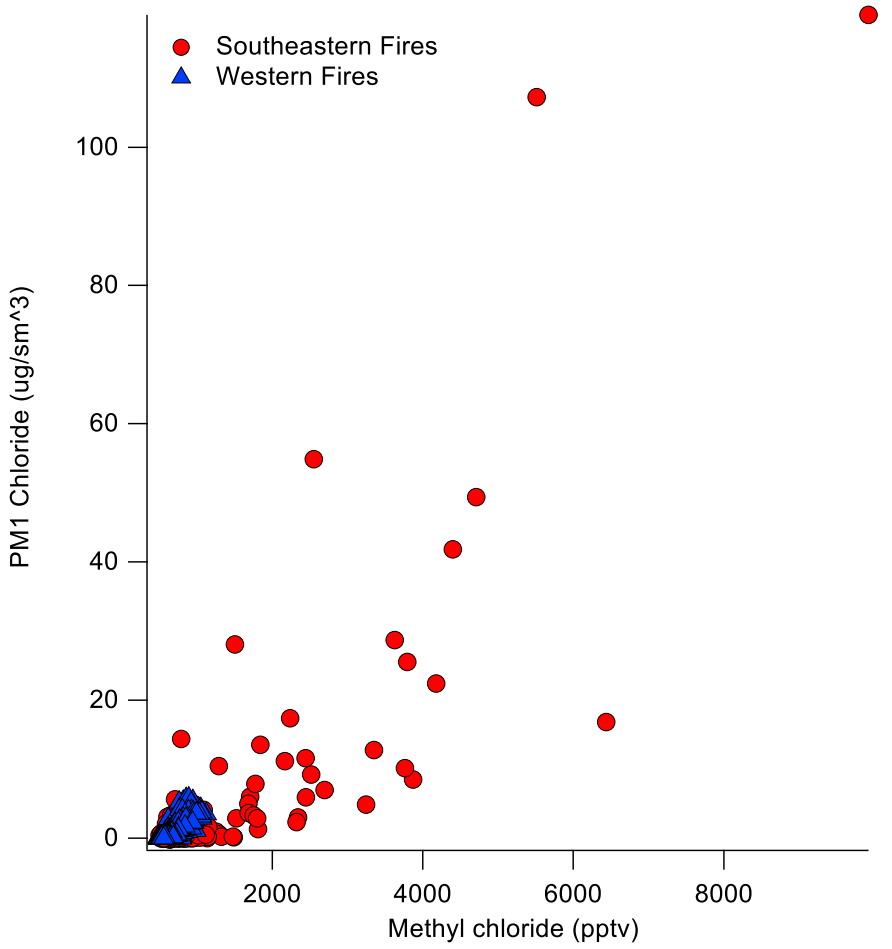

Figure 6.5 Standard mass concentration of chloride in non-refractory, sub-micron particulate matter plotted against the observed methyl chloride concentration.

Figure 6.4 shows the vast difference in PM_1 chloride content observed between western wildfires and southeastern agricultural fires. Notably, there appears to be a factor of 100 difference between the types of fires. There are some samples collected in the southeastern US that exhibit the same ratio as samples collected in the west, however upon further inspection it was discovered that these samples were collected over the Blackwater River State Forest fire – a

prescribed forest fire in western Florida. Figure 6.5 shows that chlorine does not appear to be preferentially loading into aerosols versus trace gas formation, it appears that the agricultural fires simply emit more chlorine than forest fires.

A likely source of chlorine for agricultural biomass are pesticides that are applied to the crops. Crop growers in the US use a combination of pesticides depending on the type of crop being grown. Corn accounts for 40% of the pesticide use in the US, and a total of 516 million pounds of pesticide were used in the US in 2008 (USDA 2014). More than 90% of the acres of corn planted in the US are treated with some form or combination of pesticide (e.g., herbicide, insecticide) (USDA 2014). Of the eleven most used pesticides, seven contain active ingredients which have at least one molecule of chlorine (Table 6.2; USDA 2014). This corresponds to 71.3 million pounds of chlorinated compounds applied to crops in 2008 alone (USDA 2014). These compounds remain in the soil and can be taken up by plants. Therefore, these chlorinated compounds could remain in the detritus and other biomass left over after the harvest, which are then burned.

Active Ingredient	% of Total Pesticide Use	Molar Mass (g/mol)	# of Chlorine Atoms	Moles of Chlorine	Mass of Chlorine (g)
Atrazine	13%	215.7	1	1.41 x 10^8	5.00 x 10^9
Acetochlor	6%	269.8	1	5.21 x 10^7	1.85 x 10^9
Metolachlor	6%	283.8	1	4.95 x 10^7	1.75 x 10^9
Dichloropropene	4%	111.0	2	1.69 x 10^8	5.98 x 10^9
2,4-D	3%	221.0	2	6.35 x 10^7	2.25 x 10^9
Chlorpyrifos	1%	350.6	3	2.00 x 10^7	7.10 x 10^8
Chlorothalonil	1%	265.9	4	3.52 x 10^7	1.25 x 10^9
Total Mass of Active Ingredient (lbs)	516 x 10^6			Total Mass of Chlorine (kg)	1.88 x 10^7
				Total Mass of Methyl Chloride (kg)	2.68 x 10^7

Table 6.2 The top seven chlorine-containing active ingredients used in pesticides, and the net mass of chlorine used per year.

Assuming every atom of chlorine in the active ingredients is completely converted to methyl chloride, then an estimated 26.8 Gg/yr of methyl chloride would be emitted to the atmosphere from the US. This figure is larger than the 9.9 Gg/yr of methyl chloride emitted from US cropland burning calculated using literature values of 26 Tg/yr of crop biomass burned, a molar emission ratio of 21.9 CH_3Cl/CO_2, and 1515 kg CO_2 emitted per Mg of crop biomass burned from Bond et al., 2004; Lobert et al., 1999; and Wiedinmyer et al., 2006; respectively. This figure might be enhanced for a few reasons. First, not all crop land area is burned after the harvest. The US EPA has been limiting the amount of cropland burning that occurs to limit its impacts on air quality. Second, the amount of applied pesticide will not be completely taken up by the biomass. Water runoff carries a portion of the applied pesticides out of the fields and into nearby watersheds. Third, not all of the chlorine present in the biomass will be converted to methyl chloride. There is a significant amount of chloride that remains in particulate matter that isn't converted to trace gas (Figure 6.5). Finally, if a fire starts in the field, then in theory the heat of the fire would boil off pesticides remaining that had not been taken up by the biomass. The pesticides listed in Table 6.2 have boiling points that range from 100 °C to 376 °C (NCBI 2021). Therefore, pesticides with boiling points at the lower end of the range that weren't taken up would boil off before the biomass began to combust at approximately 200 °C, and well before pyrolysis begins at approximately 300 °C. However, pesticides such as chlorpyrifos will remain in the fire during combustion and pyrolysis and actually begin to decompose at 160 °C, and therefore can contribute to methyl chloride formation (NCBI 2021).

So, one cannot say that all or most of the CH_3Cl observed was a result of pesticide use, but there appears to be enough chlorine available from pesticides to partly or mostly account for the observed emitted CH_3Cl.

7. Summary of Findings

7.1 Effects of Biomass Burning Emissions on Air Quality & Ozone Formation

A goal of this research was to determine how biomass burning emissions affect local air quality in cities and other urban centers. One way to get a quantitative look at these effects is to simulate a smoke plume entering an urban center within a chemical box model.

Box modeling has fast become one of the most powerful tools in the atmospheric sciences community, and has seen significant advances in power and scope just over the past few decades. A general schematic of the box modeling process is shown in Figure 7.1.

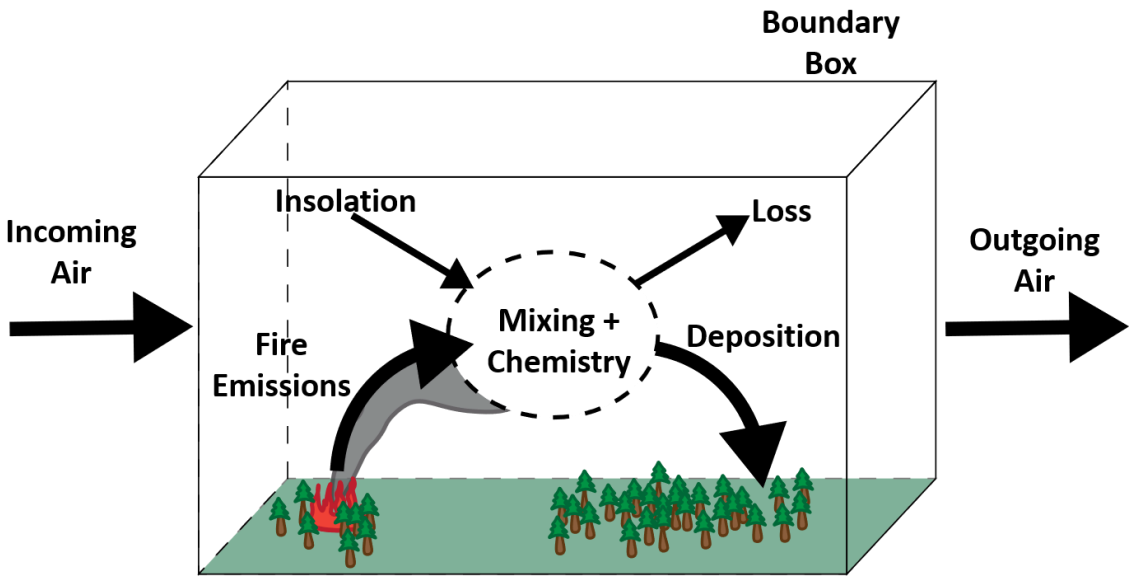

Figure 7.1 General schematic of a chemical box model.

The box model used for this analysis is the BOXMOX program – a 3-D box modeling program that is based on the Kinetic PreProcessor (KPP) developed at the Virginia Polytechnic Institute and the Max Planck Institute of Chemistry (Sandu & Sander, 2005). BOXMOX is an extension of the KPP designed for creating the box model while the KPP generates and solves the corresponding differential equations. The model was run using conditions representative of an urban air plume in a summertime environment (i.e., 30°C temperature, 1 km boundary layer height). The modeled emissions were created based on measurements collected in Pasadena, CA during a non-smoke impacted period in the summer of 2020. The model was configured to run over the course of eight hours with ten-minute time steps, which represents the average photochemically active period of time during the day. The model was run three times with identical environments, boundary layer heights, photolysis rates, and deposition rates. The only aspect that changed was the emissions, which were injected continuously during the first hour, after which the emissions were switched off to observe the chemistry. The modeled emissions are coded to mix instantaneously, and mixing with background air was removed to keep the model variation to a minimum (Sandu & Sander, 2005).

The first model run was set up with emissions solely based on the Pasadena observations and no additional emissions from biomass burning. The second model run was set up with emissions representative of enhancements in trace gases from biomass burning, which were calculated based on observations during the height of the Bobcat Fire, which took place just outside of Pasadena in September 2020.

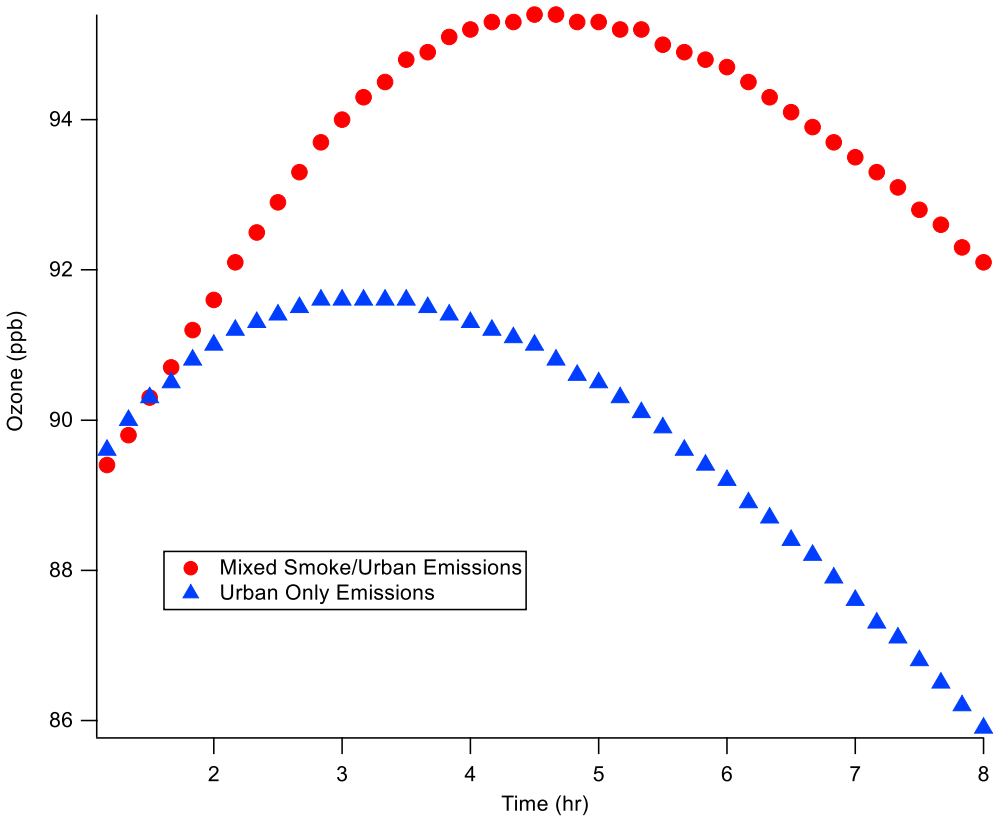

Figure 7.2 Box modeling results of an urban plume with and without an injection of biomass burning emissions.

Figure 7.2 shows the results of the urban and urban-mixed box model runs. Ozone exhibits a 3.8 ppb enhancement in the mixed smoke-urban plume compared to a non-smoke-impacted urban environment. A similar enhancement in ozone was observed between the 2008 ARCTAS campaign, where the Central Valley was smoke impacted, and the 2019 FIREX-AQ campaign, which was not smoke impacted. The average ozone concentration around the southern Central Valley was 52 ppbv during FIREX-AQ, but was enhanced to 79 ppb in the same region when it was impacted by smoke in 2008. The increase in 3.8 ppb predicted by the model may

seem small as an absolute figure, but the key is that there is an enhancement in the ozone production during smokey periods. Differences between the model prediction and *in situ* observations are likely caused by the limitations of the model set up, such as lack of smoke particulates, turbulent mixing, and variations in emission rates that might be expected throughout the day. These results show that even a short burst of smoke (1 hr) can increase the ozone production for the urban area long after the smoke clears.

Urban areas have been shown to be sensitive to VOC emissions. The method for tracking sensitivity to ozone production is to construct an ozone isopleth for the region of study. The isopleth plot is formed by plotting NOx versus the summed VOC species by carbon. The combination of these species most conducive to forming ozone is an 8:1 VOC-to-NOx ratio (Kleinman et al., 2000).

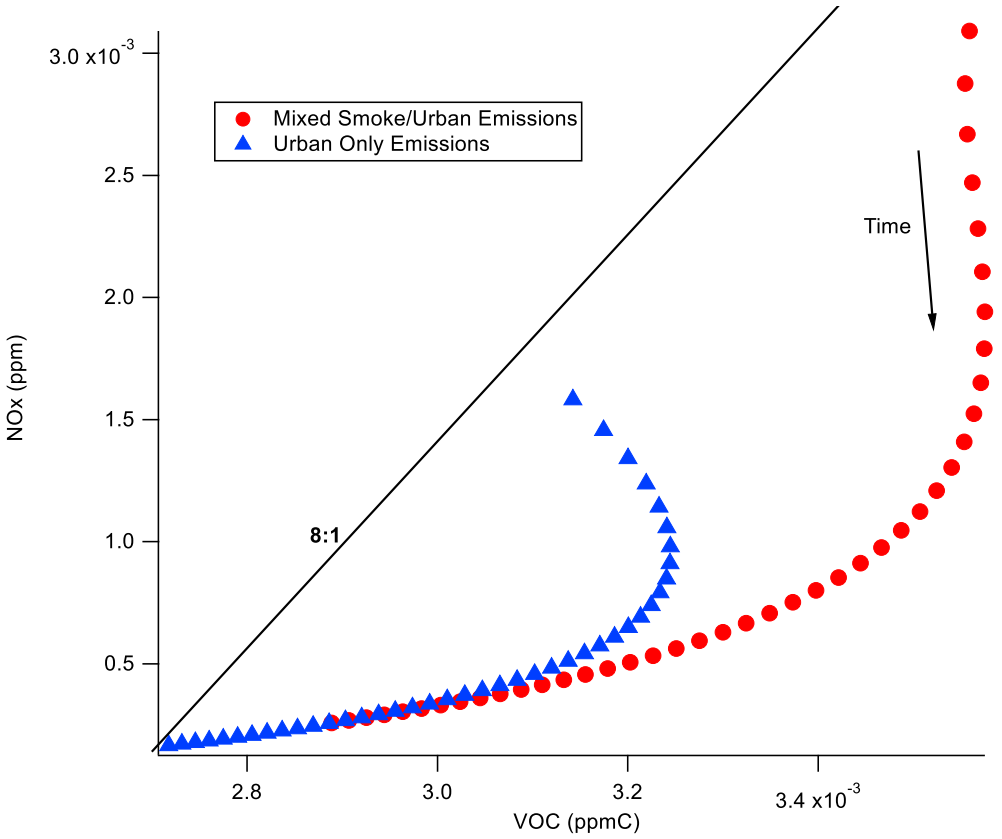

Figure 7.3 Ozone isopleth for the urban plume box model, with adjustments for smoke injection.

Figure 7.3 shows an ozone isopleth for the smoke-impacted urban and urban cases. An 8:1 line is plotted for reference. The impact of the smoke emissions swayed the chemical regime of the air mass from near the 8:1 line to a more strongly NOx-limited regime, and from the 8:1 VOC-to-NOx line where ozone production it most efficient. It appears that in this case the ozone production was most efficient at the start of the model run as the burst of emissions entered the box. As the gases were left to react, the chemical regime transitioned to more NOx-limited, and ozone production slowed. However, as the air mass became more and more smoke impacted, the

farther up the “hill” of ozone production the air mass traveled, the crest of which lies along the 8:1 reference line (see Figure 1.6).

These modeling results were then compared to real-world observations. During 2020, daily air samples were collected at the California Institute of Technology (CalTech) to examine trends in ambient trace gas concentrations throughout the lockdowns and subsequent reopening of the state during the COVID-19 pandemic. Caltech is located in Pasadena, CA, which itself is located within the LA Air Basin, and is a good representation of an urban area with corresponding emission sources (i.e., traffic, industry, etc.). Figure 7.4 shows the time series for carbon monoxide as observed in the daily sampling conducted by the Rowland-Blake Lab, as well as hourly ozone data for Pasadena, reported by the South Coast Air Quality Management District (SCAQMD).

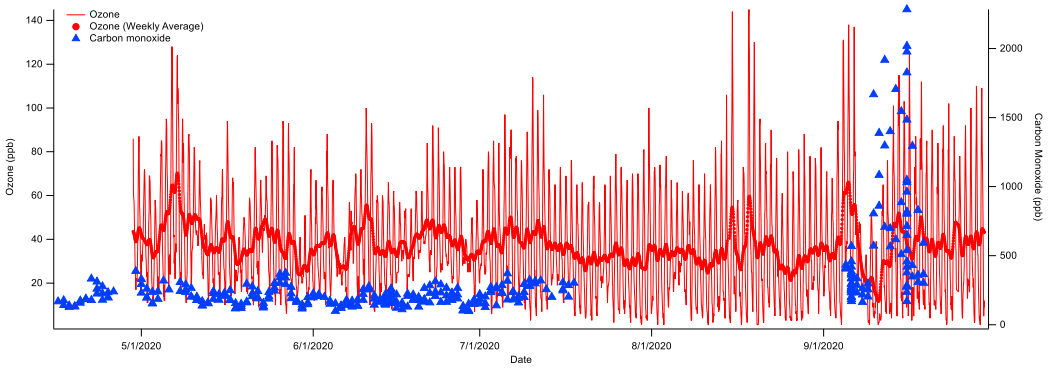

Figure 7.4 Time series for carbon monoxide as observed in daily canister sampling, and an hourly ozone time series as reported by the SCAQMD.

On September 6th, 2020, the Bobcat Fire began in the Los Angeles National Forest just to the northeast of Pasadena. Smoke from the fire and other fires in northern California filled the LA Basin, and was observed in the daily sampling measurements. Figure 7.4 highlights the period of

days just prior to ignition and the days following until easterly winds started to blow smoke out of the basin.

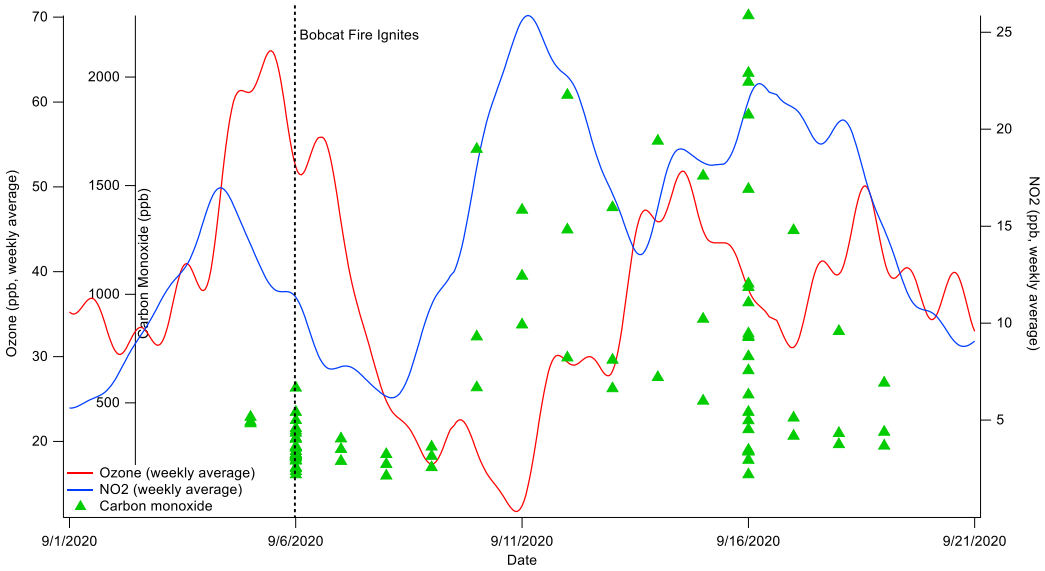

Figure 7.5 Time series of carbon monoxide, ozone (weekly average), and NO_2 (weekly average) during the 2020 Bobcat Fire in the mountains just north of Pasadena.

Figure 7.5 shows the enhancement in carbon monoxide from emissions from the Bobcat Fire, as well as the observed ozone and NO_2 concentrations. Interestingly, decreases in ozone concentration were observed following the influx of smoke to the LA Basin from the Bobcat Fire. Additionally, NO_2 was enhanced following the smoke influence, likely caused by NO_x emissions from the biomass burning. The decrease in ozone may be from NO_x titration, which would explain the increase in NO_2 and decrease in ozone, and has been observed in very fresh smoke plumes (Stedman et al., 1973; Eq. 2.1).

$$NO + O_3 \rightarrow NO_2 + O_2 \qquad \text{Eq. 2.1}$$

These results are also compared to results from a 14 km resolution chemical box model covering the continental US, which was run for the purposes of this research by Dr. Louisa Emmons at NCAR. The box model is the National Center for Atmospheric Research's (NCAR) Atmospheric Chemistry Observations and Modeling (ACOM) branch's Multi-Scale Infrastructure for Chemistry and Aerosols (MUSICA) framework, a version of the NCAR ACOM Community Atmosphere Model with Chemistry (CAM-Chem) base model with 14 km regional refinement. CAM-Chem uses the Model for Ozone and Related chemical Tracers (MOZART) reactions inventory. Included are results from both the MOZART-TS1 and MOZART-TS2 versions. MOZART-TS1 is the base tropospheric mechanism with included halogen chemistry to represent stratospheric chemistry, and the MOZART-TS2 mechanism includes further development in terpene oxidation reactions and mechanisms. The fire emissions used are from the ACOM Fire Inventory from NCAR (FINN) v2 fire emissions inventory. The anthropogenic emissions were calculated using the CAMSv4.2_R2.1 inventory, and biogenic emissions were calculated based on the NCAR MEGAN inventory. The model was nudged to the Modern-Era Retrospective analysis for Research and Applications, Version 2 (MERRA2) meteorological conditions. The purpose of the model was to examine the large-scale effects of wildfires on tropospheric ozone production across the continental US.

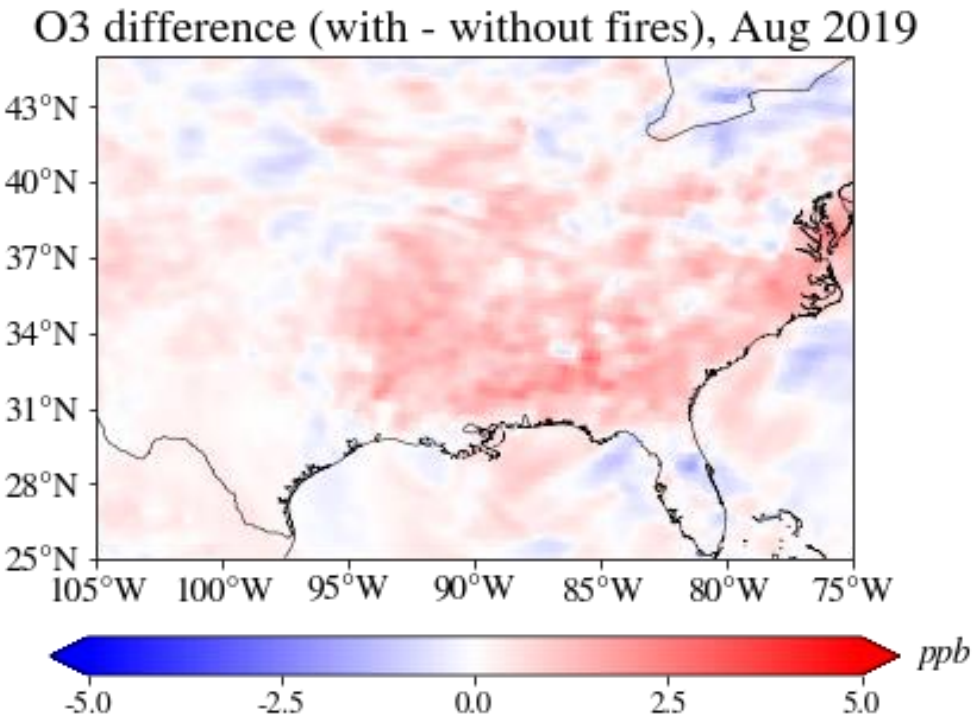

Figure 7.6 Difference in ambient ozone concentration as predicted by the model for August 2019 (reproduced with permission from Louisa Emmons).

The model predicts a maximum enhancement of 5 ppb in certain regions of the US, especially in the southeast (Figure 7.6). This value is larger than the value predicted by the BOXMOX model, which makes sense as this is a much more refined and accurate model, and correspondingly requires more computational power than a laptop can handle. However, the model apparently underpredicts the actual 27 ppb enhancement observed in the Central Valley during FIREX-AQ. The reason for this difference likely lies in the resolution of the model. At 14 km resolution, this model would have a difficult time predicting large spikes in ozone enhancement over small areas such as an active fire or a large city. What is being modeled is the general trends in ozone enhancement over the region. Still, a 5 ppb enhancement in ozone is

significant, especially for those living in areas that are routinely impacted by fire smoke, and therefore will be routinely exposed to enhanced ozone concentrations.

7.2 Effects of Chlorine Emissions from Biomass Burns on Ozone Depletion

Biomass burning appears to be a larger source of chlorine and bromine than previously reported. Agricultural burns are likely volatilizing residual pesticides in the detritus left over in fields after the harvest, which form halocarbons during the combustion process.

An understanding of the enhancement of methyl halide emissions can be gained via a naïve calculation to obtain a decent approximation (within an order of magnitude) for the enhancement in methyl halide from agricultural fires. First, the Fargo fire - a small cornfield fire - was chosen as the fire for this calculation because it was one of the freshest fires sampled (it had just been lit as the sampling began) and because there were five data points associated with the smoke plume compared to three to four points for most other crop fires.

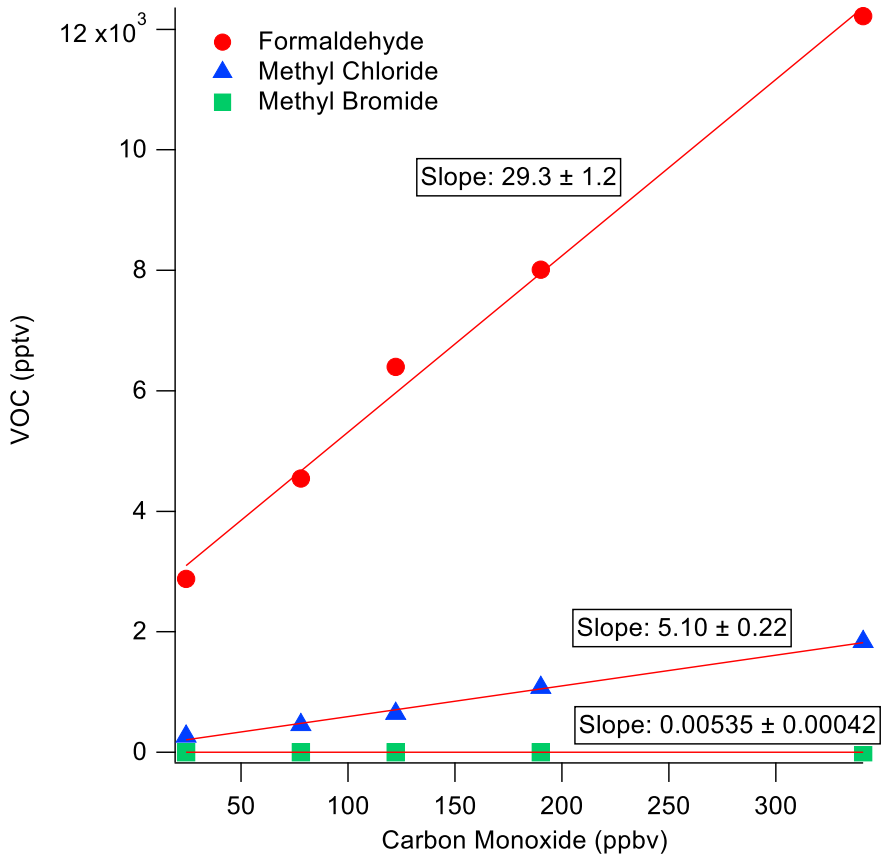

Figure 7.7 Emission ratios of formaldehyde, methyl chloride, and methyl bromide versus carbon monoxide as observed in the Fargo fire.

Figure 7.7 shows the emission ratios for three gases – formaldehyde, methyl chloride, and methyl bromide – that were emitted from the Fargo fire. The plot shows an excellent linear relationship between carbon monoxide and the three trace gases ($R^2 > 0.95$).

Emission factors for methyl chloride reported in the literature are used to estimate the average mass of methyl chloride released to the atmosphere by cropland fires per year in the continental US. Lobert et al. 1999 estimated a release of 107 Gg/yr of methyl chloride to the

atmosphere as a result of burning croplands across the planet. This figure was calculated again to estimate emissions from the US only using literature values of 26 Tg/yr of crop biomass burned in the US (Bond et al., 2004), a molar emission ratio of 0.57×10^{-3} CH_3Cl/CO (African fire emission ratio; Blake et al., 1996), and 70 kg CO emitted per Mg of crop biomass burned (Wiedinmyer et al., 2006). The result is an estimate of 1.9 Gg/yr of methyl chloride emitted to the atmosphere from cropland burning in the US alone.

26 Tg	0.57×10^{-3} mol CH_3Cl	70 kg CO	50.49 g CH_3Cl	1 mol CO
yr	1 mol CO	Mg	1 mol CH_3Cl	28.01 g CO

= **1.9 Gg CH_3Cl / yr**

Using the results of this research coupled with literature values for total amounts of crop area burned used in the previous calculation, an estimate for the emissions of methyl chloride to the atmosphere based on the FIREX-AQ measurements are presented. The emission ratio for CH_3Cl to CO was taken from the southeastern fire emission ratio results from the previous chapter, 6.2×10^{-3} CH_3Cl/CO, taken from the average of the five greatest observed emission ratios. The result is an estimated 20 Gg/yr of methyl chloride emitted to the atmosphere from cropland burns in the contiguous US.

26 Tg	$6.2x10^{-3}$ mol CH_3Cl	70 kg CO	50.49 g CH_3Cl	1 mol CO
yr	1 mol CO	Mg	1 mol CH_3Cl	28.01 g CO

= **20 Gg CH_3Cl / yr**

The estimated emissions worldwide from agricultural burning are estimated using the value of 475 Tg/yr of agricultural residue burned reported by Bond et al., 2004. The result is an estimated 370 Gg of CH_3Cl emitted from biomass burning across the planet each year. However, this value is assuming that all farmers use chlorinated pesticides, which is not necessarily the case. Therefore this value can be considered an upper bound to the CH_3Cl emission per year.

475 Tg	$6.2x10^{-3}$ mol CH_3Cl	70 kg CO	50.49 g CH_3Cl	1 mol CO
yr	1 mol CO	Mg	1 mol CH_3Cl	28.01 g CO

= **370 Gg CH_3Cl / yr**

Methyl chloride has an ozone depletion potential of 0.02 (Wuebbles 1983; Claxton et al., 2018). This means that CH_3Cl is only 2% as effective at destroying ozone per unit emitted as compared to a unit of CFC-11 emitted. Using literature values of -0.34 Dobson units (DU) per 1 Tg of CFC-11 emitted (Fleming et al., 2019) and the results above, and assuming all of the emitted CH_3Cl reaches the stratosphere, then the overall impact of cropland fires in the contiguous US alone is an estimated decrease of $1.4x10^{-4}$ Dobson units (DU) of ozone per year.

-0.34 DU	0.02 CFC-11	20 Gg CH_3Cl
1 Tg CFC-11	1 CH_3Cl	yr

= **-1.4×10^{-4} DU/yr**

If the value is scaled to include all the croplands burned on the surface of the Earth per year based on the figure calculated based on 475 Tg burned per year from Bond et al., the value increases to 2.5×10^{-3} DU/yr of ozone loss.

-0.34 DU	0.02 CFC-11	370 Gg CH_3Cl
1 Tg CFC-11	1 CH_3Cl	yr

= **-2.5×10^{-3} DU/yr**

This loss of ozone from agricultural fire emissions is miniscule compared to the ozone loss caused by other sources (e.g., Montzka et al., 2018). Also, the amount of crop residue burned in the field per year is tiny compared to the amount of biomass burned per year in forest fires. Yet, the amount of methyl chloride emitted from cropland fires is disproportionately large compared to these fires. The combined global emissions from forest fires are estimated to be 348 Gg/yr of methyl chloride.

1939 Tg	0.85×10^{-3} mol CH_3Cl	117 kg CO	50.49 g CH_3Cl	1 mol CO
yr	1 mol CO	Mg	1 mol CH_3Cl	28.01 g CO

= **348 Gg CH_3Cl / yr**

So, despite only burning 24% of the biomass of forest fires (475 Tg/yr cropland versus 1939 Tg/yr forest; Bond et al., 2004), cropland fires emit almost as much methyl chloride to the atmosphere as forest fires. While the ozone layer may not be in any imminent danger from agricultural fire emissions, understanding that agricultural burning is a larger source of CH_3Cl than previously expected is important for global modeling, and for air quality management districts.

8. Conclusion

Biomass burning has been shown to be a major source of trace gases, including hazardous air pollutants, reactive gases, and carbon oxides to the troposphere. Previously the extent of these emissions was not well understood. To address this issue, several large-scale field campaigns have been conducted to gather data on large western wildfires and smaller agricultural prescribed burns in the United States.

The goal of this research was to examine the effects of biomass burning emissions on local and regional air quality, the differences in emissions between forest fires and agricultural fires, and to see how biomass burning emissions affect human health and the health of the Earth's climate.

First, a positive matrix factorization model was run for three airborne biomass burning campaign datasets, from the ARCTAS, WE-CAN, and SARP projects. The data collected during these campaigns used in this research focused on the Central Valley region of California, an area known for its poor air quality and urban smog. The ARCTAS and WE-CAN campaigns occurred during a high wildfire activity period in California, and during the flights the majority of the Central Valley (especially the northern end) was filled with fresh and lingering smoke. The SARP flights were conducted during a very low wildfire period in California, in fact the only fire occurring was a brush fire near Santa Barbara, and the prevailing wind blew the smoke plume out over the ocean. During the high fire period sampling, enhancements in several HAP species were observed throughout the Central Valley. The goal of the PMF model was to determine how much of each HAP was coming from the fires, and how much was already present in the Central Valley from local emission sources.

The results from the PMF model indicate that biomass burning was responsible for over 50% of the ambient concentrations of seven of the nine HAPs analyzed, and up to 90% of the ambient concentration for benzene.

Second, southeastern fires were studied to determine the effects of their emissions on regional abundances of trace gases, and their effects on local air quality. In addition to analyzing the raw observations measured during the campaign, a 3-D chemical box model was run to model the emissions of these smaller regional fires over the entire southeastern US.

It was discovered that trace gas emission ratios are fairly similar between western wildfires and southeastern crop fires, with the notable exception of methyl chloride and methyl bromide. These two gases exhibited a significantly different emission ratio from crop fires than from grassland or forest fires. The box model also predicted enhancements in ozone, carbon monoxide, PAN, and other fire-borne emissions throughout the entire southeastern US. A local chemical box model was run to examine the effects of these emissions on urban air quality. First, the model was run for twenty-four hours with two injections of urban-only emissions. As expected, the model showed an enhancement in ozone, hydroxyl radical, and NOx. The second model was set up with identical background conditions, and was also run for twenty-four hours with the only difference from the first model being an augmented emissions inventory based on observations from previous research for the first injection to simulate a smoke plume passing over an urban area. The results of these models show that even a single injection can drastically change the ozone production efficiency in the urban area by changing the chemical regime in which the urban air mass lies. Also, the HOx chemistry changed drastically, which supports the chemical regime shift observed (Westberg et al., 1971).

Finally, methyl halide emissions measured during the agricultural burn portion of the FIREX-AQ campaign were analyzed. It has been shown in the literature that methyl halides are produced during biomass burning, and that crop burns in particular emit a significant amount of methyl halides. However, the amount of methyl halides emitted has not been well quantified, and the absolute impacts on climate have not been reported in recent years (Wiedenmyer et al., 2006; Stockwell et al., 2014). It was discovered that corn and rice residue burns produced huge amount of methyl chloride and methyl bromide compared to past literature values. In conjunction with estimates of total burned area of croplands from the literature, it was estimated that 13 Gg of methyl chloride are released to the atmosphere as a result of cropland burning per year (Randerson et al., 2012). This mass of methyl chloride in turn corresponds to an approximate decrease in 0.00025 DU of ozone per year solely from crop burns (Wuebbles, 1983). Compared to forest and grassland fires, crop fires are, gram-for-gram, 1.7 times more effective at depleting ozone despite their vastly smaller burn area.

Fire emissions present a threat to not only the climate, but are also a danger to farm workers, firefighters, and underrepresented communities. While ambient concentrations of HAPs from fires may not exceed OSHA limits for hazardous gases, these communities will be repeatedly exposed to smoke from biomass burning over the course of their lives. Firefighters obviously put themselves into environments where burning is occurring, and therefore breathe in smoke for hours at a time as they work. Anecdotes from ground samplers during FIREX-AQ recount working alongside wildland firefighters - none of whom wore respiratory PPE while working, despite standing directly in fresh smoke emissions. Farm hands and workers who handle the prescribed burns during the crop burn season bear some of the greatest risk, as they will be repeatedly exposed to crop fire and land use burn emissions year after year. Additionally,

those who live near the fields in local communities will also bear the brunt of the harm from these burns. Especially in areas with low air flow, such as the southeastern US, the smoke emissions can linger for days. If there are multiple burns occurring at once and/or if the burns are staggered, then this effect can last for weeks in extreme cases.

Oftentimes it is the most disadvantaged groups that see the worst effects of climate change. This is also true for the effects of fires. Effects from wildfires are not as discriminating as they often occur in remote areas, and can happen anywhere where there is enough dry fuel. Nowadays that is most of the western US, but there are cases such as those observed during ARCTAS and WE-CAN where communities very far downwind of the actual fire in the Central Valley were still experiencing the detrimental effects of the smoke.

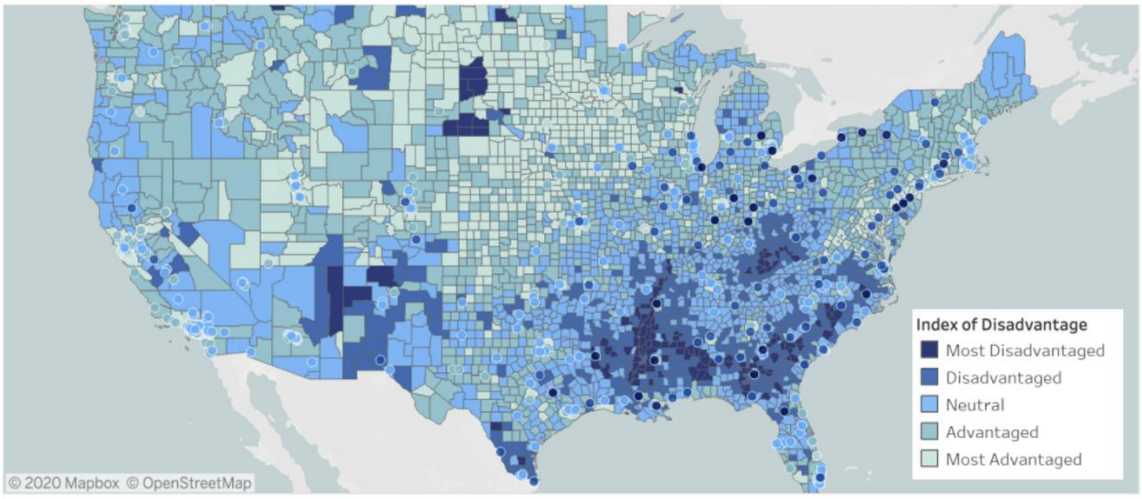

Figure 8.1 Map of community advantage or disadvantage across the continental US (adapted from Schaefer et al., 2020).

Figure 8.1 shows a map of advantaged and disadvantaged communities throughout the continental US (Schaefer et al., 2020). The amount of disadvantage associated with a community is determined by factors such as the poverty level, infant birth weight, life expectancy, and

intergenerational mobility (Schaefer et al., 2020). Note that there are a few counties in the California Central Valley that are disadvantaged that experience the same smoke as some of the neutral and advantaged communities in neighboring counties. Here we see that the wildfires in the western US affect communities of all types – advantaged and disadvantaged.

However, according to Figure 8.1, the Mississippi River Delta region and surrounding areas are some of the most socially disadvantaged areas in the entire US. Yet, these communities are the ones that will experience the effects of hundreds of croplands and land use fires each year. These communities will be disproportionately affected by the ubiquitous effluvium from these many small fires which release myriad hazardous gases. The repeated exposure to these gases, for all exposed – firefighter, field hand, and neighbor alike, will increase the risk of cancer from exposure to carcinogens like benzene in the smoke, even if only slightly.

Wildfires are increasing in frequency and severity (Abatzaglou & Williams, 2016). Unfortunately, fires are also a necessity for many parts of the world. They are intrinsically tied to our environment through millennia of evolution, and even if humans learn to stop starting them, they will always be around. However, prescribed burns for land use are a different story. It has been shown that these fires disproportionately damage the environment and air quality, and also disproportionately affect those who can stand to bear the burden the least – the US's most disadvantaged communities. Therefore, steps should be taken to limit the amount of cropland burns in particular that occur, as these have shown the greatest detriment. Fire may have been humanity's oldest friends, but blood is thicker than water, and we need to take care of our brothers in humanity first.

References

A., D. & D., S. Methods and Applications of Deoxygenation for the Conversion of Biomass to Petrochemical Products. Biomass Now - Cultiv. Util. (2013). doi:10.5772/53983

Abatzoglou, J. T. & Williams, A. P. Impact of anthropogenic climate change on wildfire across western US forests. Proc. Natl. Acad. Sci. U. S. A. 113, 11770–11775 (2016).

Abatzoglou, J. T. & Williams, A. P. Impact of anthropogenic climate change on wildfire across western US forests. Proc. Natl. Acad. Sci. U. S. A. 113, 11770–11775 (2016).

Abatzoglou, J. T., Williams, A. P. & Barbero, R. Global Emergence of Anthropogenic Climate Change in Fire Weather Indices. Geophys. Res. Lett. 46, 326–336 (2019).

Achakulwisut, P. et al. Uncertainties in isoprene photochemistry and emissions: Implications for the oxidative capacity of past and present atmospheres and for climate forcing agents. Atmos. Chem. Phys. 15, 7977–7998 (2015).

Air, R. Rethinking the Ozone Problem in Urban and Regional Air Pollution. Rethinking the Ozone Problem in Urban and Regional Air Pollution (1991). doi:10.17226/1889

Akagi, S. K. et al. Emission factors for open and domestic biomass burning for use in atmospheric models. Atmos. Chem. Phys. 11, 4039–4072 (2011).

Andreae, M. O. & Merlet, P. Emission of trace gases and aerosols from biomass burning. Global Biogeochem. Cycles 15, 955–966 (2001).

Andreae, M. O. et al. Methyl halide emissions from savanna fires in southern Africa. J. Geophys. Res. Atmos. 101, 23603–23613 (1996).

Apel, E. C. et al. Low molecular weight oxygenated volatile organic compound (OVOC) emissions during FIREX-AQ: Distributions, reactivity, chemical evolution, and comparison with other measurements. in AGU Fall Meeting Abstracts, A224-0011 (2020).

Apel, E. C. et al. Upper tropospheric ozone production from lightning NOx-impacted convection: Smoke ingestion case study from the DC3 campaign. J. Geophys. Res. Atmos. 120, 2505–2523 (2015).

Atkinson, R. & Arey, J. Atmospheric Degradation of Volatile Organic Compounds. Chem. Rev. 103, 4605–4638 (2003).

Atkinson, R. Atmospheric Chemistry of VOCs and Nitrogen Oxides. Atmos. Environ. 34, 2063–2101 (2000).

Bajpai, P. Hardwood Anatomy. Biermann's Handbook of Pulp and Paper (2018). doi:10.1016/b978-0-12-814240-0.00005-7

Baker, A. K. et al. Measurements of nonmethane hydrocarbons in 28 United States cities. Atmos. Environ. 42, 170–182 (2008).

Blake, D. (1984). Increasing concentrations of atmospheric methane: 1979-1983. University of California, Irvine: Ph.D. Thesis.

Blake, N. J., Blake, D. R., Sive, B. C., Chen, T.-Y. & Rowland, F. S., Biomass burning emissions and vertical distribution of atmospheric methyl halides and other reduced carbon gases in the South Atlantic region. J. Geophys. Res. 101, 24,151-24,164 (1996).

Blake, N. J., Blake, D. R., Sive, B. C., Chen, T.-Y. & Rowland, F. S., Biomass burning emissions and vertical distribution of atmospheric methyl halides and other reduced carbon gases in the South Atlantic region. J. Geophys. Res. 101, 24,151-24,164 (1996).

Bond, T. C. et al. A technology-based global inventory of black and organic carbon emissions from combustion. J. Geophys. Res. Atmos. 109, 1–43 (2004).

Bond, T. C. et al. A technology-based global inventory of black and organic carbon emissions from combustion. J. Geophys. Res. Atmos. 109, 1–43 (2004).

Brewer, A. W. Evidence for a world circulation provided by the measurements of helium and water vapour distribution in the stratosphere. Q. J. R. Meteorol. Soc. 75, 351–363 (1949).

Burling, I. R. et al. Laboratory measurements of trace gas emissions from biomass burning of fuel types from the southeastern and southwestern United States. Atmos. Chem. Phys. 10, 11115–11130 (2010).

Bytnerowicz, A. & Fenn, Mark & Allen, Edith & Cisneros, Ricardo. Ecologically relevant atmospheric chemistry. 107-128. (2015)

Cellulose. (2020, August 10). Retrieved September 22, 2021, from https://chem.libretexts.org/@go/page/394

Clark, J. E. D. Prehistoric Europe: The Economic Basis. (Methuen & Company Limited, 1952).

Claxton, T., Hossaini, R., Wild, O., Chipperfield, M. P. & Wilson, C. On the Regional and Seasonal Ozone Depletion Potential of Chlorinated Very Short-Lived Substances. Geophys. Res. Lett. 46, 5489–5498 (2019).

Coggon, M. M. et al. Emissions of nitrogen-containing organic compounds from the burning of herbaceous and arboraceous biomass: Fuel composition dependence and the variability of commonly used nitrile tracers. Geophys. Res. Lett. 43, 9903–9912 (2016).

Colman, J. J. et al. Description of the analysis of a wide range of volatile organic compounds in whole air samples collected during PEM-Tropics A and B. Anal. Chem. 73, 3723–3731 (2001).

Crutzen, P. J. & Andreae, M. O. Biomass burning in the tropics: Impact on atmospheric chemistry and biogeochemical cycles. Science (80). 250, 1669–1678 (1990).

Crutzen, P. J. & Gidel, L. T. A two-dimensional photochemical model of the atmosphere. 2: The tropospheric budgets of the anthropogenic chlorocarbons CO, CH4, CH3Cl and the effect of various NO(x) sources on tropospheric ozone. J. Geophys. Res. 88, 6641–6661 (1983).

Crutzen, P. J. et al. Tropospheric chemical composition measurements in Brazil during the dry season. J. Atmos. Chem. 2, 233–256 (1985).

Crutzen, P. J., Heidt, L. E., Krasnec, J. P., Pollock, W. H. & Seiler, W. Biomass burning as a source of atmospheric gases CO, H2, N 2O, NO, CH3Cl and COS. Nature 282, 253–256 (1979).

Delany, A. C., Haagensen, P., Walters, S., Wartburg, A. F. & Crutzen, P. J. Photochemically produced ozone in the emission from large-scale tropical vegetation fires. J. Geophys. Res. 90, 2425–2429 (1985).

Dodge, M.C., Combined effects of organic reactivity and nmhc/nox ratio onphotochemical oxidant formation—a modeling study. Atmos. Environ. 18 (8),1657–1665 (1984)

Dohrenwend, P. B., Le, M. V., Bush, J. A. & Thomas, C. F. The Impact on emergency department visits for respiratory illness during the southern California wildfires. West. J. Emerg. Med. 14, 79–84 (2013).

Falster, D. S. et al. BAAD: a Biomass And Allometry Database for woody plants. Ecology 96, 1445 (2015).

Fernandez-Cornejo, J. et al. Pesticide Use in U. S. Agriculture: 21 Selected Crops, 1960-2008. USDA Econ. Inf. Bull. 8–9 (2014).

Fischer, E. V. WECAN Project Manager Report. (2019).

Fleming, E. L., Newman, P. A., Liang, Q., & Daniel, J. S., The impact of continuing CFC-11 emissions on stratospheric ozone. J. Geophys. Res.: Atmospheres, 125, doi:10.1029/2019JD031849 (2020).

Gelencsér, A., Siszler, K. & Hlavay, J. Toluene-benzene concentration ratio as a tool for characterizing the distance from vehicular emission sources. Environ. Sci. Technol. 31, 2869–2872 (1997).

Gilman, J. B., Lerner, B. M., Kuster, W. C. & De Gouw, J. A. Source signature of volatile organic compounds from oil and natural gas operations in northeastern Colorado. Environ. Sci. Technol. 47, 1297–1305 (2013).

Gilman, J. B., Lerner, B. M., Kuster, W. C. & De Gouw, J. A. Source signature of volatile organic compounds from oil and natural gas operations in northeastern Colorado. Environ. Sci. Technol. 47, 1297–1305 (2013).

Goldan, P. D., Kuster, W. C., Fehsenfeld, F. C. & Montzka, S. A. Hydrocarbon measurements in the southeastern United States: The Rural Oxidants in the Southern Environment (ROSE) Program 1990. J. Geophys. Res. 100, 25945 (1995).

Gordon, M. et al. Determining air pollutant emission rates based on mass balance using airborne measurement data over the Alberta oil sands operations. Atmos. Meas. Tech. 8, 3745–3765 (2015).

Gossard, E. E. & Moninger, W. R. The Influence of a Capping Inversion on the Dynamic and Convective Instability of a Boundary Layer Model with Shear. J. Atmos. Sci. 32, 2111–2124 (1975).

Greenberg, J. P., Zimmerman, P. R., Heidt, L. & Pollock, W. Hydrocarbon and carbon monoxide emissions from biomass burning in Brazil. J. Geophys. Res. 89, 1350–1354 (1984).

Hammer, G. et al. Natural Gas. in Ullman's Encyclopedia of Industrial Chemistry 739–791 (Wiley-VCH, 2012). doi:10.1002/14356007.a17

Harrigan, D. L. et al. Anthropogenic emissions during Arctas-A: Mean transport characteristics and regional case studies. Atmos. Chem. Phys. 11, 8677–8701 (2011).

Harriss, R. C. The Amazon Boundary Layer Experiment (ABLE 2A): dry season 1985. J. Geophys. Res. 93, 1351–1360 (1988).

Hobbs, P. V, Reid, J. S., Kotchenruther, R. A., Ferek, R. J. & Weiss, R. Direct Radiative Forcing by Smoke from Biomass Burning. Science (80-.). 275, 1776–1778 (1997).

Hoke, J. E. & Anthes, R. A. The Initialization of Numerical Models by a Dynamic-Initialization Technique. Mon. Weather Rev. 104, 1551–1556 (1976).

Hoover, K. & Hanson, L. A. Wildfire Statistics. Congr. Res. Serv. 2 (2021).

Hopke, P. K. A Guide To Positive Matrix Factorization. (2000).

Huber, G. W. & Corma, A. Synergies between bio- and oil refineries for the production of fuels from biomass. Angew. Chemie - Int. Ed. 46, 7184–7201 (2007).

Hughes, S. (2018). Characterization of Trace Gases During the Front Range Air Pollution and Photochemistry Experiment (FRAPPÉ) Field Campaign. University of California, Irvine: Ph.D. Thesis.

IPCC, 2021: Climate Change 2021: The Physical Science Basis. Contribution of Working Group I to the Sixth Assessment Report of the Intergovernmental Panel on Climate Change [Masson-Delmotte, V., P. Zhai, A. Pirani, S.L. Connors, C. Péan, S. Berger, N. Caud, Y. Chen, L. Goldfarb, M.I. Gomis, M. Huang, K. Leitzell, E. Lonnoy, J.B.R. Matthews, T.K. Maycock, T. Waterfield, O. Yelekçi, R. Yu, and B. Zhou (eds.)]. Cambridge University Press. In Press.

IPCC. Climate Change 1995: The science of climate change - Contribution of Working Group 1 to the Second Assessment Report of the Intergovernmental Panel on Climate Change. (1996). doi:10.1007/978-3-662-03925-0_1

IPCC. Climate Change: The Intergovernmental Panel on Climate Change Scientific Assessment. The Intergovernmental Panel on Climate Change: Working Group 1 365 (1990).

Jiang, X., Wiedinmyer, C. & Carlton, A. G. Aerosols from fires: An examination of the effects on ozone photochemistry in the Western United States. Environ. Sci. Technol. 46, 11878–11886 (2012).

Jinno, K. (2002). Detection principle, in: Cazes, J. (Ed.), Encyclopedia of Chromatography, On-line Published, Marcel Dekker, Inc., New York.

Karion, A. et al. Methane emissions estimate from airborne measurements over a western United States natural gas field. Geophys. Res. Lett. 40, 4393–4397 (2013).

Kawamoto, H. Lignin pyrolysis reactions. J. Wood Sci. 63, 117–132 (2017).

Kleinman, L. I. et al. Ozone production in the New York City urban plume. J. Geophys. Res. Atmos. 105, 14495–14511 (2000).

Knote, C. et al. Influence of the choice of gas-phase mechanism on predictions of key gaseous pollutants during the AQMEII phase-2 intercomparison. Atmos. Environ. 115, 553–568 (2015).

Krokene, P. Conifer Defense and Resistance to Bark Beetles. Bark Beetles: Biology and Ecology of Native and Invasive Species (Elsevier Inc., 2015). doi:10.1016/B978-0-12-417156-5.00005-8

Lareau, N. P. & Clements, C. B. The mean and turbulent properties of a wildfire convective plume. J. Appl. Meteorol. Climatol. 56, 2289–2299 (2017).

Le Canut, P. Le, Andreae, M. O., Harris, G. W., Wienhold, F. G. & Zenker, T. Airborne studies of emissions from savanna fires in southern Africa 1. Aerosol emissions measured with a laser optical particle counter. J. Geophys. Res. 101, 23,615-23,630 (1996).

Lee, J. D. et al. Ozone production and precursor emission from wildfires in Africa. Environ. Sci. Atmos. (2021).

Lewis, A. C. et al. The influence of biomass burning on the global distribution of selected non-methane organic compounds. Atmos. Chem. Phys. 13, 851–867 (2013).

Lin, Y. C., Cho, J., Tompsett, G. A., Westmoreland, P. R. & Huber, G. W. Kinetics and mechanism of cellulose pyrolysis. J. Phys. Chem. C 113, 20097–20107 (2009).

Lin, Y. C., Cho, J., Tompsett, G. A., Westmoreland, P. R. & Huber, G. W. Kinetics and mechanism of cellulose pyrolysis. J. Phys. Chem. C 113, 20097–20107 (2009).

Lindaas, J. et al. Emissions of Reactive Nitrogen from Western U.S. Wildfires During Summer 2018. J. Geophys. Res. Atmos. 126, 1–21 (2021).

Liu, X. et al. Airborne measurements of western U.S. wildfire emissions: Comparison with prescribed burning and air quality implications. J. Geophys. Res. 122, 6108–6129 (2017).

Liu, X. et al. Airborne measurements of western U.S. wildfire emissions: Comparison with prescribed burning and air quality implications. J. Geophys. Res. 122, 6108–6129 (2017).

Lobert, J. M., Keene, W. C., Logan, J. A. & Yevich, R. Global chlorine emissions from biomass burning: Reactive Chlorine Emissions Inventory. J. Geophys. Res. Atmos. 104, 8373–8389 (1999).

Lobert, J. M., Keene, W. C., Logan, J. A. & Yevich, R. Global chlorine emissions from biomass burning: Reactive Chlorine Emissions Inventory. J. Geophys. Res. Atmos. 104, 8373–8389 (1999).

Ma, S. et al. Variations and determinants of carbon content in plants: A global synthesis. Biogeosciences 15, 693–702 (2018).

Marcy, T. P. et al. Measurements of trace gases in the tropical tropopause layer. Atmos. Environ. 41, 7253–7261 (2007).

Martin, M. V., Kahn, R. A. & Tosca, M. G. A global analysis of wildfire smoke injection heights derived from space-based multi-angle imaging. Remote Sens. 10, (2018).

Mayer, E. W. et al. Methane: Interhemispheric concentration gradient and atmospheric residence time. Proc. Natl. Acad. Sci. 79, 1366–1370 (1982).

McClure, C. D. & Jaffe, D. A. Investigation of high ozone events because of wildfire smoke in an urban area. Atmos. Environ. 194, 146–157 (2018).

McRae, R. H. D., Sharples, J. J. & Fromm, M. Linking local wildfire dynamics to pyroCb development. Nat. Hazards Earth Syst. Sci. 15, 417–428 (2015).

Mohanakumar, K. Stratosphere Troposphere Interactions: An Introduction. (Springer Netherlands, 2008). doi:10.1007/978-1-4020-8217-7

Molina, M. J. & Rowland, F. S. Stratospheric sink for chlorofluoromethanes: chlorine atom-catalysed destruction of ozone. Nature 249, 810–812 (1974).

Montzka, S. A., Dutton, G. S., Yu, P., Ray, E., Portmann, R. W., Daniel, J. S., et al., An unexpected and persistent increase in global emissions of ozone-depleting CFC-11. Nature, 557(7705), 413–417 (2018).

National Center for Biotechnology Information. "PubChem Compound Summary for CID 2730, Chlorpyrifos" PubChem, pubchem.ncbi.nlm.nih.gov/compound/Chlorpyrifos. (2021)

National Center for Biotechnology Information. "PubChem Compound Summary for CID 4169, Metolachlor" PubChem, pubchem.ncbi.nlm.nih.gov/compound/Metolachlor. (2021)

Nauslar, N. J., Abatzoglou, J. T. & Marsh, P. T. The 2017 north bay and southern California fires: A case study. Fire 1, 1–17 (2018).

Norris, G., Duvall, R., Brown, S. & Bai, S. EPA Positive Matrix Factorization (PMF) 5.0 Fundamentals and User Guide. (2014).

O'Dell, K. et al. Hazardous Air Pollutants in Fresh and Aged Western US Wildfire Smoke and Implications for Long-Term Exposure. Environ. Sci. Technol. 54, 11838–11847 (2020).

Paatero, P. Least squares formulation of robust non-negative factor analysis. Chemom. Intell. Lab. Syst. 37, 23–35 (1997).

Paatero, P. The Multilinear Engine—A Table-Driven, Least Squares Program for Solving Multilinear Problems, Including the n-Way Parallel Factor Analysis Model. J. Comput. Graph. Stat. 8, 854–888 (1999).

Paris, J. D. et al. Wildfire smoke in the Siberian Arctic in summer: Source characterization and plume evolution from airborne measurements. Atmos. Chem. Phys. 9, 9315–9327 (2009).

Penkett, S. A. et al. Methyl Bromide. in Scientific Assessment of Ozone Depletion: 2006 10.1-10.26 (2007).

Permar, W. et al. Emissions of Trace Organic Gases from Western U.S. Wildfires Based on WE-CAN Aircraft Measurements. J. Geophys. Res. Atmos. 126, 1–29 (2021).

Pétron, G. et al. Hydrocarbon emissions characterization in the Colorado Front Range: A pilot study. J. Geophys. Res. Atmos. 117, 1–19 (2012).

Pfister, G. G. et al. The multi-scale infrastructure for chemistry and aerosols (MUSICA). Bull. Am. Meteorol. Soc. 101, E1743–E1760 (2020).

Polissar, A. V., Hopke, P. K. & Poirot, R. L. Atmospheric aerosol over Vermont: Chemical composition and sources. Environ. Sci. Technol. 35, 4604–4621 (2001).

Randerson, J. T., Chen, Y., Van Der Werf, G. R., Rogers, B. M. & Morton, D. C. Global burned area and biomass burning emissions from small fires. J. Geophys. Res. G Biogeosciences 117, (2012).

Randerson, J. T., Chen, Y., Van Der Werf, G. R., Rogers, B. M. & Morton, D. C. Global burned area and biomass burning emissions from small fires. J. Geophys. Res. G Biogeosciences 117, (2012).

Rossabi, S. & Helmig, D. Changes in Atmospheric Butanes and Pentanes and Their Isomeric Ratios in the Continental United States. J. Geophys. Res. Atmos. 123, 3772–3790 (2018).

Rudolph, J., Khedim, A., Koppmann, R. & Bonsang, B. Field study of the emissions of methyl chloride and other halocarbons from biomass burning in Western Africa. J. Atmos. Chem. 22, 67–80 (1995).

San Joaquin Valley Unified Air Pollution Control District. Appendix A: Ambient 1-Hour Ozone Data Analysis. (2013).

Sandu, A. & Sander, R. KPP-2.1 User's Manual. (2005).

Santoso, M. A., Christensen, E. G., Yang, J. & Rein, G. Review of the Transition from Smouldering to Flaming Combustion in Wildfires. Front. Mech. Eng. 5, (2019).

Schwantes, R. et al. Comprehensive isoprene and terpene chemistry improves simulated surface ozone in the southeastern U.S. Atmos. Chem. Phys. Discuss. 1–52 (2019). doi:10.5194/acp-2019-902

Scott, R. P. W. (2001a). Katharometer detector for GC, in: Cazes, J. (Ed.), Encyclopedia of Chromatography, Marcel Dekker, Inc., New York, Basel, pp. 465-466.

Scott, R. P. W. (2001b). Electron capture detector, in: Cazes, J. (Ed.), Encyclopedia of Chromatography, Marcel Dekker, Inc., New York, Basel, pp. 285-287.

Scott, R. P. W. (2001c). Gas chromatography-mass spectrometry, in: Cazes, J. (Ed.), Encyclopedia of Chromatography, Marcel Dekker, Inc., New York, Basel, pp. 366-371.

Seigneur, C. Meteorology: General Circulation. in Air Pollution: Concepts, Theory, and Applications 33–50 (Cambridge University Press, 2019). doi:10.1017/9781108674614.003

Sekimoto, K. et al. High-and low-temperature pyrolysis profiles describe volatile organic compound emissions from western US wildfire fuels. Atmos. Chem. Phys. 18, 9263–9281 (2018).

Shaefer, H. L., Edin, K. & Nelson, T. Understanding Communities of Deep Disadvantage: An Introduction. (2020).

Shine, K. P., Derwent, R. G., Wuebbles, D. J. & Morcrette, J. J. Radiative forcing of climate. Clim. Chang. IPCC Sci. Assess. 41–68 (1990).

Sillman, S. Chapter 12 The relation between ozone, NOx and hydrocarbons in urban and polluted rural environments. Dev. Environ. Sci. 1, 339–385 (2002).

Simpson, I. J. et al. A biomass burning source of C1 - C4 alkyl nitrates. Geophys. Res. Lett. 29, 2–5 (2002).

Simpson, I. J. et al. Air quality in the Industrial Heartland of Alberta, Canada and potential impacts on human health. Atmos. Environ. 81, 702–709 (2013).

Simpson, I. J. et al. Boreal forest fire emissions in fresh Canadian smoke plumes: C1-C10 volatile organic compounds (VOCs), CO2, CO, NO2, NO, HCN and CH3CN. Atmos. Chem. Phys. 11, 6445–6463 (2011).

Simpson, I. J. et al. Boreal forest fire emissions in fresh Canadian smoke plumes: C1-C10 volatile organic compounds (VOCs), CO2, CO, NO2, NO, HCN and CH3CN. Atmos. Chem. Phys. 11, 6445–6463 (2011).

Simpson, I. J. et al. Characterization of trace gases measured over Alberta oil sands mining operations: 76 speciated C2-C10 volatile organic compounds (VOCs), CO2, CH4, CO, NO, NO2, NOy, O3 and SO2. Atmos. Chem. Phys. 10, 11931–11954 (2010).

Simpson, I. J. et al. Characterization of trace gases measured over alberta oil sands mining operations: 76 speciated C2-C10 volatile organic compounds (VOCs), CO2, CH4, CO, NO, NO2, NOy, O3 and SO2. Atmos. Chem. Phys. 10, 11931–11954 (2010).

Simpson, I. J. et al. Characterization, sources and reactivity of volatile organic compounds (VOCs) in Seoul and surrounding regions during KORUS-AQ. Elem. Sci. Anthr. 8, (2020).

Singh, H. B. & Hanst, P. L. Peroxyacetyl Nitrate (Pan) in the Unpolluted Atmosphere: An Important Reservoir for Nitrogen Oxides. Geophys. Res. Lett. 8, 941–944 (1981).

Singh, H. B. & Hanst, P. L. Peroxyacetyl Nitrate (Pan) in the Unpolluted Atmosphere: An Important Reservoir for Nitrogen Oxides. Geophys. Res. Lett. 8, 941–944 (1981).

Singh, H. B. et al. Impact of biomass burning emissions on the composition of the South Atlantic troposphere: Reactive nitrogen and ozone. J. Geophys. Res. 101, 24,203-24,219 (1996).

Stedman, D. H., Daby, E. E., Stuhl, F. & Niki, H. Analysis of ozone and nitric oxide by a chemiluminescent method in laboratory and atmospheric studies of photochemical smog. J. Air Pollut. Control Assoc. 22, 260–263 (1972). Jorgensen, S & Fath, B. Encyclopedia of Ecology. (Elsevier Science, 2008).

Stockwell, C. E. et al. Trace gas emissions from combustion of peat, crop residue, domestic biofuels, grasses, and other fuels: Configuration and Fourier transform infrared (FTIR) component of the fourth Fire Lab at Missoula Experiment (FLAME-4). Atmos. Chem. Phys. 14, 9727–9754 (2014).

Stockwell, C. E. et al. Trace gas emissions from combustion of peat, crop residue, domestic biofuels, grasses, and other fuels: Configuration and Fourier transform infrared (FTIR) component of the fourth Fire Lab at Missoula Experiment (FLAME-4). Atmos. Chem. Phys. 14, 9727–9754 (2014).

Stockwell, C. E. et al. Trace gas emissions from combustion of peat, crop residue, domestic biofuels, grasses, and other fuels: Configuration and Fourier transform infrared (FTIR) component of the fourth Fire Lab at Missoula Experiment (FLAME-4). Atmos. Chem. Phys. 14, 9727–9754 (2014).

Strum, M. & Scheffe, R. National review of ambient air toxics observations. J. Air Waste Manag. Assoc. 66, 120–133 (2016).

Sullivan, P. R., Campbell, M. J., Dennison, P. E., Brewer, S. C. & Butler, B. W. Modeling wildland firefighter travel rates by terrain slope: Results from gps-tracking of type 1 crew movement. Fire 3, 1–14 (2020).

Thapa, L. et al. Observations from inside a Wildfire-Driven Thunderstorm: The 2019 FIREX-AQ Field Experiment. in AGU Fall Meeting Abstracts, A234-09 (2020).

Tilmes, S. et al. Description and evaluation of tropospheric chemistry and aerosols in the Community Earth System Model (CESM1.2). Geosci. Model Dev. 8, 1395–1426 (2015).

Tsai, W. T. Fate of chloromethanes in the atmospheric environment: Implications for human health, ozone formation and depletion, and global warming impacts. Toxics 5, (2017).

U.S. EPA. 2017 National Emissions Inventory: January 2021 Updated Release, Technical Support Document. (2021).

Vasileva, A. et al. Emission ratios of trace gases and particles for Siberian forest fires on the basis of mobile ground observations. Atmos. Chem. Phys. 17, 12303–12325 (2017).

Wadhwani, R., Sutherland, D., Moinuddin, K. A. M. & Joseph, P. Kinetics of pyrolysis of litter materials from pine and eucalyptus forests. J. Therm. Anal. Calorim. 130, 2035–2046 (2017).

Wang, Q., Geng, C., Lu, S., Chen, W. & Shao, M. Emission factors of gaseous carbonaceous species from residential combustion of coal and crop residue briquettes. Front. Environ. Sci. Eng. China 7, 66–76 (2013).

Wang, S. et al. Chemical Tomography in a Fresh Wildland Fire Plume: a Large Eddy Simulation (LES) Study. J. Geophys. Res. Atmos. (2021). doi:10.1029/2021jd035203

Warneke, C. et al. Fire Influence on Regional to Global Environments and Air Quality (FIREX-AQ). White Paper (2018).

Wei, M., Zhang, Z., Long, T., He, G. & Wang, G. Monitoring Landsat Based Burned Area as an Indicator of Sustainable Development Goals. Earth's Future. 9, (2021).

Wertime, T. A. Pyrotechnology: Man's First Industrial Uses of Fire: The Neolithic Revolution introduced man to the new energy resources to be had from agriculture and those to be gained by applying fire to fuels and earths. 61, 670–682 (1973).

Westberg, K., Cohen, N. & Wilson, K. W. Carbon Monoxide: Its Role in Photochemical Smog Formation. Science (80-.). 171, 1013–1015 (1971).

Westberg, K., Cohen, N. & Wilson, K. W. Carbon Monoxide: Its Role in Photochemical Smog Formation. Science (80-.). 171, 1013–1015 (1971).

Whittaker, R. H.: Communities and Ecosystems, 2nd Revised Edition, MacMillan Publishing Co., New York, USA, 1975.

Wiedinmyer, C. et al. Estimating emissions from fires in North America for air quality modeling. Atmos. Environ. 40, 3419–3432 (2006).

Wiedinmyer, C. et al. Estimating emissions from fires in North America for air quality modeling. Atmos. Environ. 40, 3419–3432 (2006).

Wiedinmyer, C. et al. Estimating emissions from fires in North America for air quality modeling. Atmos. Environ. 40, 3419–3432 (2006).

Wooster, M. J., Roberts, G., Perry, G. L. W. & Kaufman, Y. J. Retrieval of biomass combustion rates and totals from fire radiative power observations: FRP derivation and calibration relationships between biomass consumption and fire radiative energy release. J. Geophys. Res. Atmos. 110, 1–24 (2005).

Wuebbles, D. J. Chlorocarbon emission scenarios: Potential impact on stratospheric ozone. J. Geophys. Res. 88, 1433–1443 (1983).

Wuebbles, D. J. Chlorocarbon emission scenarios: Potential impact on stratspheric ozone. J. Geophys. Res. 88, 1433–1443 (1983).

Yokelson, R. J., Griffith, D. W. T. & Ward, D. E. Open-Path Fourier Transform Infrared Studies of Large-Scale Laboratory Biomass Fires. J. Geophys. Res. 101, 21067–21080 (1996).

Zhang, Q. et al. Understanding atmospheric organic aerosols via factor analysis of aerosol mass spectrometry: A review. Anal. Bioanal. Chem. 401, 3045–3067 (2011).